HYDROGENATION OF AQUEOUS ACETIC ACID TO BIOETHANOL OVER TiO_2-SUPPORTED Ru-Sn AND Ni-Sn CATALYSTS

YUANYUAN ZHAO

Content

Chapter 1
Introduction

Chapter 2
TiO_2-supported Ni-Sn as an effective hydrogenation catalyst for aqueous acetic acid to ethanol

Chapter 3
Hydrogenation of aqueous acetic acid over $Ru-Sn/TiO_2$ catalyst in a flow-type reactor, governed by reverse reaction

Chapter 4
Effects of water boiling on hydrogenation of aqueous acetic acid over Ni-Sn/TiO_2 and Ru-Sn/TiO_2 in a flow type reactor

Chapter 5
Stability of Ni-Sn/TiO_2 and Ru-Sn/TiO_2 catalysts in hydrogenation of aqueous acetic acid into ethanol

Chapter 6
Concluding remarks

List of figures

List of tables

Chapter 1

Introduction

1.1 World energy shortage and environment issues

In the past 300 years, human society started to use fossil fuels after the industrial revolution (British Petroleum (BP), 2020). The development of human lives and society are inseparable from the use of fossil energy. In 2019, fossil energy accounts for 84% of total world energy consumption, of which oil 33%, natural gas 24%, and coal 27% (British Petroleum (BP), 2020). According to the IEA's annual forecast, global energy demand will continue to grow and without continuous improvement in energy efficiency as global growth and poverty reduction, would require twice as much energy as it does today (International Energy Agency (IEA), 2019). In fact, the estimated years of extraction remaining for coal, natural gas, and cured oil are 132, 50, and 49.8years, respectively, in 2019 (British Petroleum (BP), 2020). However, fossil resources are derived from fossils of animals and plants in the ancient geological age, their reserves are limited and exhaustible. Therefore, it is clear that the reliance on fossil fuels is unsustainable and the remaining reserves of fossil fuels will not be able to support the development of human society for long.

On the other hand, along with the large amounts of fossil fuel consumption many environmental issues were caused, such as air pollution, climate change destroyed the species-rich wild forests, acid rain, and ozone layer depletion. Among these, the most serious problem is global warming, which is increasing the earth’s average surface temperature, due to greenhouse gases released by the burning of fossil fuels. It also causes other relating more environmental problems such as the rise of the sea level, increasing rate of snow and ice melting, extreme weather, and so on. The world average temperature has risen by 0.85°C over the last 100 years, and about two-thirds of this increase has occurred since 1975 (International Energy Agency (IEA), 2013). In

addition, it is predicted that until the end of the 21st century, the increase of global mean surface temperature relative to 1986–2005 is likely to be 0.3°C to 4.8°C based on the representative concentration pathways (Intergovernmental Panel on Climate Change (IPCC), 2014). The Earth's sea level has risen by 21 cm (8 inches) since 1880 (Church and White, 2011). Perennial ice cover in the Arctic is melting at the rate of 11.5% per decade and the thickness of the Arctic ice has decreased by 48% since 1960 (Comiso and Hall, 2014).

If these environmental issues continue to proceed, the impact of global warming on the earth's ecological environment is devastating. Therefore, it is necessary to address to the emission problem of carbon dioxide and reduce dependence on fossil energy, promptly.

1.2 Biomass energy

Biomass is organic material produced from water and atmospheric carbon dioxide by photosynthesis using sunlight energy, and this includes wood, crops, agricultural waste, animal feces, and industrial waste (S. Saka, 2001). Production or fuel from biomass is sustainable and its does not increase the net atmospheric carbon dioxide through regeneration of plants. Furthermore, use of biomass use can lead to net carbon dioxide emission reductions when used in place of fossil fuels. This makes the biomass gain attention as a carbon natural energy resource. Since, biomass can be continuously produced as long as the sun exits. Moreover, unlike fossil fuel resources, biomass does not disturb the carbon balance in earth ecosystem. Therefore, biomass energy has played an important role in developing the sustainable energy, and some international agency claim the demands of biomass for future world energy supply. In 2015, energy produced from renewable resources accounted for 12.2 % of TPES worldwide. In detail, the proportions of energy produced from biomass and hydropower were 9.7 % and 2.5 %, respectively, with the remaining 1.5 % coming from other

renewable resources such as geothermal power, solar power, wind power, tide/wave/ocean power (Hasan et al., 2017). The united states environmental protection agency's claim in the "rapidly changing world with stabilizing policies (RCWP)" that the commercialized biomass energy will supply for 25.8% and 31.7% of the world primary energy demands in 2025 and 2050, respectively (Lashof, D.A.; Tirpak, 1990).

Utilization of biomass resource include, firewood, charcoal, pellet liquid biofuel such as biodiesel and bioethanol, biogas, and so on (Simmons et al., 2008; Voloshin et al., 2016). Among of these, biodiesel and bioethanol have been paid more attention due to the advantages of the utilization for transportation fuel (Balat et al., 2008; Ma and Hanna, 1999). Especially, bioethanol not only can use as transportation fuel, but also same as ethanol can work as industrial raw material.

1.3 Bioethanol

Bioethanol refers to ethanol for fuel produced from biomass. As an alternative fuel, since bioethanol contains oxygen in the molecule, it exhibits properties different from hydrocarbon fuels. The calorific value per weight is small for bioethanol, but when it burning no soot is produced and NOx and CO emissions can be reduced than gasoline (S. Saka, 2001). And Al-Hasan reported that mixing unleaded gasoline with ethanol can increase braking power, torque, volume and braking thermal efficiency, and fuel consumption, while reducing the unit fuel consumption and equivalent air-fuel ratio of the brake (Al-Hasan, 2003). And it is a liquid, which is advantages in terms of storage. Besides, bioethanol can use as same ethanol as a common solvent for industrial chemical synthesis (Clarke et al., 2018), or as a disinfection material for medical usages, such as 62%–71% ethanol can reduce coronavirus infectivity within 1 minute (Kampf, 2020).

The world production of bioethanol in 2000 was around 17 billion liters, and the amount had increased to approximately 98.6 billion liters in 2016 (Hasan et al., 2017).

Especially, due to the effects of coronavirus, the demand of ethanol and bioethanol is even rising in modern world.

1.3.1 Bioethanol production process

1.3.1.1 Current bioethanol production process

The alcoholic fermentation process is the traditional method for producing bioethanol. Currently, the raw materials for bioethanol are mainly used starch such as corn and molasses such as sugar cane, which is "first generation" bioethanol production technology. Starch resources are composed of amylose and amylopectin. After hydrolyzing starch with amylase, the product glucose is converted to ethanol by alcoholic fermentation. Molasse is composed of glucose, fructose and sucrose, which can be directly fermented by yeast *Saccharomyces cerevisiae* and anaerobic bacterium *Zymomonas mobilis* (Shiro Saka, 2010). However, given the growing demand for human food as well as energy and accompanying the world's increasing population with the priority of starving human society, these raw materials for bioethanol products have a problem causing competition with food demand (Brown, 1980; Johansson and Azar, 2007; Rathmann et al., 2010).

Therefore, the "second generation" bioethanol production method using lignocellulosics such as wood, rice straw and bagasse, which are non-edible biomass resources, have attracted attention. Lignocellulose is the main component of plant cell wall, and it is composed of lignocellulose are cellulose (40–60% of the total dry weight), hemicellulose (20–40%) and lignin (10–25%)(Kang et al., 2014).Crystalline cellulose is the most abundant organic compound on the earth, which accounts for approximately 30-50% of the plant (Chen, 2014). However, lignocellulose contains lignin which consists of an irregular aromatic compound as a main component, that makes wood

very rigid and is difficult to decompose. For this reason, pretreatment is necessary for second generation bioethanol production. Acid and enzymatic hydrolysis with dilute or concentrated sulfuric acid and supercritical water have been applied (S. Saka, 2001). In enzymatic saccharification method, preliminary treatment of delignification is necessary, whereas such pretreatment is unnecessary for acid hydrolysis, and hence research on acid hydrolysis has been actively carried out in recent years. However, because calcium hydroxide ($Ca(OH)_2$) is required for neutralization of sulfuric acid, a large amount of gypsum ($CaSO_4$) is generated. Hence a separation step to remove gypsum is necessary (Bon and Ferrara, 2010). Attention is being paid to the hydrolysis of biomass by supercritical technology. This is a technology that hydrolyzes biomass by increasing the water density and hydrogen ion concentration by utilizing the specificity of ion products and the permittivity of water in the supercritical state(Matsumura et al., 2006; Rabemanolontsoa and Saka, 2016). With this method, it is unnecessary to add neither acid nor enzyme to the process, which is expect as a novel process with a simple post-processing (Saka et al., 2005).

After the saccharification step, lignocellulosics are decomposed into hexose, pentose, oligosaccharides and Uronic acids. However, with the conventional yeasts and bacteria, only hexoses can be used as the substrate for bioethanol production. In addition, the reaction of ethanol fermentation as shown in equation 1.1, one molar hexose is converted into 2 molar ethanol and 2 molar carbon dioxides, which means that 4 of 6 carbon atoms contained in one hexose molecule can be converted to ethanol, while the remaining 2 carbons are discharged as CO_2.

$$C_6H_{12}O_6 \rightarrow 2C_2H_5OH + 2CO_2 \qquad (1.1)$$

1.3.1.2 Advanced bioethanol production process

As discuss above, in the alcoholic fermentation the carbon is wasted as carbon dioxide exhaust which makes the carbon utilization efficiency is low. Hence, our laboratory has proposed a new bioethanol production process by using acetic acid fermentation to improve the carbon utilization efficiency as shown in Fig.1-1. Bioethanol can be produced by hydrogenating acetic acid that is produced by acetic acid fermentation, and the process consists by three steps: hot-compressed water treatment to lignocellulose, acetic acid fermentation and hydrogenation of fermented acetic acid to ethanol (Saka et al., 2019).

There are two advantages for this new acetic acid fermentation process. Firstly, various types of compounds can be utilized as substrates for acetic acid fermentation. Hexoses, pentose and other degradation products can be fermented in the co-culture environment of *Clostridium thermoaceticum* and *Clostridium thermocellum* (*Moorella thermoacetica*)(Eggeman and Verser, 2006). Some of the lignin-derived monomeric products can also be utilized. The second is its inherent carbon utilization efficiency. As shown in equation 1.2, 1 molar of hexose produces 3 molars of acetic acid theoretically. By hydrogenation of acetic acid intermediate, in formula 1.3, 3 molars of ethanol are produced from 1 molar of hexose, but no CO_2 is produced.

Consequently, by using acetic acid fermentation, it is expected to produce ethanol with high carbon utilization efficiency while minimizing CO_2 by reduction.

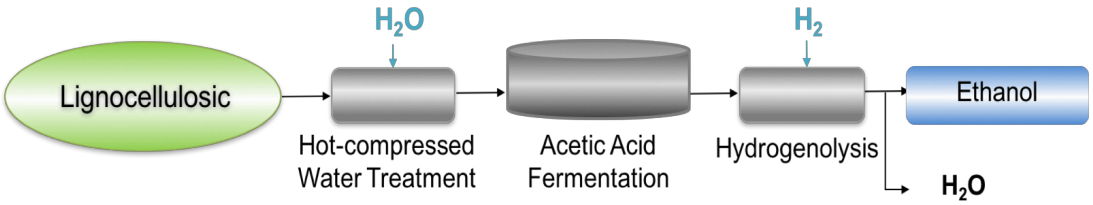

Fig. 1-1 Bioethanol production process from lignocellulosics, consisting of three steps: hot-compressed water treatment, acetic acid fermentation and hydrogenation (Saka et al., 2019).

$$C_6H_{12}O_6 \rightarrow 3CH_3COOH \quad (1.2)$$

$$3CH_3COOH+6H_2 \rightarrow 3C_2H_5OH+3H_2O \quad (1.3)$$

$$C_6H_{12}O_6 +6H_2 \rightarrow 3C_2H_5OH+3H_2O \quad (1.4)$$

1.4 Catalytic hydrogenation of acetic acid to ethanol

1.4.1 Catalyst for two step and one step bioethanol conversion

Hydrogenation of acetic acid have been studied since the first half of 20th century. Through the long times of investigation, Two different pathways have been reported for the hydrogenation of acetic acid: a two-step reaction via ethyl acetate to ethanol, and direct conversion to ethanol (Adkins and Folkers, 1931; Adkins and Wojcik, 1933; Folkers and Adkins, 1932; Rachmady and Vannice, 2000; Voeste and Buchold, 1984). As shown in Fig. 1- 2, acetic acid can be converted to ethanol via ethyl acetate (equation 1.5-1.7), or acetic acid can be directly hydrogenated into ethanol (one step method) (Voeste and Buchold, 1984).

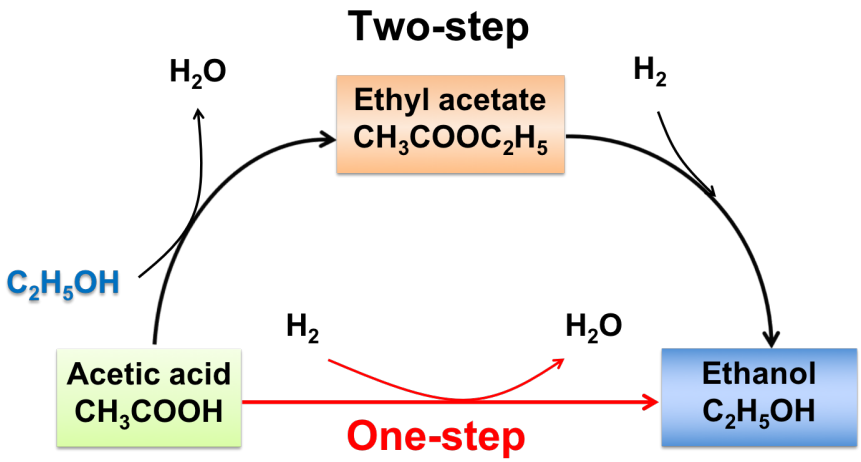

Fig. 1-2 Bioethanol production by hydrogenolysis of acetic acid.

$$CH_3COOH + C_2H_5OH \rightarrow CH_3COOC_2H_5 + H_2O \quad (1.5)$$

$$CH_3COOC_2H_5 + 2H_2 \rightarrow 2C_2H_5OH \quad (1.6)$$

$$CH_3COOH + 2H_2 \rightarrow C_2H_5OH + H_2O \quad (1.7)$$

Two-step method is a well-established way via acetate particularly by the use of Cu-Zn catalyst (Phaiboonsilpa et al., 2020). It was reported that a high yield of 98.7 mol% of ethanol was achieved under the conditions of 250 °C/ 2.0 MPa, molar ratio H_2/EtOAc=80/1 (Phaiboonsilpa et al., 2020). However, since esterification of acetic acid is an equilibrium reaction with proceeding of the reverse reaction by water, it is necessary to remove the water which is formed during the reaction for completing of the esterification reaction. From the viewpoint of efficiency, one step method would be more beneficial.

Investigation of direct hydrogenation of acetic acid have been conducted under gas or aqueous phase with a flow or a batch type reaction system. Rachmady et al. reported that with supported platinum catalysts 8% ethanol can be converted under vapor environments, and Zhang et al. found 97% ethanol converted from acetic acid on steam with Pt-Sn/CNT catalysts (Rachmady and Vannice, 2000; Zhang et al., 2013).

However, gas phase reaction is necessary to gasify the aqueous acetic acid, and it was reported that the gas-phase hydrogenation proceeds more efficiently than aqueous phase (Olcay et al., 2014). Considering the energy efficiency, the aqueous phase hydrogenation is more advantageous for hydrogenation of acetic acid.

Hydrogenation of aqueous acetic acid in a flow type reaction system is reported by Olcay et al. and the results are summarized in Table 1.1-1.3. At here, the notation of the catalyst is defined as "catalytic metal/supporting carrier". The conversion rate, selectivity, and yield are defined by the formula of 1.8-1.10. In these researches, the catalytic activity of seven transition metals were investigated which include Ru-ruthenium, Pd-palladium, Ni-nickel, Cu-copper, Ir-iridium, Pt-platinum. Ru was reported to show the highest activity (Olcay et al., 2010). Selectivity of ethanol formation was reported to increase when hydrogen pressure becomes higher (Olcay et al., 2014). In hydrogenation of aqueous acetic acid in a batch type reaction system, Chen et al. repoted that Ru/C catalyst can convert 16.6 mol%of ethaol under 6.4 MPa at 150 °C (Chen et al., 2011); Eilliott et al. reported that Ru/C catalyst had greater catalyst activity than Pt/C, but the main products become ethane and carbon dioxide (Elliott and Hart, 2009). Wan et al. reported that Ru/C showed the highest conversion rate and ethanol selectivity than Ru/ Al_2O_3, Pt/C ,Pt/Al_2O_3, Pd/C and Pd/Al_2O_3 at a low temperature of 150 °C (Wan et al., 2013).

Table 1-1 The results of hydrogenation of aqueous acetic acid in a flow type reaction system (Olcay et al., 2010).

Catalyst	Temperature (℃)	Acetic acid Conversion rate (mol%)	Ethanol Selectivity (mol%)	Ethanol Yield (mol%)
5%Ru/C	150	12.3	80.2	9.8
5%Ru/C	175	16.6	74.0	12.3
5%Rh/C	260	15.2	3.7	0.6
5%Pt/C	260	45.1	27.9	12.6
5%Pd/C	260	4.8	9.8	0.5
5%Ir/Al_2O_3	260	7.5	68.1	5.1
Raney Ni (93.9% Ni)	260	87.8	32.1	28.2
Raney Cu (98.9% Cu)	260	5.9	75.6	4.5

(10g/L Acetic acid, 5.17MPa）

Table 1-2 The results of hydrogenation of aqueous acetic acid in a flow type reaction system (Wang et al., 2014).

Catalyst	Temperature (℃)	Acetic acid Conversion rate (mol%)	Ethanol Selectivity (mol%)	Ethanol Yield (mol%)
4%Ir-MoO_x/SiO_2 (Mo/Ir=0.13)	100	75.9	62.2	47.2

(10 g/L acetic acid, 6 MPa）

Table 1-3 The results of hydrogenation of aqueous acetic acid in a flow type reaction system (Chen et al., 2011).

Catalyst	Temperature (℃)	Acetic acid Conversion rate (mol%)	Ethanol Selectivity (mol%)	Ethanol Yield (mol%)
1%Ru/C	150	23.3	71.1	16.6
1%Ru/C	180	56.4	25.9	14.6
1%Ru/C	190	76.9	6.9	5.3

(0.83 mol/L acetic acid, 6.4 MPa)

$$Convertion\ rate(\text{mol\%}) = \frac{Acetic\ acid\ consumption(\text{mol})}{Acetic\ acid\ input(mol)} \times 100 \quad (1.8)$$

$$Selectivity\ of\ product\ \boldsymbol{X}(\text{mol\%C}) = \frac{Yield\ of\ product\ X(molC)}{Total\ product\ yield(molC)} \times 100 \quad (1.9)$$

$$Yield\ of\ Product\ Y(\text{mol\%C}) = \frac{Yield\ of\ product\ Y\ (\text{molC})}{Acetic\ acid\ input\ (\text{molC})} \times 100 \quad (1.10)$$

（mol%C：Yield based on carbon）

1.4.2 Lewis acid-supported catalyst for one-step hydrogenation

1.4.2.1 Role of Lewis acid

As shown in Fig.1-3(a) low reactivity of acetic acid for direct hydrogenation to acetic acid originates from less effective polarization of the carbonyl carbon of acetic acid, which decrease the reactivity with the hydrogen anion that is activated on catalyst (Kawamoto et al., 2016). Lewis acid can improve this reactivity by the coordination of the vacant orbital of the Lewis acid to the lone pair of oxygen atoms of acetic acid, effectively which improves the polarizability ($\delta+$) of the carbonyl carbon (Fig. 1-3 (b)) (Kawamoto et al., 2016).

Titanium oxide is a solid Lewis acid that is often utilized as a catalyst support, Fujii of our laboratory evaluated the hydrogenation reactivity of acetic acid over titanium oxide-supported platinum catalyst (Pt/TiO_2) compared with the activated carbon-supported platinum catalyst (Pt/C) investigate the effect of Lewis acid support on the hydrogenation activity of acetic acid in both polar (THF) and non-polar (Hexane) solvents (Kawamoto et al., 2016). The results as shown in Table 1-4. When acetic acid was hydrogenated by 4wt% Pt/TiO_2, both ethanol yield and acetic acid conversion rate are higher than use 3wt%Pt/C. The reaction mechanism has been cleared as shown in Fig.1-4. Titanium oxide acting as a Lewis acid coordinates to the lone pairs of oxygen atoms of acetic acid, which significantly improves the polarization of the carbonyl carbon. Due to the resulting greater δ+ character acetic acid becomes more susceptible to the nucleophilic attack of the hydrogen activated on Pt with the similar mechanism, the formation of ethyl acetate was also catalyzed via the activated acetic acid when hexane and THF were used as solvents.

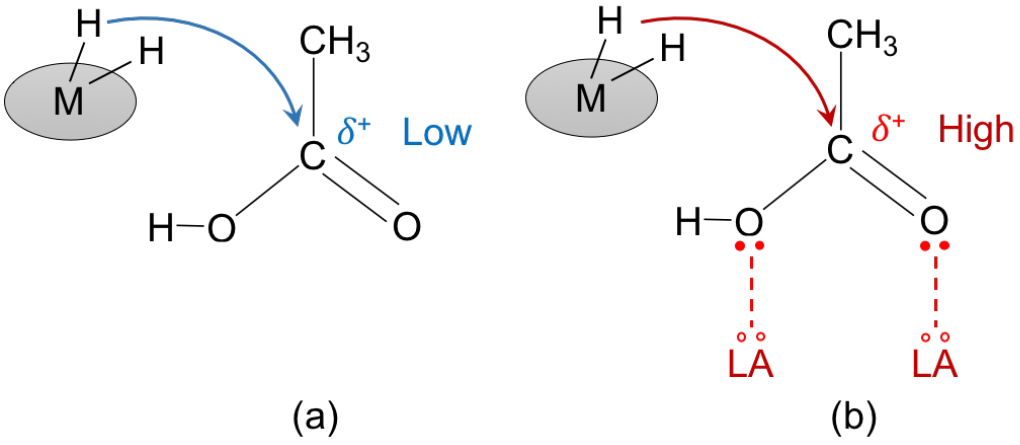

Fig.1-3 Role of the Lewis acid to increasing polarizability (δ+) of the carbonyl carbon of acetic acid for improving catalytic activity(Olcay et al., 2014). M: catalyst metal; LA: Lewis acid; (a) without Lewis acid; (b) with Lewis acid

In addition, according to the table 1-4, by using THF as a solvent, the selectivity of ethanol formation increased and by-production of ethyl acetate are significantly suppressed as compared with the case of using hexane. This result has been explained by the coordination of the oxygen atom of THF to the Lewis acid site of TiO_2. Meanwhile, the coordination of THF inhibits the ethanol access to acetic acid activated on the catalyst, and the selectivity of ethanol formation enhanced because of the suppression of the by-production of ethyl acetate (Kawamoto et al., 2016).

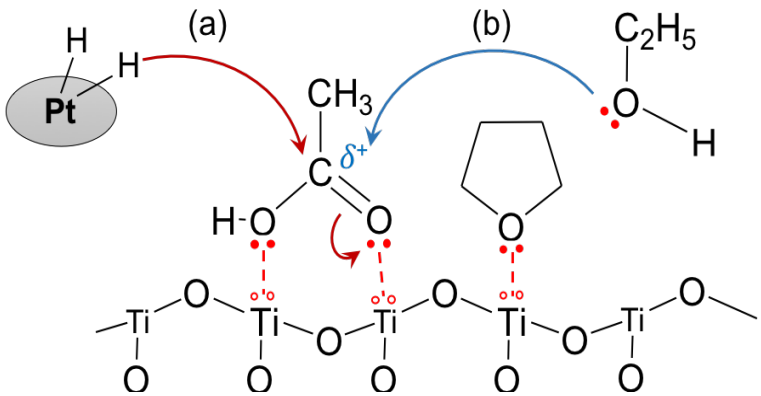

Fig. 1-4 Influence of Lewis acid support on catalytic activity of Pt/TiO_2 catalyst for hydrogenation to ethanol (a) esterification to ethyl acetate (b) with the role of solvent THF.

Table 1-4 Influence of solvent conditions on hydrogenation of acetic acid by 4wt%Pt/ TiO_2 and 3wt%Pt/C (Kawamoto et al., 2016).

Ex No	Catalyst	Catalyst (wt%)	Solvent	AcOH (g/L)	Temperature (°C)	H_2 (MPa)	Yield (mol%)		
							AcOH	EtOH	EtOAc
1	3wt%Pt/C	1	Hexane	10	130	6.0	99.1	0.2	0.7
2			H_2O		200	15.0	86.6	8.4	0
3	4wt%Pt/ TiO_2	1	Hexane	10	130	2.0	18.9	22.1	29.5
4						6.0	1.3	45.2	26.8
5						10.0	0	68.9	15.5
6						15.0	0	85.8	7.1
7			THF	10	130	2.0	79.6	13.3	7.2
8		10	H_2O	100	130	15.0	71.5	23.3	0
10		1	H_2O	10	130	15.0	91.6	2.2	0
					150		70.1	25.5	0
					200		31.2	61.1	0
					225		4.3	67.4	0

(Reaction time: 12 h)

1.4.2.1. Ru-Sn/TiO_2 catalyst

The order of activity of seven transition metals for aqueous acetic acid hydrogenation was reported by Olcay et al. as shown in the formula 1.11 (Olcay et al., 2010). Ruthenium is reported to exhibit highest activity for acetic acid hydrogenation, Ito et al. has loaded ruthenium on TiO_2 support to prepare Ru/TiO_2 for hydrogenation of aqueous acetic acid. They reported that under the conditions of 130 °C/ 15 MPa/ 12 h, 71.3 mol% of ethanol was obtained from 10 g/L aqueous acetic acid. However, some gaseous production such as methane and ethane were produced, which decrease the ethanol yield. By co-loading of tin (Sn) with ruthenium, the gasification was effectively suppressed. Thus the bimetal catalyst 4wt%Ru-4wt%Sn/TiO_2 has been found as an effective catalyst for converting aqueous acetic acid (10 g/L) to ethanol in 98.2 mol% under the conditions of 170 ° C/ 15 MPa/ 12 h, and Sn was worked as a very effective parts for suppressing the acetic acid gasification under such conditions (Ito et al., 2016).

Ru is a precious metal, but inexpensive catalysts are preferable for hydrogenation of aqueous acetic acid. According to Olcay et al. reports order, the price of each metal are summarized in Table 1-5. It was obviously that Ni is a non-precious metal candidate that can be applied to TiO_2-based catalysts instead of Ru. However, Ni/TiO_2 catalyst has not been investigated for catalytic hydrogenation of aqueous acetic acid, which will be investigated in our current paper

$$Ru > Rh \fallingdotseq Pt > Pd \fallingdotseq Ir > Ni > Cu \qquad (1.11)$$

Table 1-5 Metal price (Dec./ 8/ 2020)

Metal	Price (US$/ Kg)
Pt	34166
Rh	540000
Pd	78066
Ir	56166
Cu	8
Ru	9000
Ni	16
Sn	19

("InvestmentMine: http://www.infomine.com/investment/metal-prices/")

1.4.3 Hydrogenation with different type of reactor

Batch type reactor is the simplest reactor system, which usually a tank reactor with a stirrer, the raw materials are added to the reactor at one time until the reaction reaches the specified conversion rate to obtain the reactant. It is easy operation for small amount reaction which makes it often using for catalyst activity, characteristic and reaction kinetics investigation. Many of the catalyst investigation for hydrogenation of acetic acid also used batch type reactor. The reactivity of Ru-Sn/TiO_2 and Pt/TiO_2 for hydrogenation of acetic acid to ethanol were investigated with batch reactor (Ito et al., 2016; Kawamoto et al., 2016). And Lawal et al. reported the kinetics of hydrogenation of acetic acid over Pt/TiO_2 (Lawal et al., 2019).

On the other hand, flow type reactor flow reactor normally keeps a higher efficient of producing production, since the raw materials are continuously fed to the reactor and the products can be collected simultaneously from the outlet of the reactor. Flow reactors are often installed for large scale of a chemical production.

Recently there were some research reported that using a flow reactor for solid-catalyzed reactions has many advantages over batch reactors (Hartman et al., 2011; Hessel, 2009; Hessel et al., 2007; Roberge et al., 2008b, 2008a; Wiles and Watts, 2012). Continuous flow hydrogenation has also been shown to reduce reaction times and improve operational selectivity and safety (Durndell et al., 2015; Gómez-Quero et al., 2011; Numwong et al., 2012; Olcay et al., 2014; Osako et al., 2017; Wang et al., 2018; Yu et al., 2020). Numwong et al. reported that in the flow type reactor, the hydrogenation rate of polyunsaturated fatty acid methyl esters over Pd/C was 4 to 5 times faster in the batch-type reactor (Numwong et al., 2012). Durndell et al. reported that the reactivity and selectivity of C=O activation in hydrogenation of cinnamaldehyde over Pt/SiO_2 are improved (Durndell et al., 2015). Moreover, as discussed before, Olcay. et al. used flow reactor to investigate the hydrogenation reaction of various catalysts including Ru/C for hydrogenation of aqueous acetic acid, and they found that increasing the hydrogen pressure would increase the selectivity of ethanol (Olcay et al., 2014).

1.5 Objectives of this dissertation

Highly efficient of hydrogenation of acetic acid to ethanol is very important for the advance bioethanol production process (Saka et al., 2019). Instead of gas phase acetic acid hydrogenation, the aqueous phase hydrogenation is more advantageous on the energy efficient (Olcay et al., 2014). The transition metals supported on Lewis acid sites catalysts were found able for direct hydrogenation of aqueous acetic acid (Olcay et al., 2010). Ito et al. obtained 98 mol% of ethanol from hydrogenation of 10 g/L aqueous acetic acid over 4wt%Ru-4wt%Sn/TiO_2 catalyst (170 ℃/ 15MPa/ 12h) in batch type reactor (Ito et al., 2016). However, Ru is a precious metal, inexpensive catalysts are always more preferable for hydrogenation of aqueous acetic acid and the advance bioethanol production process. And it was reported that a flow reactor for

solid-catalyzed reactions has many advantages over batch reactors, such as higher conversion or selectivity (Hartman et al., 2011; Hessel, 2009; Hessel et al., 2007; Roberge et al., 2008b, 2008a; Wiles and Watts, 2012). Therefore, the main objectives of this dissertation is investigating highly efficient catalysts for hydrogenation of aqueous acetic acid with both batch and flow type reactor.

Ni as a cheaper metal than Ru and relatively shows activity on hydrogenation of aqueous acetic acid were used to investigate the new catalyst. In chapter 2, various Ni and Ni-Sn catalysts supported on TiO_2 were prepared and the catalytic activities were evaluated and compared with Ru-Sn/TiO_2 for ethanol formation from aqueous acetic acid with batch type reactor. The catalyst characterization was investigated with analytical instruments. The compared with Ru-Sn/TiO_2 in an attempt to provide more catalyst options for the bioethanol production process.

In previous study, Ru-Sn/TiO_2 is known as an effective catalyst for hydrogenation of aqueous acetic acid to ethanol. Hence a similar hydrogenation process was investigated in a flow-type rather than a batch-type reactor. The hydrogenation of aqueous acetic acid activities was investigated under different reaction conditions by passing a fix bed catalyst column which in a commercialized flow type reactor (H-Cube). The influence of type of reactor and side reactions in hydrogenation of aqueous acetic acid were mainly discussed in chapter 3. Moreover, the possibility of this method for hydrogenation of aqueous lactic acid to propane-1,2-diol was lightly reported in this chapter.

The author found Ni-Sn/TiO_2 was an efficient catalyst for hydrogenation of aqueous acetic acid to ethanol for bioethanol production. In chapter 4, Ni-Sn/TiO_2 was evaluated and compared with Ru-Sn/TiO_2 in a flow-type reactor under similar conditions as chapter 3. In this chapter, the ethanol conversion, and the ethanol yield was compared. Effects of water boiling on side reactions in hydrogenation of aqueous acetic acid and was further investigated and compared over both Ni-Sn/TiO_2 and Ru-

Sn/TiO_2 catalysts. the competitive reaction routes with hydrogenation of aqueous acetic acid are discussed in this chapter.

4wt%Ru-4wt%Sn/TiO_2 and 4wt%Ni-4wt%Sn/TiO_2, which were reported as efficient catalyst for hydrogenation of aqueous acetic acid to ethanol for bioethanol production. The durability study of 4wt%Ru-4wt%Sn/TiO_2 and 4wt%Ni-4wt%Sn/TiO_2 catalysts were investigated at by flow type reactor in chapter 5. The catalyst stability on ethanol conversion and the characteristic of recovered catalyst from durability study were investigated in chapter 5.

Finally, the catalyst investigation and the reaction mechanism of hydrogenation of aqueous acetic over both Ni-Sn/TiO_2 and Ru-Sn/TiO_2 were summarized. Prospects for the future studies to fulfill this research were further proposed in chapter 6 as conclusions.

Chapter 2

TiO_2-supported Ni-Sn as an effective hydrogenation catalyst for aqueous acetic acid to ethanol

2.1 Introduction

Fossil fuel shortage has become an urgent problem in the world, especially with regards to oil and natural gas (Pimentel et al., 2008). Biomass resources are used as a substitute for fossil resources in both developed and developing countries, particularly as biofuels (Cleveland et al., 1984; Biello , 2011). Bioethanol receives much attention as one of these biofuel alternatives to gasoline (Osei et al., 2013). Currently, alcohol fermentation predominately uses edible resources, such as sugarcane and starch, as raw materials, causing a risk of increasing food prices (Ajanovic, 2011). In addition, during the alcohol fermentation of hexoses, such as glucose, two carbon atoms are emitted as CO_2, thus decreasing the efficiency of carbon utilization (Rodríguez et al., 2010).

To improve carbon efficiency and avoid food competition, our research group has proposed a highly efficient bioethanol production process via acetic acid fermentation from lignocelluloses, which are non-edible resources (Saka et al., 2019). With acetic acid fermentation, all carbon atoms in glucose can be converted into acetic acid, and thus the carbon efficiency is expected to be improved (Nakamura et al., 2011)(Rabemanolontsoa et al., 2016). This new bioethanol production process includes three steps: hot-compressed water treatment to hydrolyze lignocellulose, acetic acid fermentation of resulting hydrolyzates, and hydrogenation of acetic acid into ethanol. The current research is focused on the last step, hydrogenation of acetic acid.

Two different pathways have been reported for the hydrogenation of acetic acid: a two-step reaction via ethyl acetate to ethanol, and direct conversion to ethanol (Adkins and Folkers, 1931; Adkins and Wojcik, 1933; Folkers and Adkins, 1932; Rachmady and Vannice, 2000; Voeste and Buchold, 1984). The direct hydrogenation from

aqueous acetic acid is desirable for practical use because the two-step reaction via ethyl acetate requires dehydration of acetic acid, which is energetically and economically burdensome (Chien et al., 2004; Lei et al., 2004).

Several papers reported the direct hydrogenation of aqueous acetic acid into ethanol. Elliott and Hart (2009) conducted the catalytic hydrogenation of aqueous acetic acid as a constituent of fast pyrolysis oil over Pd/C and Ru/C under the conditions of 150-300 °C/ H_2 13.8 MPa/ 0.5-4 h, but the reported yields were only less than 35 mol%. Wan et al. (2013) compared the catalytic activity of various catalysts for hydrogenation of aqueous acetic acid under the conditions of 200 or 300°C/ H_2 4.8 MPa/ 1 h. They showed that Ru/C exhibited the higher conversion than Ru/Al_2O_3, Pt/C, Pd/C, Pt/Al_2O_3, Pd/C, and Pd/Al_2O_3, but most of the products were methane and ethane. Wang et al. (2014) reported the aqueous acetic acid hydrogenation over Ir-MoO_x/SiO_2 with a flow-type reactor, but the maximum ethanol yield was less than 40 mol%.

Our research group reported Ru-Sn/TiO_2 as an effective catalyst, which converted aqueous acetic acid into ethanol with a high yield of 98 mol% (Ito et al., 2016). Because the ethanol yield increased with increasing Ru-Sn content up to 8 wt% (based on TiO_2) but rather decreased with higher contents of 14 wt% and 20 wt%, a hydrogenation mechanism was proposed. The carbonyl group of acetic acid is coordinated to Ti, which is a Lewis acid site, at the interface between Ru-Sn and TiO_2, and the activated carbonyl carbon is more susceptible to attack by hydrogen activated on Ru-Sn (Ito et al., 2016; Kawamoto et al., 2016).

Ru is a precious metal, but inexpensive catalysts are preferable for hydrogenation of aqueous acetic acid. Olcay et al. (2010) compared the relative catalytic activities of seven transition metals for the hydrogenation of aqueous acetic acid and reported that the catalytic activities were higher in the following order: Ru>Rh≒Pt>Pd≒Ir>Ni>Cu. According to this order, Ni is a non-precious metal candidate that can be applied to TiO_2-based catalysts instead of Ru. However, Ni/TiO_2 catalyst has not been investigated for catalytic hydrogenation of aqueous acetic acid.

Therefore, this research investigated various Ni- and Ni-Sn catalysts supported on TiO_2 for bioethanol production. The properties compared to the previous catalyst, Ru-Sn/TiO_2, were also described.

2.2 Experimental

Titanium isopropoxide (>95% purity), nickel(II) chloride hexahydrate ($NiCl_2 \cdot 6H_2O$, >98%), tin(II) chloride dihydrate ($SnCl_2 \cdot 2H_2O$, >97%), sodium hydroxide (NaOH, >97%), 2-propanol (>99%) and hydrochloric acid (HCl, 6 mol/L) were used for the catalyst preparation steps. All of the reagents were purchased from Nacalai Tesque, Inc., Kyoto, Japan.

2.2.1 Catalyst preparation

For catalyst preparation, our preliminary study revealed that the sol-gel sedimentation method could achieve a high dispersion of Ni and better catalytic activity than the sol-gel method. To prepare Ni/TiO_2 and Ni-Sn/TiO_2 catalysts with the sol-gel method, designated amounts of $NiCl_2 \cdot 6H_2O$, $SnCl_2 \cdot 2H_2O$, or both were added to water (100 mL, 60 °C) as Ni and Sn precursors, respectively. Using a magnetic stirrer, a mixture of IPA (20.0 mL) and TTIP (37.2 mL) was added dropwise before waiting for 0.5 h to produce precipitates of TiO_2 by hydrolysis of TTIP. The obtained solution was evaporated and dried with a rotary evaporator, then the precipitates were dried in an oven at 105 °C for 12 h.

The oven-dried precipitates were placed in a quartz combustion boat in a glass tube and calcined at 450 °C for 1 h under an airflow, and then reduced under an H_2 flow (100 mL/min) at 400 °C for 5 h. The Ni/TiO_2 and Ni-Sn/TiO_2 catalysts were thus obtained. Therefore, Ni/TiO_2 and Ni-Sn/TiO_2 catalysts were prepared by the sol-gel sedimentation method.

Designated amounts of $NiCl_2 \cdot 6H_2O$, $SnCl_2 \cdot 2H_2O$, or both were added to water (100 mL, 60 °C) as Ni and Sn precursors, respectively. Using a magnetic stirrer, a mixture of 2-propanol (20.0 mL) and titanium isopropoxide (37.2 mL) was added dropwise. After waiting for 0.5 h, precipitates of TiO_2 were produced by hydrolysis of titanium isopropoxide. Then, aqueous NaOH solution (100 mL, with sufficient concentration for neutralizing metal chlorides) was added and stirred for 0.5 h. During this period, $NiCl_2$ and $SnCl_2$ were converted to $Ni(OH)_2$ and $Sn(OH)_2$, respectively. The reaction mixture was allowed to stand for 12 h. Because $Ni(OH)_2$ and $Sn(OH)_2$ have low solubility to water, they were deposited on the TiO_2 surface to form composites. The obtained precipitates were washed with water five times and then oven-dried at 105 °C for 12 h.

The oven-dried precipitates were placed in a quartz combustion boat in a glass tube and calcined at 450 °C for 1 h under an airflow, and then reduced under an H_2 flow (100 mL/min) at 400 °C for 5 h. The Ni/TiO_2 and $Ni\text{-}Sn/TiO_2$ catalysts were thus obtained.

2.2.2 Catalyst characterization

The obtained catalysts were analyzed by X-ray diffraction (XRD; RINT 2000V, Rigaku Corp., Tokyo, Japan), and the XRD patterns were identified by comparison to a database (AtomWork, National Institute for Materials Science, Ibaraki, Japan). The catalyst surface, dispersion of metals, and particle size were observed by scanning electron microscope (SEM; SU6600, Hitachi High-Technologies Corp., Tokyo, Japan) with an energy dispersive X-ray spectroscope (EDS; XFlash 5010, Bruker Corp., MA, USA), and field emission transmission electron microscope (FE-TEM; JEM-2100F, JEOL Ltd., Tokyo, Japan) with EDS (JED-2300T, JEOL Ltd.). The states of metals on catalyst surface were determined by X-ray photoelectron spectroscopy (XPS; JPS-9030, JEOL Ltd., Tokyo, Japan).

The reducibility of non-reduced Ni, Sn, Ni-Sn, and Ni-Sn/TiO_2 samples were investigated by temperature-programmed reduction (TPR; AutoChemII 2920, Micromeritics Corp., GA, USA). The sample was pretreated at 200 °C for 0.3 h under He (50 mL/min) atmosphere. The reduction was carried out from 80 to 1000 °C (10 °C/min) under 5 vol% H_2 in Ar with a flow rate of 50 mL/min.

Lewis acid points of the catalysts were determined with infrared spectroscopy (IR; IRTracer-100, Shimazu Corp., Kyoto, Japan) by using pyridine as a probe molecule (Kikuchi, 2013). Each catalyst sample was filled in a cup of a diffuse reflectance measuring device, and heated to 120 °C under vacuum pressure as a pretreatment, and then gradually cooled to 40 °C to measure the background. After that, pyridine in a 30-mL glass container was introduced, and the IR spectrum was measured.

2.2.3 Hydrogenation of aqueous acetic acid to ethanol

Hydrogenation was conducted in a 100-mL batch-type reactor made of Hastelloy C-278 (Model 4560, Parr Instrument Company, IL, USA). The prepared Ni/TiO_2 or Ni-Sn/TiO_2 catalyst (1.20 g) was placed in the reactor with water (20 mL), and activated with stirring at 120 °C under 2 MPa of H_2 (99.9%, Imamura Sanso KK., Otsu, Japan) for 1 h. After cooling and opening the reactor, acetic acid and water were added, adjusting the amount and concentration of aqueous acetic acid solution to be 30 mL and 10 g/L, respectively.

After sealing the reactor again, the inside of the reactor was purged and pressurized to approximately 5.4–6.6 MPa with H_2. This pressure range of H_2 provides sufficient excess and approximately 30–37 times of the required amount for hydrogenation; 1 mole of acetic acid requires 2 moles of H_2. Hydrogenation of the aqueous acetic acid was then performed with stirring at the temperature between 170–280 °C for 3–12 h. When the temperature of the reactor was increased, the inside pressure increased. Therefore, the initial H_2 pressure mentioned above was adjusted to

let the pressure be about 10 MPa during the reaction.

After hydrogenation, the reactor was cooled and the reaction mixture was collected. The products in the reaction mixture were analyzed by high-performance liquid chromatography (HPLC; LC20 system, Shimadzu Corp., Kyoto, Japan) under the following conditions: column, Aminex HPX-87H (300 × 7.8 mm, Bio-Rad Laboratories, Inc., CA, USA); eluent, 5 mM sulfuric acid in water; flow-rate, 0.6 mL/min; column temperature, 45 °C; detector, refractive index detector (RID-20A, Shimadzu Corp.).

2.3 Results and discussion

2.3.1 Influence of preparation method on catalyst activity

The catalytic activity of 4wt%Ni/TiO_2 and 4wt%Ni-4wt%Sn/TiO_2 catalysts prepared by the sol-gel method (A) and sol-gel sedimentation method (B) were investigated for hydrogenation of aqueous acetic acid (10g/L), and the results are shown in Table 2-1. The 4wt%Ni-4wt%Sn/TiO_2 catalyst prepared by method B achieved a higher ethanol yield (87 mol%) than that by method A even under lower H_2 pressure. This indicates that method B can synthesize the Ni-Sn/TiO_2 catalyst in high activity. Therefore, method B was mainly used for further investigation.

In the case of method A, the ethanol yield increased obviously from 1 mol% to 21 mol% at 170 °C and 10 MPa when Sn was loaded. The ethanol yield increased further to 27 mol% as the temperature and pressure were raised to 220 °C and 15 MPa, respectively. These results indicate that the addition of Sn can increase the reactivity of acetic acid hydrogenation, and high temperature and pressure could lead to improved reactivity.

Table 2-1. Effect of preparation method and tin addition on catalyst activity.

Catalyst	Preparation method	Temperature (˚C)	Pressure （MPa）	Yield （mol%）	
				Acetic acid	Ethanol
4wt%Ni/TiO_2	A	170	10	92	1
4wt%Ni-4wt%Sn/TiO_2		170	10	86	22
4wt%Ni-4wt%Sn/TiO_2		220	15	66	27
4wt%Ni/TiO_2	B	220	10	91	5
4wt%Ni-4wt%Sn/TiO_2		220	10	4	87

(10 g/L acetic acid, 12 h)

2.3.2 Influence of Sn loading on the catalytic activity of Ni/TiO_2

The catalytic activity of 4wt%Ni/TiO_2 (metal basis on TiO_2) was investigated under the conditions of 220 °C/10 MPa, but the ethanol yield was only 5 mol% (Table 2-1). However, when the 4wt%Ni-4wt%Sn/TiO_2 catalyst was used, the ethanol yield increased significantly to 87 mol% under the same reaction conditions (Table 2-1). These results indicate that adding Sn promoted the catalytic activity of Ni/TiO_2 for hydrogenation of aqueous acetic acid.

The influence of Sn addition was fairly different from that observed for 4wt%Ru/TiO_2 (Ito et al., 2016). The Ru catalyst itself had a quite high catalytic activity for hydrogenation of aqueous acetic acid into ethanol, but the ethanol yield was limited due to the gas formation as a side reaction. The addition of Sn to Ru was dramatically suppressed the gas formation, improving the selectivity of ethanol production. In contrast, 4wt%Ni/TiO_2 exhibited almost no catalytic activity, and the addition of Sn was necessary for the conversion of aqueous acetic acid.

To determine the optimum Sn content, the Sn content was varied from 0 to 16 wt% with a fixed Ni content of 4 wt%. The catalytic activities of the prepared catalysts

were investigated under the conditions of 200 °C/10 MPa for 12 h, and the results are shown in Fig. 2-1. When the Sn content increased to 2 wt% and 4 wt%, the ethanol yield was sharply improved to 51.8 mol% and 92.5 mol%, respectively. However, as the Sn content further increased to 6 wt% and 8 wt%, the ethanol yield decreased. When the Sn content reached 16 wt%, the ethanol yield drastically decreased to 9.2 mol%. Further, while increasing the Sn content from 2 wt% to 16 wt%, the color of the catalyst (as-prepared) changed from black to yellow. The reason for this color change is discussed in subsection 3.3. These results indicate that approximately equal weights of Ni and Sn are optimal for the synthesis of highly efficient catalysts for hydrogenation of acetic acid.

As for the selectivity of hydrogenation, although the ethanol yield varied with the Sn content, the total yield of ethanol and acetic acid was almost 100 mol%. Therefore, the selectivity of Ni-Sn/TiO_2 for hydrogenation was found to be high, and there was no undesirable side reaction, such as gasification, under the given reaction conditions.

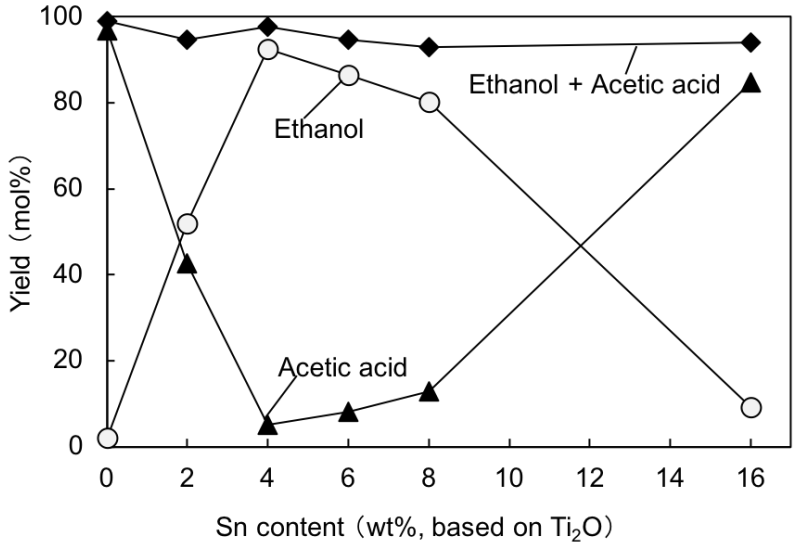

Fig. 2-1The effect of Sn content on ethanol yield by hydrogenation of aqueous acetic acid (10 g/L) with 4wt%Ni-Xwt%Sn/TiO_2, (200 °C / 12 h/ H_2/10 MPa).

2.3.3 Characterization of Ni-Sn/TiO_2 catalyst by SEM and TEM

SEM images of a fresh 4wt%Ni-4wt%Sn/TiO_2 catalyst are shown in Fig. 2-2 along with a line mapping of elements by EDS. In the SEM images, lumps of the catalyst of several hundred micrometers were observed, but the detailed structures could not be observed even when the scale was enlarged. In the line mapping curves, which represent the amount of each element, no apparent change was observed for Ni and Sn, indicating that the Ni-Sn alloys were evenly dispersed on TiO_2 at the nanoscale. The formation of Ni_3Sn_2 on the catalyst surface was confirmed by XRD analysis, as described later, which reasonably explains the SEM-EDS results.

The fresh 4wt%Ni-4wt%Sn/TiO_2 catalyst was observed by FE-TEM to understand the details of alloy dispersion, and the results are shown in Fig. 2-3. The average sizes of the Ni-Sn alloy and TiO_2 particles were determined to be 13±3 nm and 9±4 nm, respectively. The reason the size of Ni-Sn alloy was larger than that of the TiO_2 support might be because the Ni-Sn alloys were loaded across several TiO_2 particles.

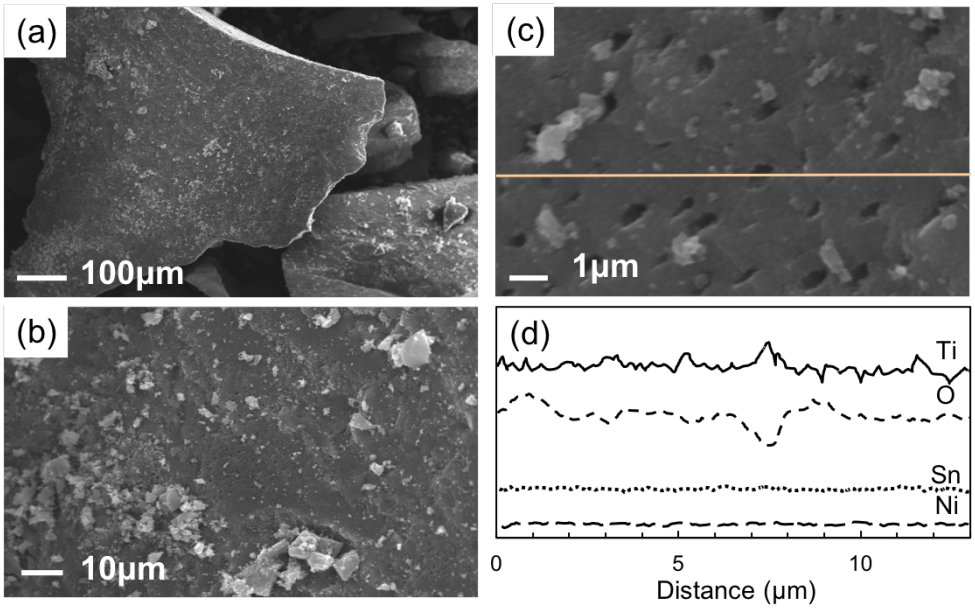

Fig. 2-2 SEM images of 4wt%Ni-4wt%Sn/TiO_2 at various scales (a-c) and a line mapping of elements on (c), as shown in (d).

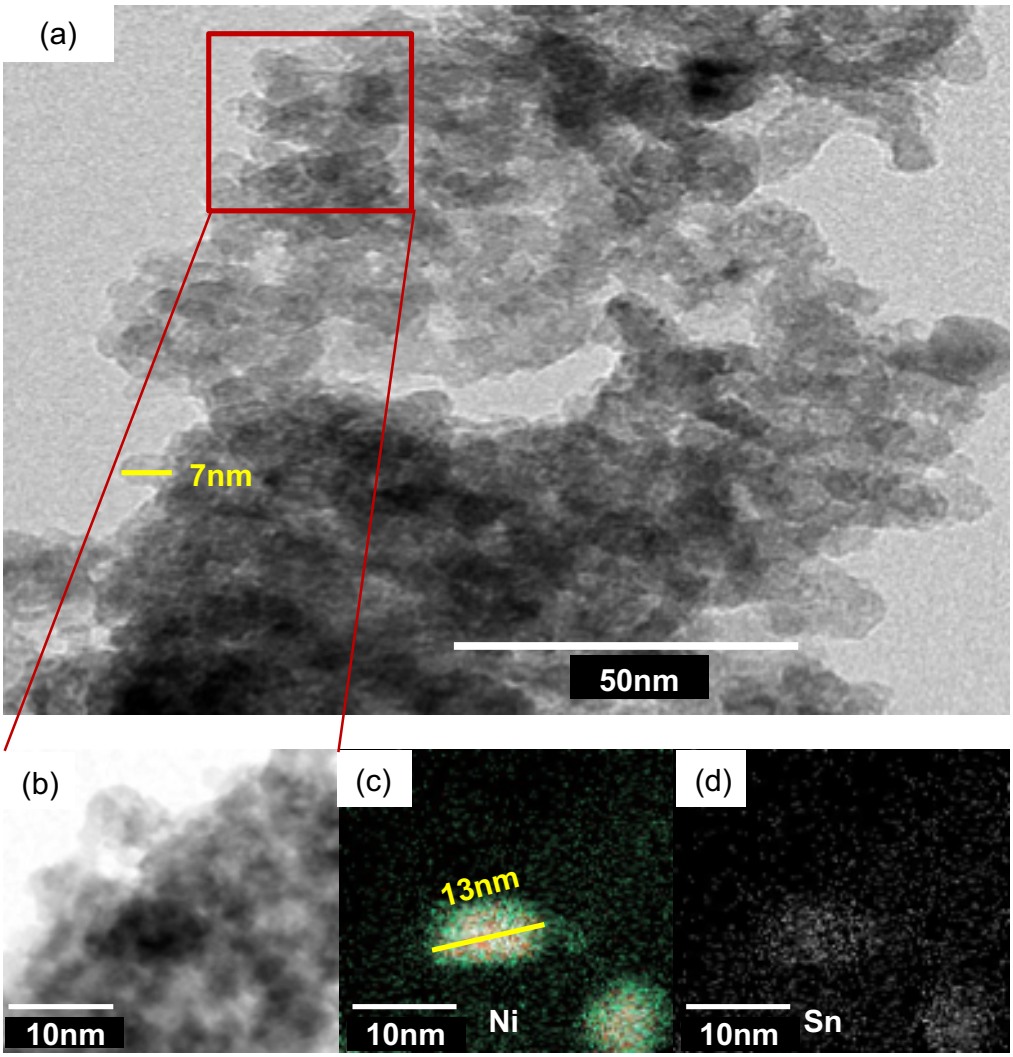

Fig. 2-3 Alloy dispersion on 4wt%Ni-4wt%Sn/TiO_2; (a) FE-TEM image, (b) enlarged FE-TEM image with (c) Ni and (d) Sn mappings.

2.3.4 Optimum ratio of Ni and Sn

To discuss the reason why the optimal ratio of Ni and Sn existed, the behavior of Ni and Sn during the reduction treatment was investigated. Because Ni and Sn are the minor components of the Ni-Sn/TiO_2 catalyst, only small XRD and TPR signals were obtained. Accordingly, only Ni and Sn precursors were utilized for this study. The same sol-gel sedimentation method in subsection 2.2 was conducted by using $NiCl_2$, $SnCl_2$, or both without dropping the titanium isopropoxide solution. The calcination and

reduction were then carried out in the same manner at 450 °C in air for 1 h to produce metal oxides and at 400 °C in H_2 for 5 h to form metals, respectively. The prepared samples were analyzed by XRD, as shown in Fig. 2-4. The TPR analysis was performed for the samples before the reduction treatment and the results are shown in Fig. 2-5.

In the XRD results, after reducing only NiO, Ni metal was detected even though the peaks of NiO remained to some extent. In the case of only SnO_2, only the peaks of SnO_2 were found even after the reduction by H_2 at 400 °C. Therefore, NiO can be easily reduced to metal, but SnO_2 is difficult to be reduced alone under the given conditions. However, when the SnO_2 was reduced in the presence of NiO, the peaks of Ni_3Sn_2 alloy appeared; similar results are reported in the literature (Rodiansono et al., 2012).

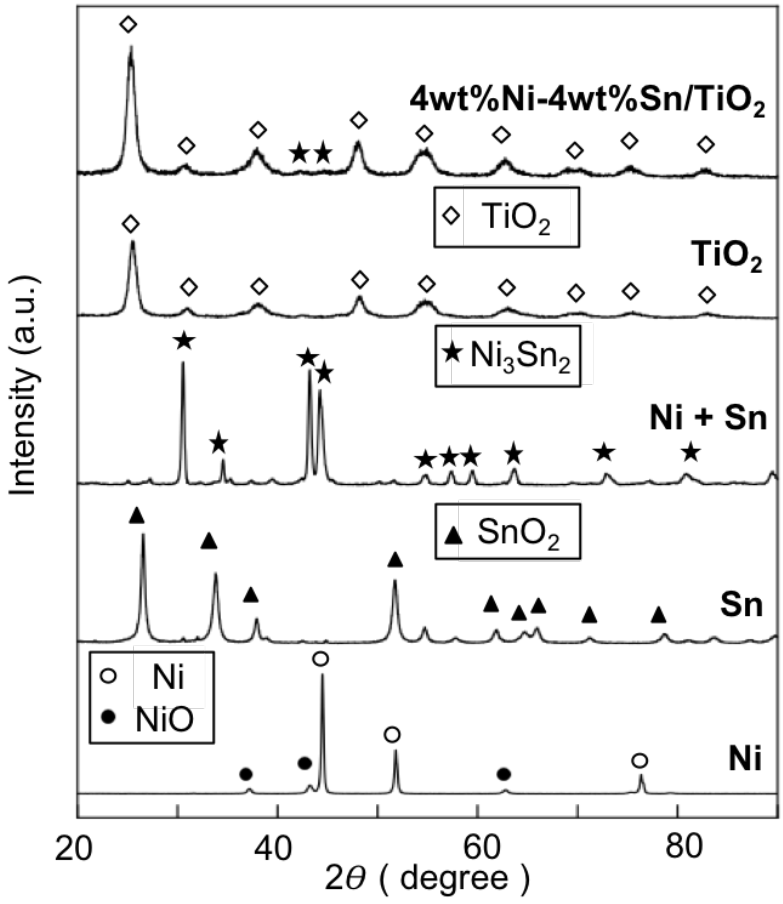

Fig. 2-4 Results of the reduction treatment with H_2 at 400 °C for NiO, SnO_2, or both (Ni:Sn = 1:1, w/w) analyzed by XRD.

In the TPR profiles in Fig. 2-5, the reduction of NiO occurred at around 300 to 430 °C, whereas the SnO_2 required higher temperatures of around 600 to 750 °C for the reduction to Sn-metal. Similar results have been reported by others (Hengne et al., 2018; Shen et al., 2019). The reduction of the mixture of Ni and SnO_2 started at around 300 °C, like NiO only, but new peaks appeared at around 430 to 500 °C. The Sn reduction seems to conclude at around 650 °C, which is lower than in the case of SnO_2 only. These new peaks and earlier reduction of SnO_2 indicate Ni-Sn alloy formation. Wang et al. (2016) and Liu et al. (2019) have reported similar behavior in TPR profiles of Ni-Sn/SiO_2. The TPR profile of 4wt%Ni- 4wt%Sn/TiO_2 also showed similar reducibility as the mixture of NiO and SnO_2.

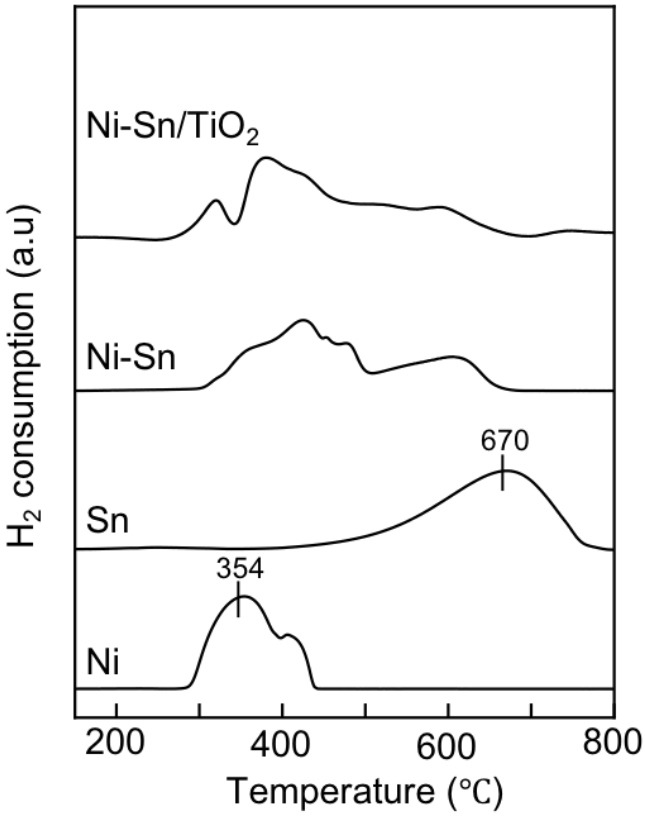

Fig. 2-5 TPR profiles of NiO, SnO_2, mixture of both (Ni:Sn = 1:1, w/w) and non reduced 4wt%Ni-4wt%Sn/TiO_2.

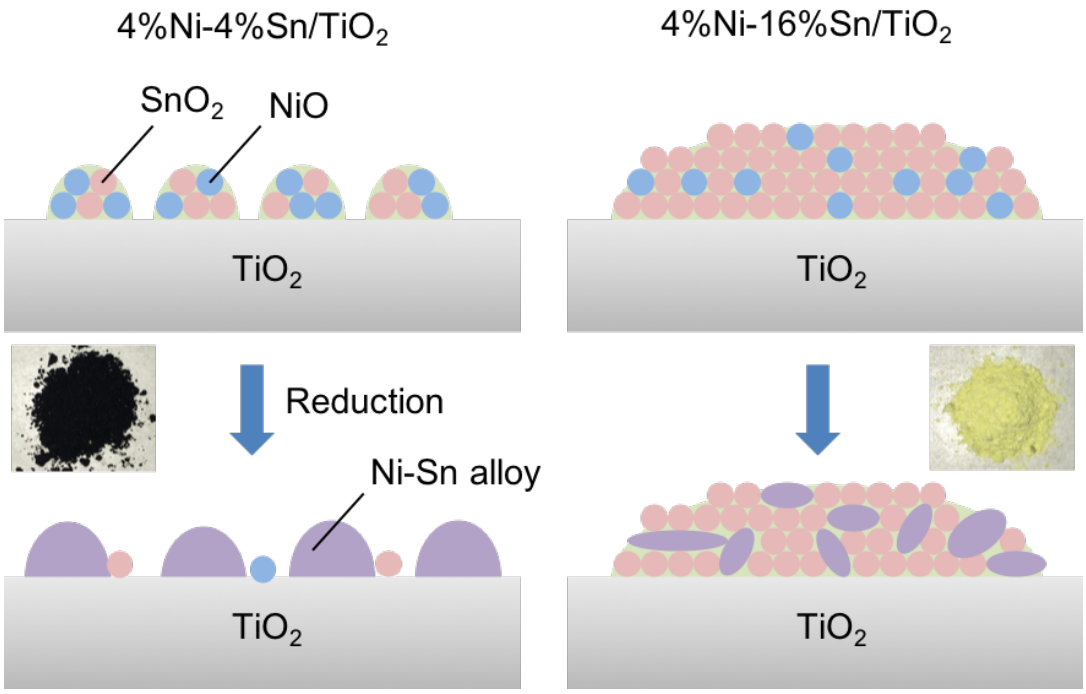

Fig. 2-6 The effect of Ni/Sn ratios on the alloy formation.

These results suggest that in the metal formation of the Ni-Sn/TiO_2 catalyst, Ni is first reduced by H_2, and then the metal Ni reduces adjacent SnO_2 to form the Ni_3Sn_2 alloy. Based on this assumption, the effect of the Ni/Sn ratio on the alloy formation process can be proposed as in Fig. 2-6. When there is an optimal Ni/Sn ratio (left figure), most of SnO_2 can be reduced to Ni-Sn alloy and it is evenly dispersed on the TiO_2 surface. However, if Sn is added excessively (right figure), only a part of SnO_2 is reduced to Ni-Sn alloy and most of the alloy is buried in the remaining SnO_2. Via this mechanism, we can also explain why the color of the catalyst changed from black to yellow when the Sn content was increased. As explained in Fig. 1, the catalytic activity was the highest for the Ni:Sn ratio of 1:1 (w/w). Because the atomic weights of Ni and Sn are 58.7 and 118.7, respectively, the weight ratio of Ni:Sn = 1:1 corresponds approximately to a molar ratio of Ni:Sn = 2:1, which is roughly similar to the stoichiometric ratio of Ni_3Sn_2 alloy. This might be the reason why the catalytic activity of the Ni-Sn/TiO_2 catalyst was high when the amounts of Ni and Sn were 4 wt% each.

2.3.5 Influence of reaction temperature and metal content

The aqueous acetic acid solution could be effectively converted to ethanol by using the 4wt%Ni-4wt%Sn/TiO_2 catalyst. To optimize the reaction temperature, the hydrogenation activity was evaluated in the temperature range of 180 to 280 °C at 10 MPa for 12 h, and the results are shown in Fig. 2-7. Ethanol reached a maximum yield of 92.5 mol% at 200 °C, and the yield tended to decrease gradually when the reaction temperature was further raised. At temperatures higher than 200 °C, the total yield of ethanol and acetic acid decreased, thus indicating that side reactions, such as gasification, proceeded. However, in the case of Ru-Sn/TiO_2 catalyst (Ito et al., 2016), gasification proceeds even at around 170 °C, so the Ni-Sn/TiO_2 catalyst is considered to have higher resistance against side reactions. Based on these results, 200 °C is the optimum temperature for hydrogenation of acetic acid with the Ni-Sn/TiO_2 catalyst. At 200 °C, the ethanol yield increased from 49 mol% to 71mol% and 93 mol% by prolonging the reaction time from 3 h to 6 h and 12 h, respectively.

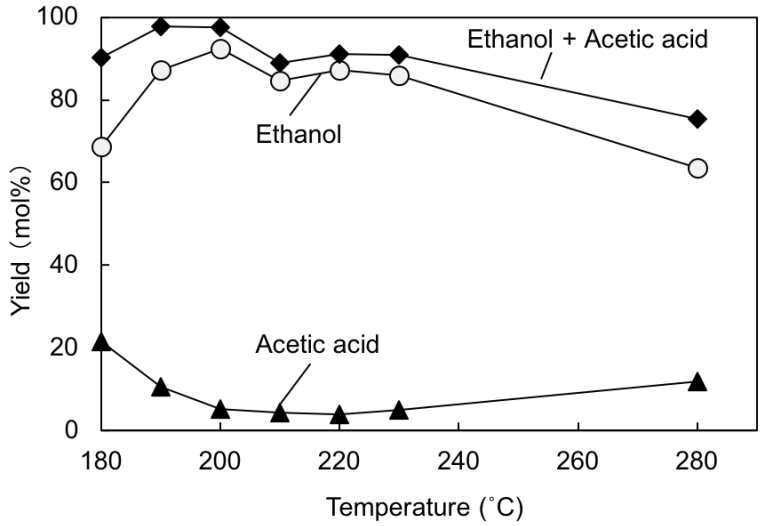

Fig. 2-7 Influence of temperature on hydrogenation activity of 4wt%Ni-4wt%Sn/TiO_2, reaction time (12 h).

For further improved catalytic activity, the content of Ni and Sn to TiO_2 was increased up to 24 wt% each with a constant Ni:Sn ratio of 1:1 (w/w) and hydrogenation activities were investigated under 10 MPa at 200 °C for 3 h, as shown in Fig. 2-8. The ethanol yield was improved from approximately 50 mol% to 85 mol% when the metal contents of Ni and Sn were increased from 4 wt% to 16 wt%. However, when the metal content was further increased to 24 wt%, the ethanol yield was reduced to 57 mol%. These results indicate that there is an appropriate value for the amount of catalyst metal and that an excessive amount leads to a decrease in catalyst activity. The balance of Ni-Sn and TiO_2 may be important because increasing the amount of Ni-Sn alloy improves hydrogen activation but reduces Lewis acid sites by covering the TiO_2 surface. In this research, the 16wt%Ni-16wt%Sn/TiO_2 catalyst showed the highest catalytic activity of the systems studied.

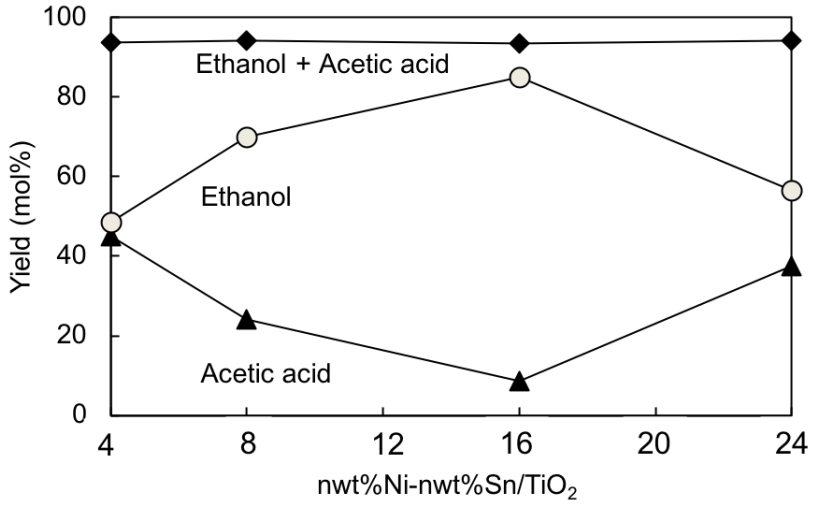

Fig. 2-8 The effect of metal loading amount on activity of aqueous acetic acid hydrogenation. (10 g/L AcOH, 10 MPa/ 3 h/ 200 °C)

2.3.6 Catalytic mechanism and comparison with Ru-Sn/TiO_2

IR analysis is useful for evaluating the acidic properties of a solid surface using pyridine as a probe molecule (Kikuchi, 2013). The acidic property of the 4wt%Ni-4wt%Sn/TiO_2 catalyst was investigated by the IR method and compared with those of TiO_2, SnO_2 and Ni_3Sn_2, and the results are shown in Fig. 2-9. The Lewis acid sites were detected at around 1440 cm^{-1} in TiO_2 and 4wt%Ni-4wt%Sn/TiO_2 catalyst, but there was no absorbed pyridine signal in the Ni_3Sn_2 alloy and SnO_2. This indicates that the Lewis acid sites in the catalyst were provided by TiO_2, and Ni_3Sn_2 alloys were mainly employed for activating hydrogen, although Lewis acidity of SnO_2 was used to explain the activity of Sn containing catalysts (Khder, 2008; Khder et al., 2008; Khder and Ahmed, 2009; Liu et al., 2015).

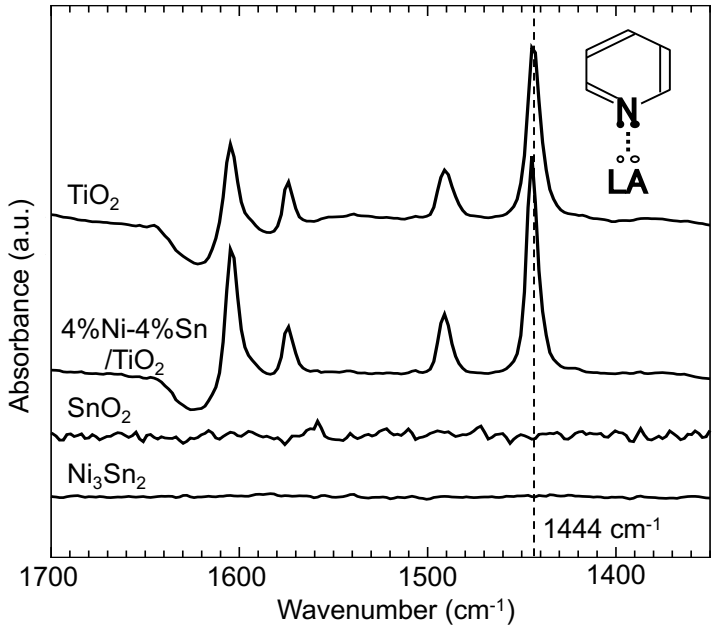

Fig. 2-9 Lewis acid point in the catalyst measured by IR.

The electronic states of Ni and Sn of 4wt%Ni-4wt%Sn/TiO_2 catalyst were evaluated by XPS (Fig. 2-10). A peak around 855 eV was assigned to Ni $2p_{3/2}$ (Li et al., 2017; Wei et al., 2004), and it contained two signals of Ni^0 with the peak at 852.1 eV (Hengne et al., 2018) and Ni^{2+} at 854.7 eV (Li et al., 2016) in Fig.10 (a). A Sn $3d_{5/2}$ signal around 486 eV, Fig.10 (b), was able to be separated into three components of Sn^0, Sn^{2+}, and Sn^{4+} with the peaks at 485, 486.2, and 487.1 eV, respectively (Li et al., 2011; Quackenbush et al., 2013; Hanyš et al., 2006). These results indicate that NiO, SnO and SnO_2 remained on the catalyst surface. Nevertheless, the analysis in Fig. 2-9 indicates that the TiO_2 support acted as the Lewis acid site, activating acetic acid in catalytic hydrogenation in aqueous solution.

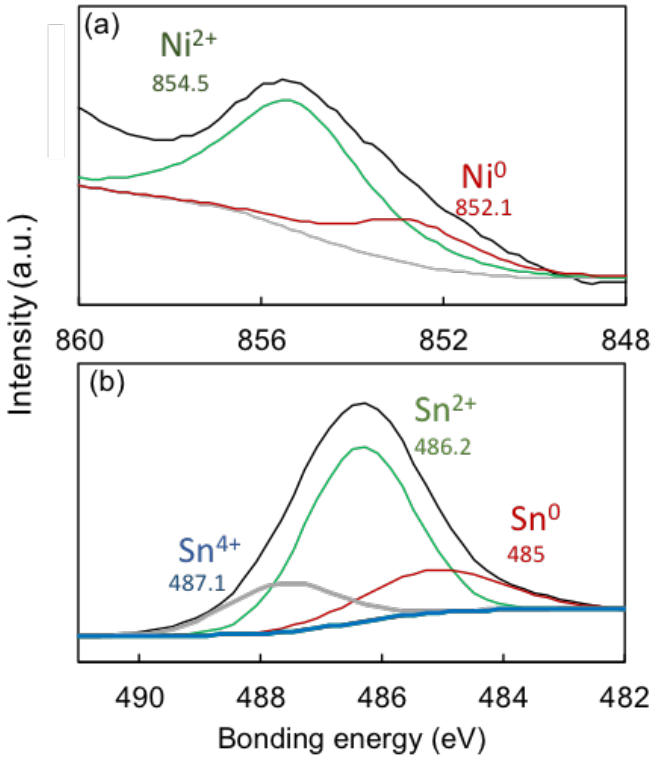

Fig. 2-10 Ni 2p spectra (a) and Sn 3d (b) spectra of fresh 4wt%Ni-4wt%Sn/TO_2 catalyst.

These results provide experimental support for the catalytic mechanism of Ni-Sn/TiO_2 to convert aqueous acetic acid into ethanol (Fig. 2-11), which was originally proposed for Ru-Sn/TiO_2 in our previous paper (Ito et al., 2016) but enough evidence

has not been presented. A lone pair of carbonyl group of acetic acid coordinates to Ti of TiO_2 as a Lewis acid, activating the acetic acid molecule by increasing the $\delta+$ character of carbonyl carbon. This makes the nucleophilic addition of hydrogen anion that is activated on Ni-Sn alloy easier. With this mechanism, hydrogenation of acetic acid occurs at the interface between Ni-Sn and TiO_2. The hydrogenation reactivity that rather decreased by using a large excess amount of Ni-Sn alloy (24 wt%, based on TiO_2, Fig. 2-8) supports this mechanism.

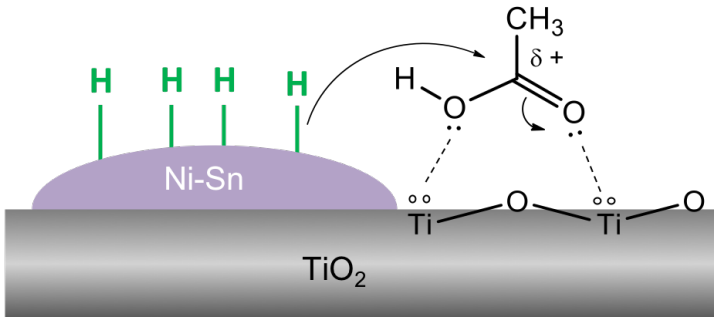

Fig. 2-11 Postulated role of TiO_2 and Ni-Sn alloy for the formation of ethanol from acetic acid.

Both Ru-Sn/TiO_2 and Ni-Sn/TiO_2 catalysts exhibited high catalytic activity for hydrogenation of aqueous acetic acid into ethanol. The yield of ethanol with Ni-Sn/TiO_2 catalyst was 93 mol% under conditions of 200 °C/ 10 MPa/ 12 h, corresponding to that (98 mol%) with Ru-Sn/TiO_2 under similar conditions of 170 °C/ 15 MPa/ 12 h (Ito et al., 2016). However, the role of Sn is quite different for these catalysts. The catalytic activity decreased by changing Ru metal to Ru-Sn alloy, but the selectivity of ethanol formation increased by suppressing gasification as a side reaction more significantly. On the other hand, the catalytic activity of Ni catalyst was dramatically enhanced by using Ni-Sn alloy, probably due to the more efficient hydrogen activation occurring on Ni-Sn alloy than Ni metal.

2.4 Summary

The Ni/TiO_2 and $Ni\text{-}Sn/TiO_2$ catalysts were investigated for hydrogenation of aqueous acetic acid to ethanol, relating to the bioethanol production from lignocellulosics.

1. Catalytic activities of Ni/TiO_2 catalysts were low but dramatically increased by the addition of Sn, and the ethanol yield reached 93 mol% with 4wt%Ni-4wt%Sn/TiO_2.
2. The optimum ratio of Ni:Sn was about 1:1 (w/w) for high catalytic activity due to the alloy (Ni_3Sn_2) formation.
3. Alloy formation of catalysts were confirmed that NiO is first reduced by H_2 into Ni metal, and then the Ni metal reduces the adjacent SnO_2 to form Ni-Sn alloy, which explained the use of an excessive amount of Sn lowered the catalytic activity.
4. The TiO_2 support was suggested to be the Lewis acid site of the catalyst.
5. Based on the present results, the catalytic hydrogenation mechanism of $Ni\text{-}Sn/TiO_2$ was proposed, which is a lone pair of carbonyl group of acetic acid coordinates to TiO_2, resulting in enhancement of the attack of hydrogen anions activated on the neighboring Ni-Sn alloys, and thus the promotion of the hydrogenation activity.

Chapter 3

Hydrogenation of aqueous acetic acid over Ru-Sn/TiO_2 catalyst in a flow-type reactor, governed by reverse reaction

3.1 Introduction

Bioethanol has drawn attention as a means of reducing our dependence on fossil fuels (Dodić et al., 2009; Kim and Dale, 2004; Owusu and Asumadu-Sarkodie, 2016; Urry, 2014; Yang et al., 2012). Currently, commercial bioethanol production involves alcoholic fermentation with yeast, which also releases two carbon atoms from glucose as CO_2 (Schell et al., 1990; Takagi et al., 1977), resulting in low carbon conversion efficiency. Therefore, we have proposed a new ethanol production process based on acetic acid fermentation that can theoretically convert all carbon atoms into acetic acid (Saka et al., 2019). Acetic acid is also a useful industrial chemical, and the global market size is 16.3 million tons in 2018 (Dimian and Kiss, 2020; Le Berre, 2001).

This new bioethanol production process consists of three steps: a hot-compressed water treatment to hydrolyze lignocellulosics, acetic acid fermentation, and hydrogenation of acetic acid (Saka et al., 2019). This research focuses on the final acetic acid hydrogenation step. Transition metals on various supports including titania (TiO_2) and alumina (Al_2O_3) have been reported for hydrogenation of organic acids (Besson et al., 2014; Cheah et al., 1992; Chen et al., 2014; Mendes et al., 2001; Tahara et al., 1997; Wan et al., 2013; Zhang et al., 2013). We have reported Pt (Kawamoto et al., 2016) and Ru (Ito et al., 2016) supported on TiO_2 as potential hydrogenation catalysts for aqueous acetic acid to ethanol, by activating acetic acid with Lewis acid site (Ti). Ethanol was obtained with a batch-type reactor using a less expensive Ru-Sn/TiO_2 catalyst in a 98 mol % yield from 10 g/L of aqueous acetic acid under the optimum conditions of 10 MPa H_2 and 170 °C, although a long reaction time of 12 h was required (Ito et al., 2016) .

The use of flow reactors for reactions on solid catalysts has many advantages over batch reactors (Durndell et al., 2015; Gómez-Quero et al., 2011; Hartman et al., 2011; Hessel, 2009; Hessel et al., 2006; Numwong et al., 2012; Olcay et al., 2014; Osako et al., 2017; Roberge et al., 2008b, 2008a; Wang et al., 2018; Wiles and Watts, 2012; Yu et al., 2020). Continuous flow hydrogenation has also recently been found to reduce reaction times and improve selectivity and safety of operation (Durndell et al., 2015; Gómez-Quero et al., 2011; Numwong et al., 2012; Olcay et al., 2014; Osako et al., 2017; Wang et al., 2018; Yu et al., 2020). For example, Numwong et al. (Numwong et al., 2012) reported that the hydrogenation rate of polyunsaturated fatty acid methyl esters over Pd/C was 4–5 times faster in a flow-type than batch-type reactor. Durndell et al. (Durndell et al., 2015) reported improved reactivity and selectivity towards C=O activation in hydrogenation of cinnamaldehyde over Pt/SiO_2. Olcay. et al. (Olcay et al., 2014) investigated the hydrogenation of aqueous acetic acid with various catalysts including Ru/C using a flow reactor, and they reported that the ethanol selectivity increased by increasing the hydrogen pressure. However, the conversion of acetic acid was only about 16.6%.

In this paper, hydrogenation of aqueous acetic acid over 4wt%Ru-4wt%Sn/TiO_2 was investigated with the use of a commercially available flow type reactor system, H-Cube. The results are compared with those obtained from a batch type reactor reported in our previous paper (Ito et al., 2016). Side reactions that compete with hydrogenation to ethanol were closely examined to better understand the reactions occurring and the role of the flow reactor. This catalytic system was also applied to hydrogenation of lactic acid to propane-1,2-diol.

3.2 Experimental

3.2.1. Materials and catalyst preparation

Titanium isopropoxide (> 95% purity), tin (II) chloride dihydrate ($SnCl_2 \cdot 2H_2O$, > 97%), sodium hydroxide (NaOH, > 97%), 2-propanol (> 99%), and hydrochloric acid (HCl, 6 mol/L) were used for catalyst preparation. Acetic acid (AcOH, > 99%) and ethanol (EtOH, > 99.5%) were used for the preparation of the aqueous solutions for hydrogenation. All the above reagents were purchased from Nacalai Tesque, Inc., Kyoto, Japan. Ruthenium (III) chloride ($RuCl_3$) was provided by Tokyo chemical industry, Co. Ltd., Tokyo, Japan, and hydrogen (H_2, > 99.9%) was provided by Imamura Sanso, Co. Ltd., Shiga, Japan.

In our previous study (Ito et al., 2016), the addition of Sn to 4wt% Ru/TiO_2 significantly improved the ethanol selectivity against gasification, and the Sn loading level of 4 wt% against TiO_2 was found to be optimal for the ethanol production from aqueous acetic acid. Therefore, 4wt%Ru-4wt%Sn/TiO_2 catalyst was selected and prepared by a sol-gel sedimentation method. A mixture of tetraisopropoxide and isopropanol was added dropwise to an aqueous solution of $RuCl_3$ and $SnCl_2$ at 60 °C. After the additional agitation for 30 min, aqueous NaOH solution (100 mL, with sufficient concentration for neutralizing metal chlorides) was added and stirred for 0.5 h. During this period, $RuCl_3$ and $SnCl_2$ were converted to $Ru(OH)_3$ and $Sn(OH)_2$, respectively, and then deposited on the TiO_2 surface. The reaction mixture was allowed to stand for 12 h. The obtained precipitates were washed with water fiver times and then oven-dried at 105 °C for overnight. The obtained solid was calcinated at 450 °C under an air flow (100 mL/min) for 1 h and then reduced at 400 °C under a H_2 flow (100 mL/min) for 2 h. The prepared catalysts (BET surface area = 80 ± 5 m^2/g) were adjusted to a powder with an average size of 50–70 μm for packing into the catalyst column.

3.2.2 Hydrogenation with flow type reactor

Fig. 3-1 shows the configuration of the flow-type reactor consisting of a flow reactor system (H-Cube Pro™, ThalesNano Inc., Budapest, Hungary) and an electric furnace (Phoenix, ThalesNano Inc., Budapest, Hungary)(Jones et al., 2006). The system allows for a reaction pressure and temperature up to 10 MPa and 450 °C. For the hydrogenation reaction, aqueous acetic acid solution (10 g/L) was fed by a high-pressure pump at a flow rate of 0.3 mL/min, and hydrogen (H_2, > 99.9%) was mixed as microbubbles through a mixer filter. The H_2 flow rate was controlled with a mass flow controller (Gas module, ThalesNano Inc., Budapest, Hungary) at 60 mL/min. The flow rates were based on the standard ambient temperature and pressure (SATP). The mixture was preheated through a heat exchanger and supplied to a packed-bed catalyst column (4wt%Ru-4wt%Sn/TiO_2) heated at a designated temperature between 160–380 °C. The resulting mixture was then cooled by the heat exchanger. The inner pressure of the reaction system was maintained at 10 MPa by a back-pressure regulator. After the pressure was released, the reaction mixture was separated into liquid and gaseous products with a liquid-gas separator and collected in a glass bottle and a gas bag, respectively. To ensure that the reaction reached a steady state, the products were collected at least 45 min after starting to operate the system under the specified conditions.

The typical reaction conditions described above were altered according to the purpose of the experiment. We used two types of catalyst columns: a narrow column (inner diameter, 3.9 mm; catalyst-packed length, 100 mm) and wide column (inner diameter, 9.4 mm; catalyst-packed length, 210 mm). The porosity φ of the catalyst-packed region was 0.66 as measured by filling with water.

The mean residence time t was calculated by the following equation:

$$t = \frac{\varphi \mathrm{V}}{F_{Aq}\frac{\rho Aq}{\rho' Aq} + F_{H_2}\frac{\rho H_2}{\rho' H_2}}, \tag{3.1}$$

where V is the volume of the catalyst-packed region, F is the flow rate, ρ and ρ' are densities at SATP and reaction conditions, respectively. The subscripts Aq and H_2 correspond to aqueous acetic acid and H_2, respectively. Density changes for the acetic acid solution and H_2 were estimated with the Soave–Redlich–Kwong model that runs on a steady-state process simulator, Pro/II version 10.1 (Schneider Electric, Rueil–Malmaison, France). Under the above typical conditions, the mean residence times in the narrow column were estimated to be 0.59 min at 160 °C, 0.47 min at 280 °C, and 0.09 min at 380 °C. The reason for the short residence time at 380 °C is that at 10 MPa, water vaporizes at approximately 310 °C. Because the inner volume of the wide column was approximately 12 times that of narrow column; the residence time was 12 times as long.

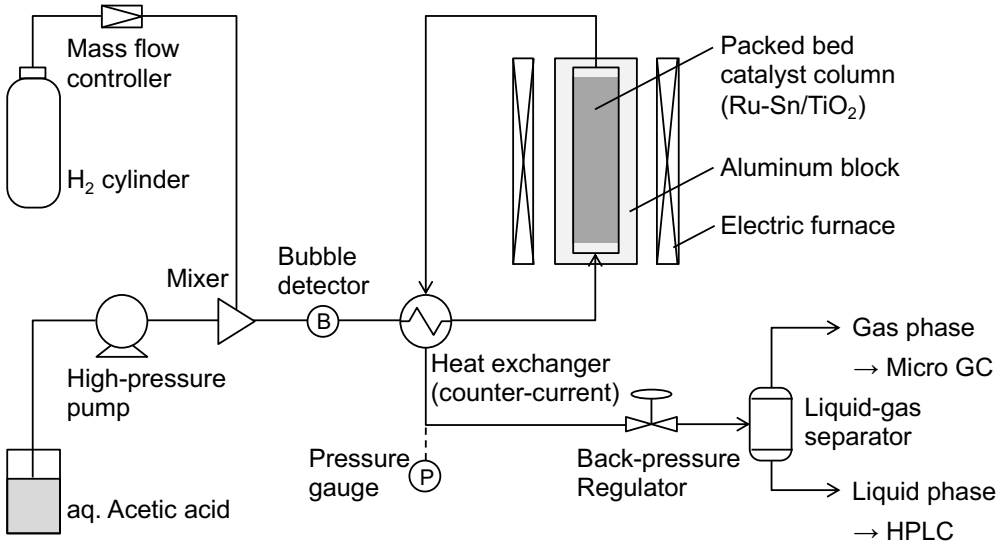

Fig. 3-1 A flow-type reactor used for hydrogenation of aqueous acetic acid to ethanol.

3.2.3 Product determination

The liquid products collected from the flow type reactor were analyzed by high-performance liquid chromatography (HPLC, LC 20 system, Shimadzu Corporation, Kyoto, Japan) under the following conditions: column, Aminex HPX-87H (300×7.8 mm, Bio-Rad Laboratories, Inc., Hercules, CA, USA); eluent, 5 mM sulfuric acid in water; flow-rate, 0.6 mL/min; column temperature, 45 °C; detector, refractive index detector (RID-20A, Shimadzu Corporation, Kyoto, Japan).

The gaseous products collected from the liquid-gas separator were analyzed with a micro gas chromatograph (Micro GC, CP 4900, Varian Medical Systems, Inc., Palo Alto, CA, USA), (Molsieve 5 A 10 m Column, PoraPLOT Q 10m Column, analysis time 120 s, pressure 550±10 kPa, temperature 100 °C). Neon (Ne) was used as an internal standard for quantification.

3.3 Results and discussion

3.3.1. Hydrogenation of aqueous acetic acid to ethanol in flow type reactor

Hydrogenation of 10 g/L aqueous acetic acid over 4wt%Ru-4wt%Sn/TiO_2 was investigated in the temperature range of 160–320 °C with the use of a narrow column at 10 MPa, and the results are shown in Fig. 3-2. The ethanol yield increased as the reaction temperature was increased to a maximum of 78 mol % at 280 °C. The optimum ethanol production temperature for the batch type reactor was 170 °C because gasification occurred at higher temperatures (Ito et al., 2016); hence, the selectivity for ethanol formation over gasification was overall improved in the flow system. The reason for this improvement will be explained later. This improvement allowed for the use of a high reaction temperature of 280 °C. High ethanol yields were achieved for a

short residence time of less than 1 min in the flow reactor, in contrast to the batch process that required reaction times as long as 12 h.

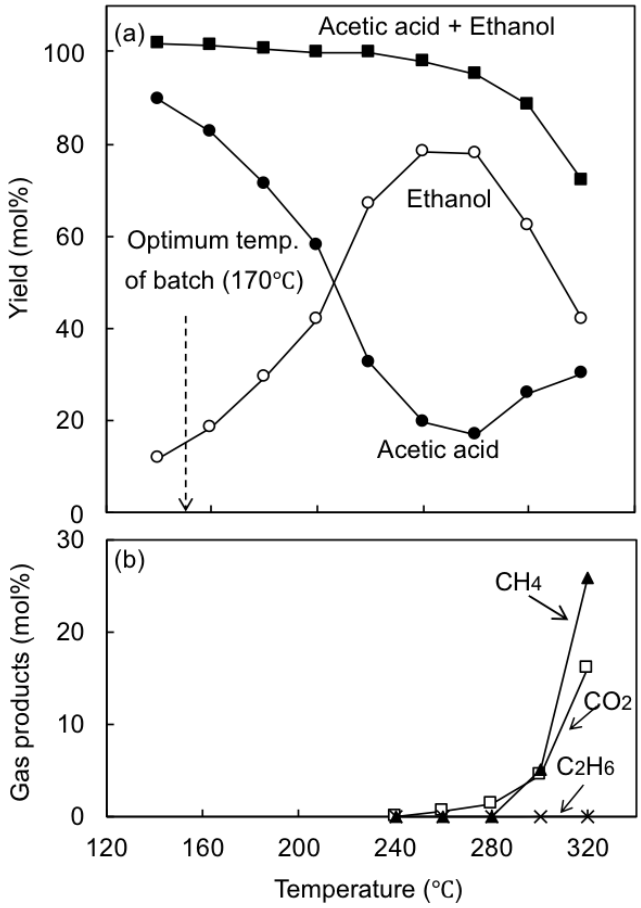

Fig. 3-2 Effect of reaction temperature on hydrogenation of aqueous acetic acid (10 g/L) to ethanol with flow reactor: (**a**) liquid products; (**b**) gaseous products (column size: 3.9-mm inner diameter, 100-mm length; pump flow rate, 0.3 mL/min; H_2 flow rate, 60 mL/min; pressure, 10 MPa).

When the reaction temperature was higher than 300 °C, the ethanol yield sharply decreased, and the recovery rate of acetic acid increased. Thus, conversion of acetic acid to ethanol was ineffective at higher temperatures. On increasing the temperature from 300 to 320 °C, the total acetic acid + ethanol yield decreased to be 72 mol %, and gaseous products, CH_4 (26 mol %), CO_2 (17 mol %), and C_2H_6 (0.1 mol %), were the

major components of the reaction mixture. Carbon dioxide started to be detected from the lower temperature at 240 °C, but CH_4 and C_2H_6 were detected above 300 °C. No carbon monoxide was detected, probably because of the occurrence of a water-gas shift reaction, as discussed later. Hydrogen might have been produced but could not be quantified because the large amount of hydrogen used in hydrogenation prevented accurate measurements. Thus, above 300 °C the ethanol yield decreased because of gasification.

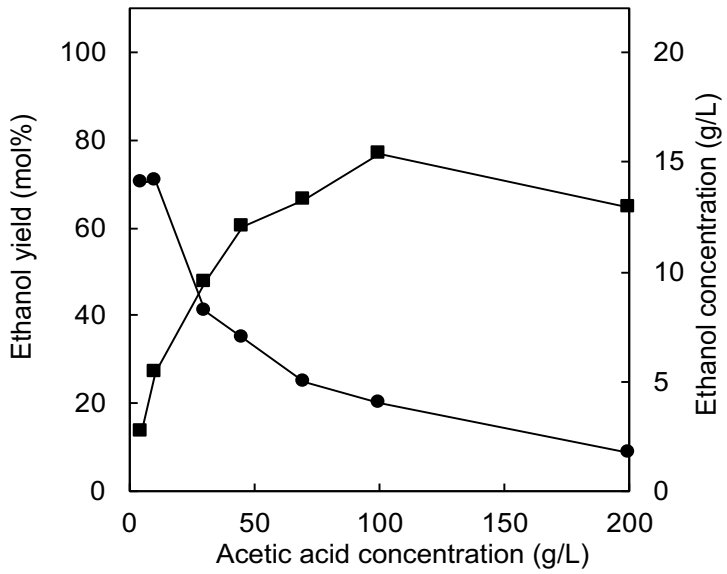

Fig. 3-3 Effect of acetic acid concentration on ethanol yield in hydrogenation of aqueous acetic acid to ethanol at 250 °C (column size, 3.9-mm inner diameter, 100-mm length; pump flow rate, 0.3 mL/min; H_2 flow rate, 60 mL/min; pressure, 10 MPa).

Fig. 3-3 shows the ethanol yields for acetic acid concentrations from 5 to 200 g/L at 250 °C under similar reaction conditions. The ethanol yield (mol %) decreased as the concentration increased, whereas the amount of ethanol obtained (g/L) stabilized in the range of 13–15 g/L. Thus, the acetic acid concentration was rate-determining up to this concentration but not above this range, where the amount of acetic acid converted to ethanol plateaued and was determined by the saturation capacity of the catalyst bed.

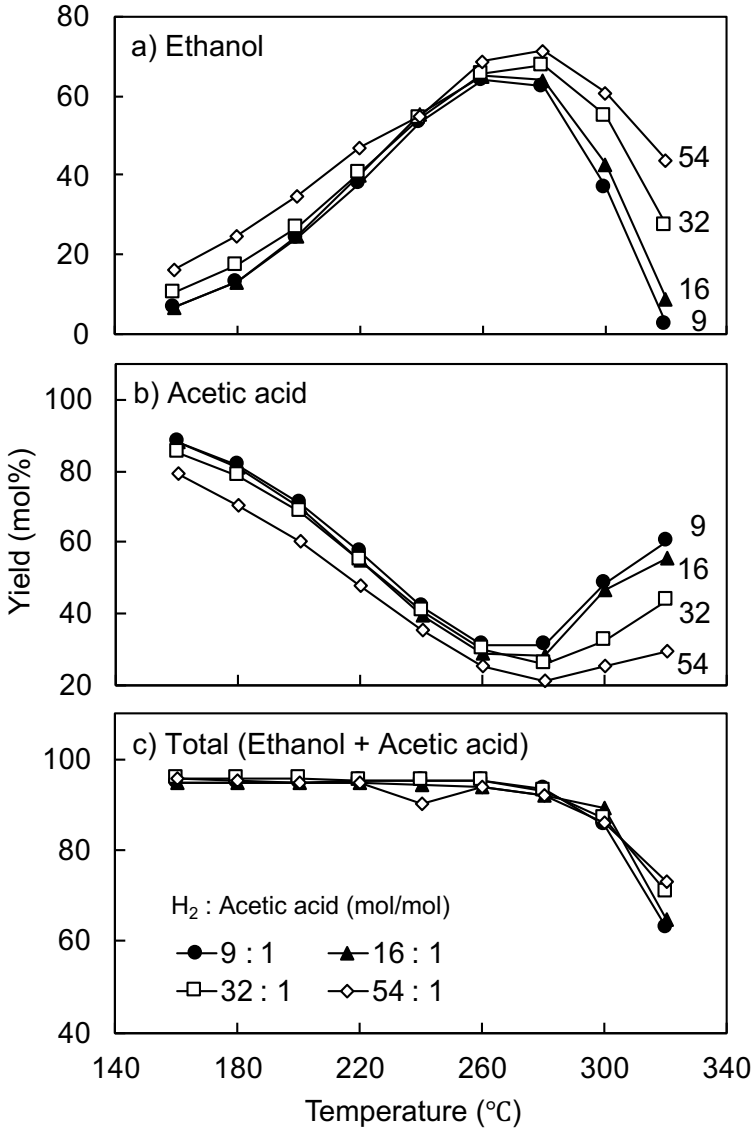

Fig. 3-4 Effect of H_2/acetic acid ratio on hydrogenation of aqueous acetic acid (10 g/L) to ethanol: (**a**) ethanol; (**b**) acetic acid; (**c**) total (ethanol + acetic acid) (column size, 3.9-mm inner diameter, 100-mm length; pump flow rate, 0.3 mL/min, H_2 flow rate, 10–60 mL/min; pressure, 10 MPa).

The influence of H_2 on the hydrogenation of 10 g/L of acetic acid was investigated under similar reaction conditions at various H_2/AcOH molar ratios. This ratio was varied through the use of different hydrogen flow rates of 60, 36, 18, and 10

mL/min, while the aqueous acetic acid flow rate was maintained (0.3 mL/min), corresponding to H_2/AcOH molar ratios of 54:1, 32:1, 16:1, and 9:1, respectively. These ratios indicate 27:1, 16:1, 8:1, and 4.5:1 times molar in excess of the required H_2, respectively, because 2 molar equivalents of H_2 are used to reduce acetic acid to ethanol. As shown in Fig. 3-4, this molar ratio had a limited influence on the yields of ethanol and acetic acid below 260 °C, where the results at ratios of 9:1, 16:1 and 32:1 were quite similar. Thus, the amount of H_2 is not rate-determining for hydrogenation of acetic acid to ethanol in this temperature range. Unfortunately, we could not reduce the rate further below 9 because of limitations of the leak error detector of the H-Cube reactor. Notably, 4.5 molar equivalents or less of H_2 is sufficient to reduce acetic acid to ethanol in the flow reactor, likely because of the very efficient activation of hydrogen on the catalyst surface, as will be discussed later.

Conversely, above 280 °C, the yields of ethanol and acetic acid varied greatly depending on the H_2/AcOH ratio. As previously mentioned, the ethanol yield decreased but the acetic acid recovery rate increased at higher temperatures. However, this tendency was lessened as the amount of hydrogen was increased (i.e., a higher H_2/AcOH ratio). Thus, a higher H_2/AcOH ratio was preferable for producing ethanol in this temperature range. The temperature at which the maximum ethanol yield was achieved shifted slightly to a higher range as the hydrogen content was increased.

A decrease in the total ethanol + AcOH yield was observed above 280 °C, which we attribute to gasification being slightly suppressed through the use of more hydrogen. However, the effect was smaller than those on the yields of ethanol and acetic acid as described above.

As for the stability of catalyst, once the catalyst was filled in the column, data of each Fig. 3-2, 3-3 or 3-4 were corrected using the same catalyst column, and hence, the catalysts were utilized for long period more than 60 h. After each of the series of experiments, it was confirmed that there was no difference in catalytic activity by

performing the hydrogenation under the initial test conditions. Therefore, the Ru-Sn/TiO_2 catalyst was very stable for long-term hydrogenation.

3.3.2. Side reactions competing with ethanol production

To understand the side reactions, aqueous ethanol and aqueous acetic acid were treated under similar reaction conditions without the use of hydrogen. The recovery rates of ethanol and acetic acid are plotted against the reaction temperature in Fig. 3-5 and compared with the yields of gaseous products.

Unexpectedly, ethanol was more reactive than acetic acid in the absence of hydrogen and converted to acetic acid at temperatures as low as 200 °C. The reaction became more pronounced above 280 °C. The total ethanol + AcOH yields of approximately 100 mol % below 280 °C suggest that oxidation reactions occurred selectively above 280 °C. Oxidation is the reverse of the hydrogenation of acetic acid to ethanol, and is thus expected to affect the apparent ethanol production rate, although this model experiment did not use any hydrogen. Inefficient conversion from acetic acid to ethanol, observed above 280 °C (Fig. 3-2 and 3-4), is rationally explained by this reverse reaction. Because the efficiency of ethanol production in this temperature range is directly related to the amount of hydrogen used, the selectivity for ethanol formation rather than the reverse reaction is greater when more hydrogen used.

Large amounts of hydrogen and acetic acid were generated. The molar ratios of H_2 to AcOH in the products were 0.4:1, 0.2:1, 0.3:1, 1.7:1, and 3.2:1 at 240, 260, 280, 300, and 320 °C, respectively. Hydrogen was the only gaseous product formed in the temperature range of 240–280 °C. The simultaneous production of hydrogen and acetic acid indicates that the aqueous solvent acts as an oxidant to convert ethanol to acetic acid, although details of this mechanism are currently unknown. When water oxidizes ethanol to acetic acid, 2 equivalents of water participate in the reaction, forming 2 equivalents of hydrogen. Although the actual yields of hydrogen determined in the

temperature range of 240–280 °C were lower than the theoretical value of 2, we attribute this to hydrogen being trapped in cages formed by water molecules as clathrate hydrates [33–35]. Hydrogen clathrate hydrates are known to form under high pressure conditions in water and can store up to 5 wt% hydrogen. In the current experiments, hydrogen trapped in water may not have been completely recovered during the gas-liquid separation process.

Catalytic oxidation of aqueous ethanol to acetic acid and hydrogen has also been reported in relation to reforming of ethanol to hydrogen (Diagne et al., 2002; Nozawa et al., 2015, 2014). In most cases, acetic acid is not the major product, whereas Nozawa et al. (Nozawa et al., 2015) reported that selectivity for acetic acid production is higher for Re/TiO_2 and $Ir\text{-}Re/TiO_2$ catalysts, but long reaction times were required.

The water-gas shift reaction ($CO + H_2O \rightarrow H_2 + CO_2$) has been used to explain the high yield of hydrogen from ethanol reforming (Nozawa et al., 2015) . This reaction also explains the high yields of hydrogen at 300 and 320 °C in the current experiments. Carbon monoxide was not detected in the present ethanol conversion, which supports the above conclusions. A similar explanation can be made for the gas formation behavior in hydrogenation of acetic acid in Fig. 3-2.

Treatment of acetic acid gave only gaseous products (CH_4, CO_2, and H_2) at high temperatures of 300 and 320 °C. This temperature range is similar to that for the formation of non-hydrogen gaseous products in the model ethanol experiments. Accordingly, some acetic acid and ethanol may be gasified during hydrogenation of acetic acid to ethanol; however, this effect is limited to high temperatures above 300 °C. Conversely, gas formation was observed over the lower temperature range of 240 °C in the hydrogenation of acetic acid in Fig. 3-2 Thus, other gas formation pathways may be included in the hydrogenation of aqueous acetic acid. This topic will be discussed later in another paper.

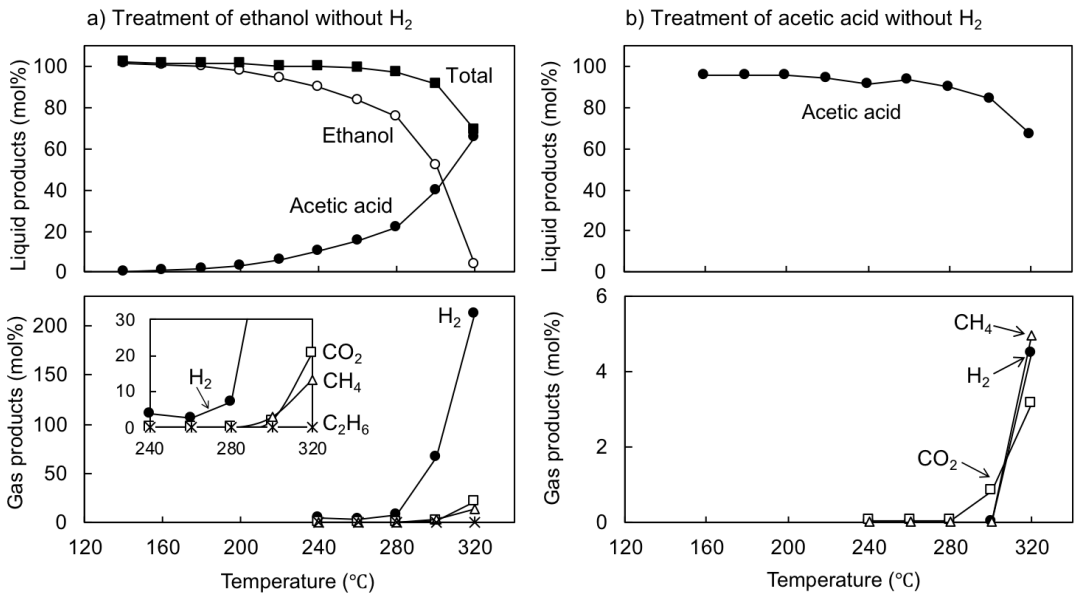

Fig. 3-5 Product yields from treatment of aqueous (a) ethanol and (b) acetic acid (10 g/L each) without H_2 (column size, 3.9-mm inner diameter, 100-mm length; pump flow rate, 0.3 mL/min; pressure, 10 MPa.

3.3.3. Influences of catalyst column size and reaction mechanism

To improve the ethanol yield, a wide column, with an inner diameter 2.4 times as wide and length 2.1 times as long as the narrow column, was used to extend the reaction time. The hydrogenation of aqueous acetic acid was conducted under similar reaction conditions to the experiments with the narrow column (Fig. 3-2). The results from the larger column are shown in Fig. 3-6. By increasing the reaction time to be effectively 12 times as long as for the original experiments, the conversion of acetic acid to ethanol proceeded almost completely at a relatively low temperature of 200 °C. A 98 mol % yield of ethanol was achieved even at a short residence time of 6.7 min. The liquid hourly space velocity (LHSV) was 1.23 h^{-1} (volume of the catalyst-packed region [14.6 mL] ÷ flow rate of aqueous AcOH [0.3 mL/min] × 60 min). Thus, in the continuous flow reactor, the reaction time was markedly reduced from 12 h (batch type) to 6.7 min.

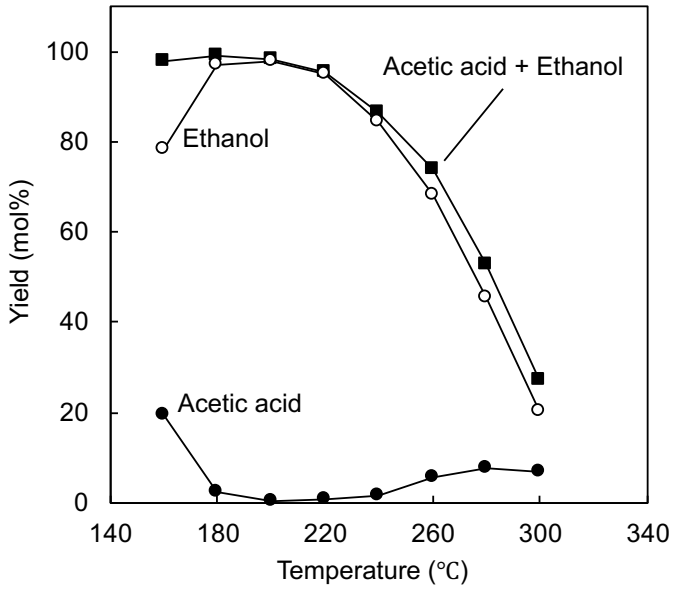

Fig. 3-6 Effect of reaction temperature on hydrogenation of aqueous acetic acid (10 g/L) to ethanol (column size, 9.4-mm inner diameter, 210-mm length; pump flow rate, 0.3 mL/min; H_2 flow rate, 60 mL/min; pressure, 10 MPa).

The ethanol yield, however, decreased when the reaction temperature was increased beyond 200 °C. At higher temperatures, the recovery rate of acetic acid increased as was the case for the narrow column (Fig. 3-2 and 3-4). Thus, the optimum temperature for ethanol production was lower in the wide column. By prolonging the reaction time up to 12 times, undesirable gasification proceeded at a lower temperature, resulting in a decrease in ethanol yield. Because the recovery of acetic acid at 200 and 220 °C was almost zero, the system was considered to be at equilibrium above 200 °C. Hence, a dynamic equilibrium was achieved between ethanol production (forward reaction) and oxidation of the product ethanol (reverse reaction).

The ethanol/acetic acid molar ratios in the reaction mixture are summarized in Table 3-1. The ratios obtained at 280 and 300 °C in Fig. 3-2 (narrow column) are also included for comparison, because the forward and reverse reactions equilibrated at the temperatures at which the acetic acid recovery rates increased. The ethanol/acetic acid molar ratios at 260, 280, and 300 °C became more similar for both types of column at

higher reaction temperatures. The ratios of 3.0:1 (wide) and 2.4:1 (narrow) at 300 °C were very similar. These results indicate that the hydrogenation reaction of aqueous acetic acid to ethanol is governed by an equilibrium reaction over prolonged reaction times, where the conversion from acetic acid to ethanol is equilibrated. This is the situation for reaction temperatures higher than 240 °C (ethanol/acetic acid ratio at the equilibrium: < 49:1). Hence, 2 mol % of acetic acid contamination of ethanol occurred at 240 °C. The prolonged reaction time produced gaseous products, because gasification is an irreversible reaction.

Table 3-1 shows the effects of temperature on the composition of ethanol/acetic acid at the equilibrium. The ratio varied considerably depending on the reaction temperature and the values were large at 200 °C (238:1) and 220 °C (120:1), where almost complete conversion from acetic acid to ethanol was realized through the prolonged reaction. Notably, the influence of the reaction temperature on the ratio at equilibrium was quite large compared with typical equilibrium reactions. The complex nature of the reactions, including three phases, may account for this result; however, further systematic studies are necessary to clarify the molecular based mechanisms.

Table 3-1. Ethanol/acetic acid molar ratio in the reaction mixture of hydrogenation of aqueous acetic acid (10g/L).

	Reaction temperature (°C)					
	200	220	240	260	280	300
Wide column	238	120	49	12	6.1	3.0
Narrow column				3.9	4.6	2.4

Wide column: 9.4 inner diameter, 210 mm length
Narrow column: 3.9 inner diameter, 100 mm length
Reaction conditions: Pump flow rate 0.3 mL/min; H_2 flow rate 60 mL/min; pressure 10 MPa

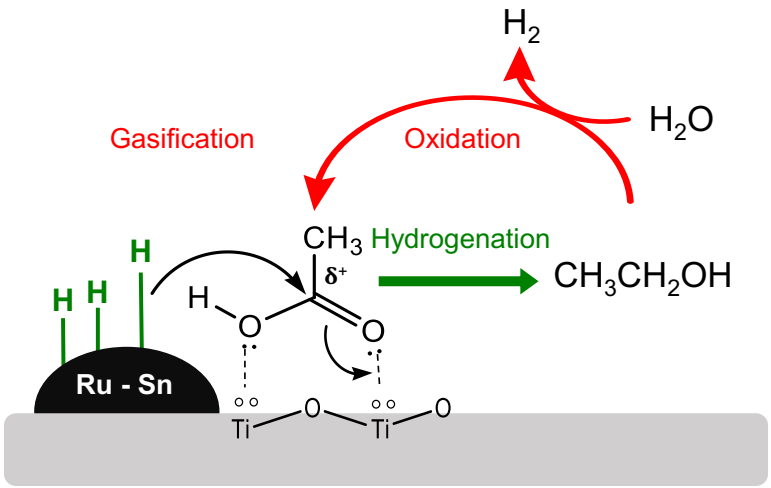

Fig. 3-7 Proposed mechanism illustrating oxidation of the product ethanol and gasification competing with hydrogenation of aqueous acetic acid to ethanol over Ru-Sn/TiO_2 catalyst in the flow type reactor.

Consequently, a hydrogenation mechanism of aqueous acetic acid over Ru-Sn/TiO_2 catalyst is proposed in Fig. 3-7, in which side reactions, oxidation of the product ethanol and gasification, compete with the desired pathway to ethanol. The oxidation of ethanol (reverse reaction) greatly affects the apparent ethanol production rate above 240 °C, where the molar ratio of ethanol/acetic acid at equilibrium is < 49:1. Under such high temperature conditions, the gasification reaction (an irreversible reaction) tends to govern the product composition for the prolonged reaction, although the gasification rate is much smaller than that of the ethanol-forming pathway.

3.3.4 Roles of flow and batch reactors

The characteristics of flow and batch reactors in hydrogenation are illustrated in Fig. 3-8. In the batch reactor (a), H_2 gas is present in the upper part, and the catalyst powder sinks into the aqueous acetic acid solution. Even when the reaction system is agitated by a stirrer, contact between the H_2 gas and the catalyst is limited. There are

fewer activated hydrogen atoms on the Ru-Sn surface, which limits hydrogenation of acetic acid and promotes oxidation of the product ethanol. The competition between hydrogenation and oxidation likely explains the long reaction time (12 h) required by the batch reactor in our previous study (Ito et al., 2016). The low optimum temperature (170 °C) is also attributed to gasification becoming more prominent for long treatments and higher temperatures.

In the flow reactor (b), aqueous acetic acid solution and H_2 microbubbles were continuously supplied and passed through the catalyst packed region. Therefore, H_2 gas had more contact with the catalyst surface than in the batch reactor. Thus, we expect that more activated hydrogen atoms are present on Ru-Sn for hydrogenation of acetic acid, and oxidation of ethanol is suppressed. This mechanism could explain why a very short reaction time was realized in the flow reactor. The short reaction time also suppressed the effects of gasification.

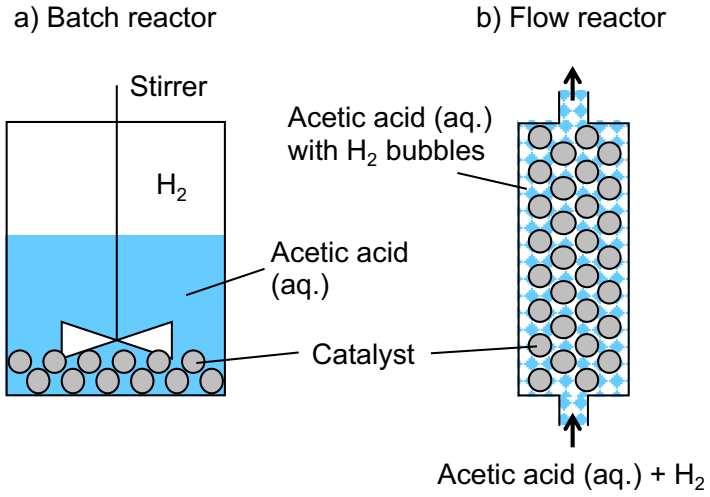

Fig. 3-8 Difference in contact behaviors between H_2 (gas), aqueous acetic acid (liquid), and catalyst (solid) in batch and flow reactors.

3.3.5 Hydrogenation of lactic acid to propane-1,2-diol

In addition to acetic acid, various biomass-based organic acids produced by microbial fermentation of sugars are used in industry, and lactic acid is one of the most widely produced organic acids (Sauer et al., 2008). Propane-1,2-diol is produced by hydrogenation of lactic acid or its esters as an industrial chemical that is used as a solvent for the production of unsaturated polyester resins, drugs, cosmetics and food, de-icing fluid, and antifreeze (Fiume et al., 2012; Luo et al., 2004; Sauer et al., 2008).

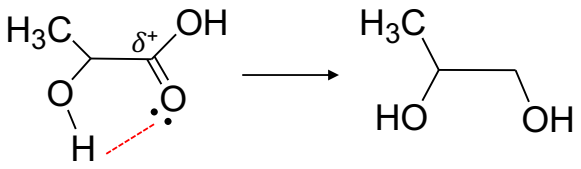

Fig. 3-9 Hydrogenation of lactic acid to propane-1,2-diol.

The present method was applied to hydrogenation of aqueous lactic acid (10 g/L) with the use of 4wt%Ru-4wt%Sn/TiO_2 in the narrow column at 10 MPa, 250 °C, and a flow rate of 0.3 mL/min (Fig. 3-9). As a result, propane-1,2-diol was obtained in 87 mol % yield and no other products were detected in the reaction mixture. Thus, lactic acid is efficiently hydrogenated from propane-1,2-diol in this system with a very short mean residence time of 0.5 min. Hydrogenation of lactic acid proceeded more efficiently than that of acetic acid, which is attributed to intramolecular hydrogen bonding of the former that increases polarization of the carbonyl group and enhances the hydrogenation reactivity. Efficient hydrogenation of acetic acid catalyzed by Ru-Sn/TiO_2 has been shown to be due to the binding of Ti (Lewis acid site) to the carbonyl oxygen of acetic acid, enhancing the δ+ character of the carbonyl carbon (Ito et al., 2016; Kawamoto et al., 2016). The carbonyl carbon of lactic acid is already activated by the intramolecular hydrogen bond. Although many papers report the hydrogenation of lactic acid (Broadbent et al., 1959; Luo et al., 2005; Mao et al., 2003; Zhang et al.,

2001) and lactate esters (Luo et al., 2004), the present hydrogenation system with a flow reactor provides a method for efficiently producing propane-1,2-diol with a short residence time.

Consequently, the present flow type hydrogenation system can be applied for production of alcohols from organic acids.

3.4 Conclusions

Hydrogenation of aqueous acetic acid (10 g/L) over 4wt%Ru-4wt%Sn/TiO_2 was investigated with a continuous flow type reactor at 10 MPa and 160–320 °C, and the following conclusions were obtained:

1. Selectivity of the acetic acid formation against gasification was markedly improved in the flow reactor, which enabled the reaction at higher temperatures. For this reason, ethanol was obtained in 78 and 98 mol % yields at 280 and 200 °C for short residence times of 0.5 and 6.7 min (LHSV: 15.1^{-1} and 1.23 h^{-1}), respectively, (batch type: 12 h).
2. Oxidation of the product ethanol to acetic acid (reverse reaction) with water as an oxidant occurred as a side reaction, which decreased the apparent rate of ethanol production.
3. The hydrogenation of aqueous acetic acid was governed by equilibrium reactions, and hence, the ethanol/acetic acid molar ratio did not change for the prolonged reaction. This limited the reaction temperature to less than 240 °C, for which the ethanol/acetic acid molar ratio at equilibrium was 49 thus giving complete conversion of acetic acid to ethanol.
4. The ethanol/acetic acid molar ratio at equilibrium varied from 238:1 to 3.0:1 depending on the reaction temperature (from 200 to 300 °C).

5. Prolonged reactions above 240 °C gave gaseous product because gasification is irreversible. Conversely, the amount of acetic acid converted to ethanol was determined by an equilibrium process.
6. The use of a flow reactor is advantageous for the efficient activation of hydrogen and increases the rate of hydrogenation of acetic acid to ethanol rather than the reverse reaction. Thus, conversion to ethanol is completed before gasification reactions start to affect the yield.
7. Lactic acid was also reduced selectively to propane-1,2-diol in an 87 mol % yield with a residence time less than 0.5 min.
8. A hydrogenation mechanism is proposed, providing insights into the development of efficient hydrogenation catalysts and reaction systems.

Chapter 4

Effects of water boiling on hydrogenation of aqueous acetic acid over Ni-Sn/TiO_2 and Ru-Sn/TiO_2 in a flow type reactor

4.1 Introduction

There is a demand to produce renewable fuels to suppress the reliance on fossil energy ("International Energy Agency (IEA):the total primary energy supply (TPES),(2017)," n.d.) and to minimize the greenhouse gas emissions for the prevention of global warming (Comiso and Hall, 2014; Intergovernmental Panel on Climate Change (IPCC), 2014; International Energy Agency (IEA), 2013). Bioethanol is attracting attention as a renewable liquid fuel alternative to gasoline (Dodić et al., 2009; Kim and Dale, 2004; Urry, 2014; Yang et al., 2012). Currently, bioethanol is produced by alcoholic fermentation using yeast, but this system wastes two carbon atoms in glucose as CO_2, which reduces the carbon utilization efficiency (Schell et al., 1990; Takagi et al., 1977). Therefore, we proposed a new bioethanol production method by acetic acid (AcOH) fermentation that can theoretically convert all carbon atoms in glucose into acetic acid (Saka et al., 2019).

This new process includes hot-compressed water treatment to hydrolyze lignocellulosics, acetic acid fermentation, and hydrogenation of acetic acid (Saka et al., 2019). This study focuses on the final hydrogenation step. Various metal catalysts supported on metal oxides such as titania (TiO_2) and alumina (Al_2O_3) have been investigated for the hydrogenation of organic acids (Besson et al., 2014; Cheah et al., 1992; Chen et al., 2014; Ito et al., 2016; Kawamoto et al., 2016; Mendes et al., 2001; Tahara et al., 1997; Wan et al., 2013; Zhang et al., 2013; Zhao et al., 2020, 2020). We reported Pt (Kawamoto et al., 2016), Ru-Sn (Ito et al., 2016) and Ni-Sn (Zhao et al., 2020) supported on TiO_2 as effective catalysts that can directly hydrogenate aqueous acetic acid to ethanol (EtOH), in which TiO_2 acts as a Lewis acid site for coordination

to the carbonyl oxygen of acetic acid, resulting in the increase in the δ^+ character to accelerate the hydrogenation of acetic acid (Kawamoto et al., 2016). More than 90 mol% of ethanol yield was achieved by hydrogenation of 10 g/L aqueous acetic acid over Ru-Sn/TiO_2 or Ni-Sn/TiO_2 catalyst with a batch reactor, although the long reaction for 12 h was required (Ito et al., 2016; Zhao et al., 2020).

Using a flow reactor has many advantages over batch type for catalytic conversion, which includes reducing the reaction time (Numwong et al., 2012) and improving the selectivity (Durndell et al., 2015; Gómez-Quero et al., 2011; Numwong et al., 2012; Olcay et al., 2014; Osako et al., 2017; Wang et al., 2018; Yu et al., 2020; Zhao et al., 2020). Olcay. et al. (Olcay et al., 2014) investigated the hydrogenation of aqueous acetic acid with various catalysts using a flow reactor, and they reported that the ethanol selectivity increased by increasing the hydrogen pressure, but the conversion of acetic acid was only about 16.6 %. Using our catalyst, 4wt%Ru-4wt%Sn/TiO_2, in a flow reactor, the 98 mol% of ethanol yield was achieved from 10 g/L aqueous acetic acid even in the short reaction for 6.7 min because the hydrogenation could be conducted in much higher temperature range due to the less efficient gas production (Zhao et al., 2020). Thus, the selectivity for the production of ethanol against gaseous product significantly increased in the flow reactor.

In our previous study (Zhao et al., 2020), oxidation of the product ethanol, the reverse reaction, was suggested to compete with the hydrogenation of acetic acid to ethanol over 4wt%Ru-4wt%Sn/TiO_2 in flow reactor, which lowered the ethanol production efficiency. Gasification was also suggested as a side reaction to decrease the ethanol yield in a relatively high temperature range. In the present study, Ni-Sn/TiO_2 catalyst was characterized for hydrogenation of aqueous acetic acid in flow reactor compared with Ru-Sn/TiO_2. Nickel is a much cheaper metal than Ru. Side reactions and the influence of reaction pressure are particularly focused, along with the role of acetaldehyde, the intermediate formed during the conversion of acetic acid to ethanol (equation 4.1).

$$\text{AcOH} \rightarrow \text{Acetaldehyde} \rightarrow \text{EtOH} \quad (4.1)$$

4.2 Experimental

4.2.1 Materials and catalyst preparation

Titanium isopropoxide (>95% purity), ruthenium (III) chloride hexahydrate ($RuCl_3$), nickel (II) chloride hexahydrate ($NiCl_2 \cdot 6H_2O$, >98%), tin (II) chloride dihydrate ($SnCl_2 \cdot 2H_2O$, >97%), sodium hydroxide (NaOH, >97%), 2-propanol (>99%), and aqueous hydrochloric acid (HCl, 6 mol/L) were used for catalyst preparation. Acetic acid (AcOH, >99%), acetaldehyde (AA, >90%), and ethanol (EtOH, >99.5%) were used as aqueous solutions for the hydrogenation reaction. $RuCl_3$ was purchased from Tokyo Chemical Industry Co. Ltd, Tokyo, Japan, and other materials were from Nacalai Tesque, Inc., Kyoto, Japan. Hydrogen (H_2, > 99.9%) was provided by Imamura Sanso, Co. Ltd., Shiga, Japan.

Catalysts were prepared by the sol-gel sedimentation method (Ito et al., 2016; Zhao et al., 2020). Designated amounts of $NiCl_2 \cdot 6H_2O$ or $RuCl_3$ with $SnCl_2 \cdot 2H_2O$ were added to water (100 mL, 60 °C) as Ni, Ru, and Sn precursors, respectively. A mixture of titanium isopropoxide and 2-propanol was added dropwise to the aqueous solution of $RuCl_3$ + $SnCl_2$ or $NiCl_2$ + $SnCl_2$ with stirring at 60 °C. After stirring for another 30 min, an aqueous NaOH solution (100 mL, sufficient concentration to neutralize the metal chlorides) was added, and the mixture was stirred for 0.5 h. During this period, $RuCl_2$, $NiCl_2$, and $SnCl_2$ were converted to $Ru(OH)_3$, $Ni(OH)_2$, and $Sn(OH)_2$, respectively, and then deposited on the TiO_2 surface. The mixture was allowed to stand for 12 h, and the obtained precipitate was washed five times with water and oven-dried at 105 °C overnight. The precipitate was calcinated at 450 °C under an air flow (100 mL/min) for 1 h and then reduced at 400 °C under a H_2 flow (100 mL/min) for 2 h. The

prepared catalysts were sieved to adjust the particle size 50–70 μm and packed into two different catalyst columns, as explained later.

4.2.2 Hydrogenation with flow type reactor

The flow-type reaction system consists of a flow-type reactor (H-Cube Pro™, ThalesNano Inc., Budapest, Hungary), an electric furnace (Phoenix, ThalesNano Inc.), and a mass flow controller (Gas Module, ThalesNano Inc.) (Jones et al., 2006). The configuration and operation of the flow-type system were introduced in detail in our previous study (Zhao et al., 2020). For hydrogenation, the aqueous solution of acetic acid, acetaldehyde, or ethanol (10 g/L) and H_2 were supplied to the catalyst column by using a pump and the mass flow controller, respectively, at designated flow rates. The pressure in the reaction system was maintained by a back-pressure regulator. After being cooled by a heat-exchanger, the resulting mixture was separated into liquid and gaseous products, and then collected in a glass bottle and a gasbag.

Two types of catalyst columns were used: a narrow column (inner diameter, 3.9 mm; catalyst-packed length, 100 mm) and a wide column (inner diameter, 9.4 mm; catalyst-packed length, 210 mm). The porosity φ of the catalyst-packed region was 0.66 as measured by filling it with water. The mean residence time t of the reactant (aqueous solution) in the catalyst-packed region was determined by the following equation:

$$t = \frac{\varphi \mathrm{V}}{F_{Aq}\frac{\rho Aq}{\rho' Aq} + F_{H_2}\frac{\rho H_2}{\rho' H_2}}, \tag{4.2}$$

where V is the volume of the catalyst-packed region, F is the flow rate, ρ and ρ' are densities at SATP and reaction conditions, respectively. The subscripts a and h correspond to aqueous solution and H_2, respectively. Density changes for the aqueous

solution and H_2 were estimated with the Soave–Redlich–Kwong model that runs on a steady-state simulator, Pro/II version 10.1 (Schneider Electric, Rueil–Malmaison, France).

4.2.3 Analytical methods

The liquid products were analyzed by high-performance liquid chromatography (HPLC, Prominence, Shimadzu Corp., Kyoto, Japan) under the following conditions: column, Aminex HPX-87H (300×7.8 mm, Bio-Rad Laboratories, Inc., Hercules, CA, USA); eluent, 5 mM sulfuric acid in water; flow-rate, 0.6 mL/min; column temperature, 45 °C; detector, refractive index detector (RID-20A, Shimadzu Corp.).

The gaseous products were analyzed with a micro gas chromatograph (Micro GC, CP 4900, Varian Medical Systems, Inc., CA, USA) under the following conditions: channel #1; column, Molsieve 5A (10 m × 0.32 mm, 0.12-μm thickness, Agilent Technologies, Inc., CA, USA); carrier gas, Ar; channel #2; column, PoraPLOT Q (10 m × 0.32 mm, 0.10-μm thickness, Agilent Technologies); carrier gas, He; oven temperature, 100 °C; thermal conductivity detector. Ne (>99.999%, Imamura Sanso) gas was used as an internal standard for quantification.

4.3 Results and discussion

4.3.1 Characterization of Ni-Sn catalyst for hydrogenation of aqueous acetic acid in flow reactor

Catalytic activity for hydrogenation of 10 g/L aqueous acetic acid was assessed by using nwt%Ni-nwt%Sn/TiO_2 (n = 4, 8 or 24), which contained metals in different proportions to TiO_2, in the temperature range of 180–380 °C with the narrow column at 10 MPa. The weight ratio of Ni and Sn was fixed at 1: 1, since this is reported to be

the best composition due to the Ni-Sn alloy formation (Zhao et al., 2020). The results are shown in Fig. 4-1. The ethanol yield tended to increase as the amount of metal loading increased and gave the maximum at 280 °C: 27.5 mol% (n = 4), 38.2 mol% (n = 8) and 50.7 mol% (n = 24). By increasing the temperature higher than 300 °C, the ethanol yield decreased, but the acetic acid recovery increased, indicating that oxidation of the product ethanol occurred for Ni-Sn/TiO_2 catalyst as reported for Ru-Sn/TiO_2 (Zhao et al., 2020). This will be discussed later more in detail.

When the reaction temperature was higher than 340 °C, the total (ethanol + acetic acid) recovery decreased, particularly for the catalyst with high metal loading (n = 24). Methane (CH_4) and carbon dioxide (CO_2) were the major gaseous products as discussed later in section 2.3. Because the corresponding temperature in the case of Ru-Sn/TiO_2 catalyst was 300 °C (Zhao et al., 2020), Ni catalyst was less effective for the production of gaseous products and exhibited better selectivity for the formation of ethanol against gaseous products than Ru catalyst at such high temperatures. This is a favorable property for the ethanol production.

The selectivity of ethanol formation also depended on the metal loading. For the catalyst with high metal loading (n = 24), the decrease in the total (ethanol + acetic acid) recovery as an indicator of gas production was great and the ethanol yield sharply decreased at such high temperatures. These results give insights into the reaction mechanism for hydrogenation of aqueous acetic acid, in which the interface between Ni-Sn alloy and TiO_2 is the active site for hydrogenation of acetic acid (Zhao et al., 2020). Acetic acid is activated by the coordination of Ti (Lewis acid site) and then attacked by the hydrogen that is activated on Ni-Sn alloy. Contrary to this, gasification may proceed on Ni-Sn, because the gas-forming reactivity was different depending on the metal species in Ni-Sn/TiO_2 and Ru-Sn/TiO_2. The above results support this hydrogenation mechanism that was proposed previously (Zhao et al., 2020), because the contribution of Ni-Sn becomes greater against that of the interface when Ni and Sn are overloaded. Similar tendency was reported in our previous paper (Zhao et al., 2020)

using a batch reactor.

Accordingly, the catalyst (n = 24) is not the intended catalyst, and the catalyst (n = 8) was used for the subsequent comparative study with 4wt%Ru-4wt%Sn/TiO_2, although the amount of metal loaded are not the same. As discussed later, Ni-Sn/TiO_2 catalyst was less efficient for the catalytic activity in hydrogenation of acetic acid to ethanol, while better in terms of the gas-by-production.

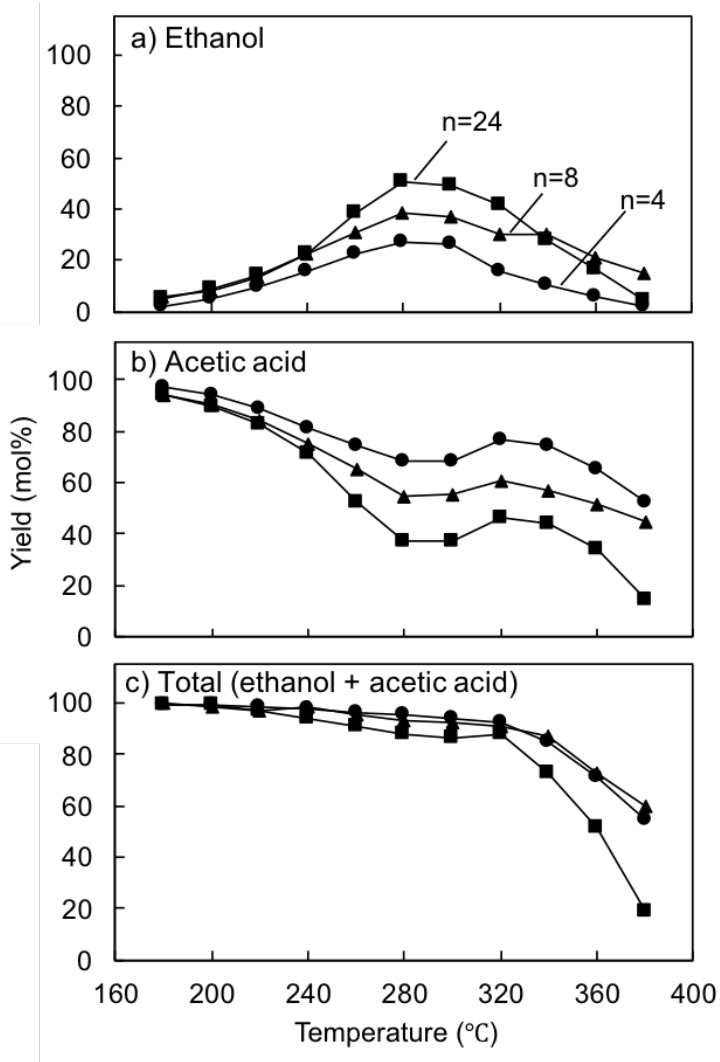

Fig. 4-1 Effect of metal loading amount on the hydrogenation of aqueous acetic acid (10g/L) over nwt%Ni-nwt%Sn/TiO_2 (n=4, 8 or 24): (a) EtOH; (b) AcOH; (c) total (EtOH + AcOH) (column size: 3.9-mm inner diameter, 100-mm length; pump flow rate, 0.3 mL/min; H_2 flow rate, 60 mL/min; pressure, 10 MPa).

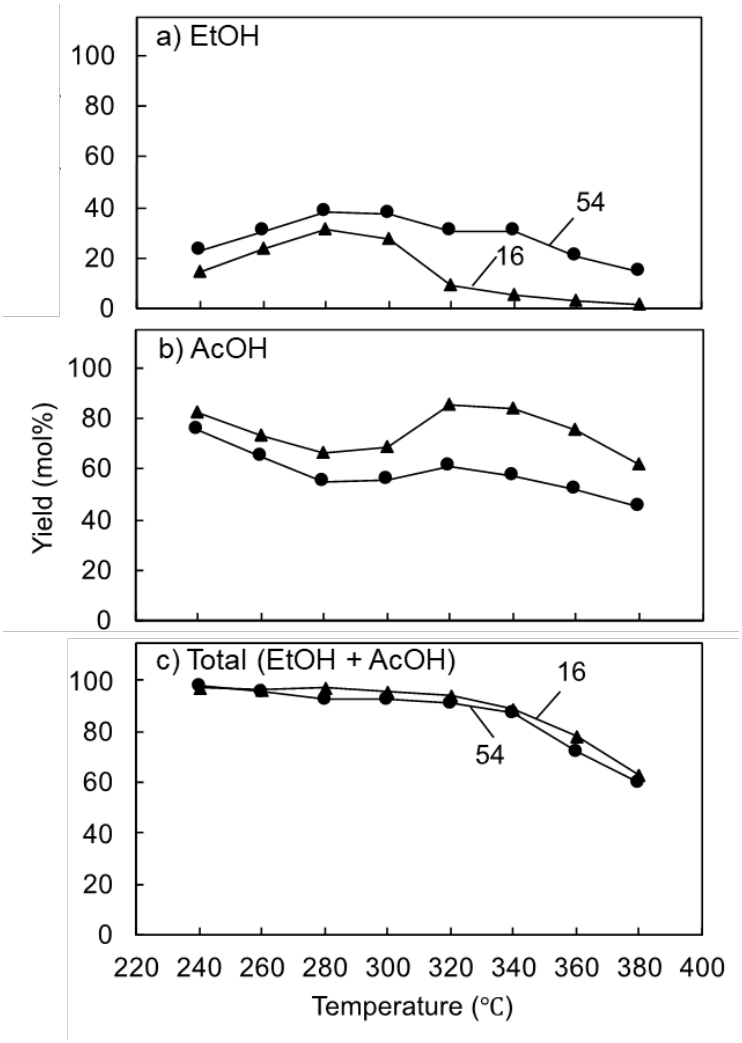

Fig. 4-2 Effect of H_2/acetic acid molar ratio on hydrogenation of aqueous acetic acid (10g/L) over 8wt%Ni-8wt%Sn/TiO_2 (column size: 3.9-mm inner diameter, 100-mm length; pump flow rate, 0.3 mL/min; H_2 flow rate, 60 mL/min; pressure, 10 MPa).

Fig. 4-2 shows the results of hydrogenation of aqueous acetic acid over 8wt%Ni-8wt%Sn/TiO_2 at the H_2/AcOH molar ratios of 16 and 54, which was changed by using different H_2 flow rates (14 and 60 ml/min) at a constant liquid flow rate of 0.3 mL/min. The ethanol yield decreased as the ratio decreased from 54 to 16, especially in the temperature range higher than 320 °C. In the case of Ru-Sn/TiO_2 (Zhao et al., 2020), similar effect was observed at temperatures higher than 280 °C, while the hydrogen amount was not rate-determining in the ethanol production at the lower temperatures.

Such difference may be due to the inefficiency of hydrogen activation by Ni-Sn/TiO_2 than by Ru-Sn/TiO_2, although further investigation is necessary to conclude it. The commonly observed effects in the higher temperature range were explained in the previous study [22] by the progress of oxidation of product ethanol, which became effective at such high temperatures. These results support the occurrence of ethanol oxidation during hydrogenation of aqueous acetic acid over Ni-Sn/TiO_2.

4.3.2 Effect of reaction pressure (water boiling)

The influences of the reaction pressure on hydrogenation of 10 g/L of aqueous acetic acid were investigated under similar reaction conditions at various pressures of 4, 6, 8.2 and 10 MPa. The results are shown in Fig. 4-3. Different temperature ranges were applied to 8wt%Ni-8wt%Sn/TiO_2 (200-380 °C) and 4wt%Ru-4wt%Sn/TiO_2 (160-320 °C) due to their different catalytic activities. Boiling of the solvent water alters the residence time by increasing the volume caused by the transition from liquid to gas. Therefore, the influences of reaction temperature on the residence time at each pressure were evaluated by the calculation with a software, Pro/II ver. 10.1 (Fig. 4-4). Table 4-1 summarizes the boiling point of water and relative residence time (liquid/gas) at each pressure. The boiling point increases by increasing the reaction pressure: 251 °C (4 MPa), 276 °C (6 MPa), 297 °C (8.2 MPa) and 312 °C (10 MPa). The relative residence time (liquid/gas) shows the opposite trend and is around 4-6, indicating that reaction time is shortened by 1/4 to 1/6 when the reaction temperature exceeds the boiling point of water. This temperature range is marked by the color bar in Fig. 4-3 and subsequent figures. Accordingly, it is necessary to consider the change in residence time and the difference in reactivity between gas and liquid phases for the following discussion.

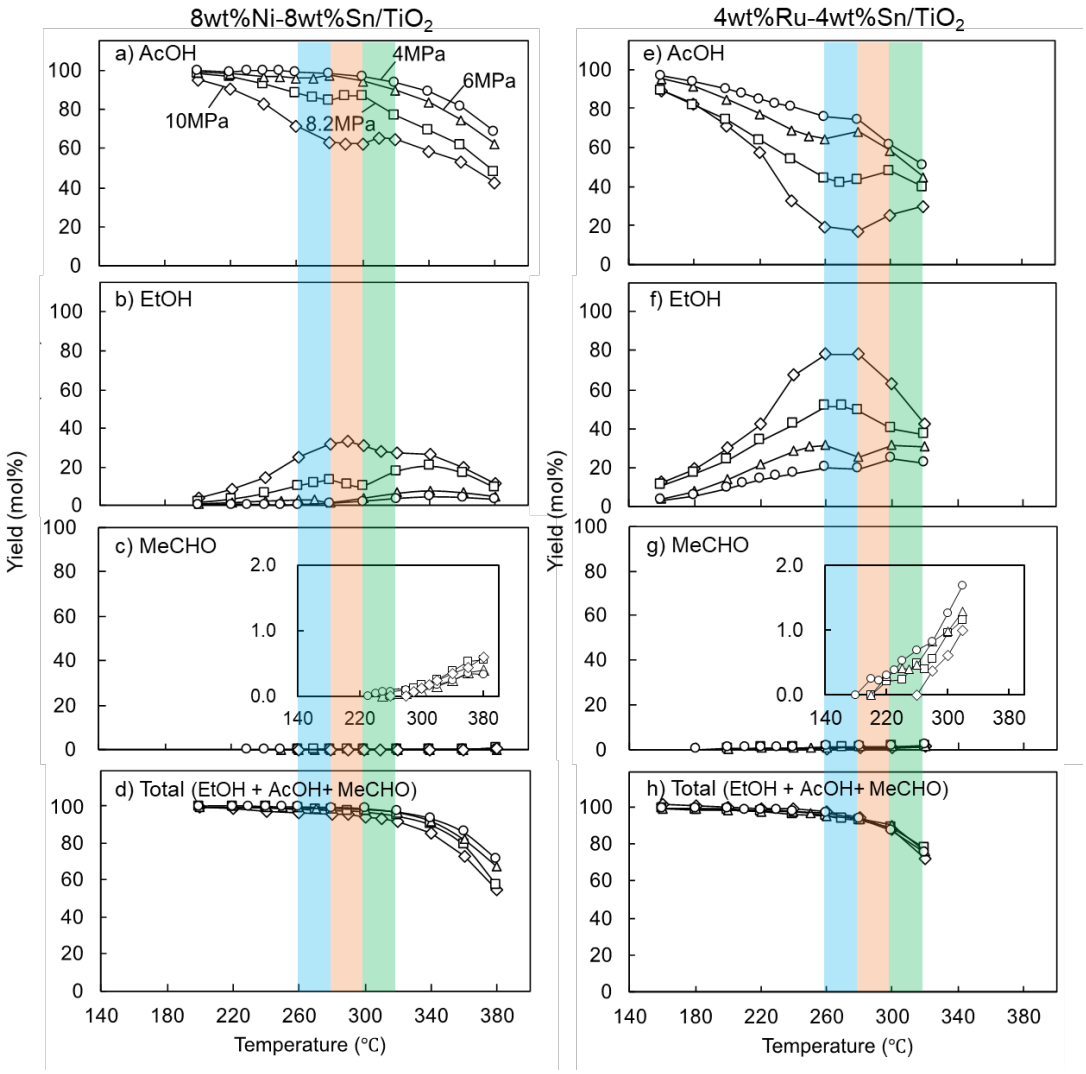

Fig. 4-3 Effect of reaction pressure on the hydrogenation of aqueous acetic acid (10g/L) over 8wt%Ni-8wt%Sn/TiO_2 and 4wt%Ru-4wt%Sn/TiO_2 at various reaction pressures of 4, 6, 8.2 and 10 MPa: (a, e) AcOH, (b, f) EtOH, (c, g) MeCHO, (d, h) total (EtOH + AcOH + MeCHO) (column size: 3.9-mm inner diameter, 100-mm length; pump flow rate, 0.3 mL/min; H_2 flow rate, 60 mL/min).

4wt%Ru-4wt%Sn/TiO_2 exhibited the better catalytic activity than 8wt%Ni-8wt%Sn/TiO_2 for the ethanol production, but the total (ethanol + acetic acid) recovery tended to be lower at >260 °C due to the gas formation (Zhao et al., 2020) (Fig. 4-3). The recovery rate of acetic acid showed the lowest value at a certain temperature and

then increased at the higher temperature range. Reaction pressure greatly affected this behavior; by lowering the reaction pressure, the temperature range with the lowest acetic acid recovery was lowered. Interestingly, this temperature range was in good agreement with the estimated boiling point of water at each pressure. Sorter residence time at the higher temperatures than the estimated boiling point of water would be a reason, while it is also necessary to pay attention to the change in reactivity due to the phase transition from the liquid phase to the gas phase. This will be discussed in the following sections.

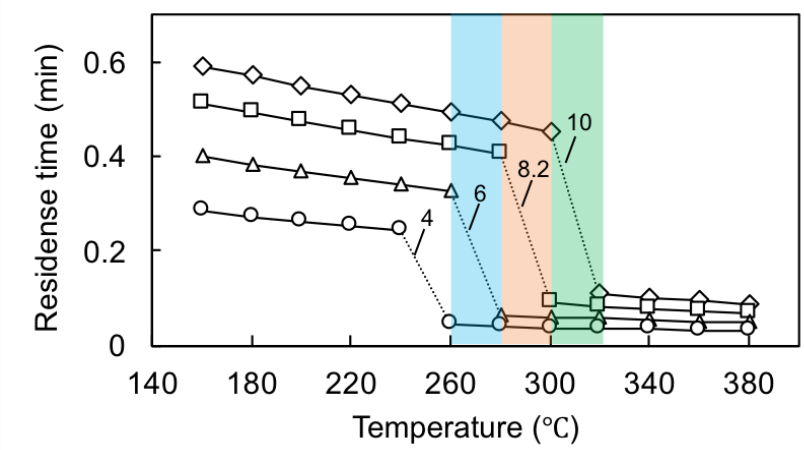

Fig. 4-4 Relationships between residence time and reaction temperature at various reaction pressures of 4, 6, 8.2 and 10 MPa (column size: 3.9-mm inner diameter, 100-mm length; pump flow rate, 0.3 mL/min; H_2 flow rate, 60 mL/min).

Table 4-1. Change of retention time and water boiling point depends on reaction pressures.

Pressure (MPa)	10	8.2	6	4
Water boiling point (°C)	312	297	276	251
Residence time liquid/ gas	4.5	4.4	5.0	5.7

4.3.3 Side reactions competing with ethanol production

In order to understand the effect of reaction pressure on hydrogenation of aqueous acetic acid solution, we investigated the side reactions in more detail, focusing on the differences between the two catalytic systems.

4.3.3.1 Oxidation of product ethanol

Conversion of aqueous ethanol (10 g/L) was performed using Ni and Ru catalysts under similar reaction conditions in the absence of hydrogen supply under the two reaction pressure conditions of 10 and 6 MPa. To understand the influence of hydrogen supply, the conversion under the hydrogenation conditions was also conducted at 6 MPa. In the absence of hydrogen supply, the reaction pressure was maintained by pumping the ethanol solution and no gas was supplied. The results are shown in Fig. 4-5.

Without the hydrogen supply, ethanol was converted to acetic acid from the temperatures as low as 200 °C and the acetic acid yield grew sharply at >280 °C and 10 MPa. This temperature range was lowered by decreasing the reaction pressure from 10 to 6 MPa and was in good agreement with the estimated boiling point of water at each pressure. Therefore, it is suggested that the oxidation reactivity was greatly improved at temperatures above the boiling point of water, where the transition from liquid water to steam (gas phase) occurred, even if the residence time was significantly shortened. Although the details of reaction mechanism are not known, steam can be activated on the catalyst surface more efficiently than liquid water. Formation of MeCHO, the intermediate of this oxidation, was very limited over the temperature range used in this study, indicating that the oxidation from ethanol to MeCHO is the

rate-determining step for this conversion, and that MeCHO is simultaneously oxidized to acetic acid on the catalyst surface.

These trends were basically the same between 8wt%Ni-8wt%Sn/TiO_2 and 4wt%Ru-4wt%Sn/TiO_2, except for the total (EtOH + AcOH + MeCHO) yield that decreased sharply at the temperatures above 300 °C at 10 MPa in the case of the Ru catalyst due to the progress of gas production. This temperature range was also lowered by lowering the reaction pressure from 10 to 6 MPa, as observed for the oxidation of ethanol. This will be discussed in the gas formation section. Therefore, some structure, which is commonly present in both catalysts, would be the active site for the oxidation of ethanol, while the efficient gasification with the Ru catalyst would occur on Ru-Sn.

The formation of ethanol was suppressed by the hydrogen supply but was not completely inhibited, which is the direct evidence for the oxidation of product ethanol that competes with the hydrogenation of acetic acid to ethanol. Reduced reaction rate of ethanol oxidation in the presence of hydrogen may be attributed to the dilution of ethanol and steam by hydrogen, because steam is suggested to act as an oxidant that is activated on the catalyst surface (Zhao et al., 2020).

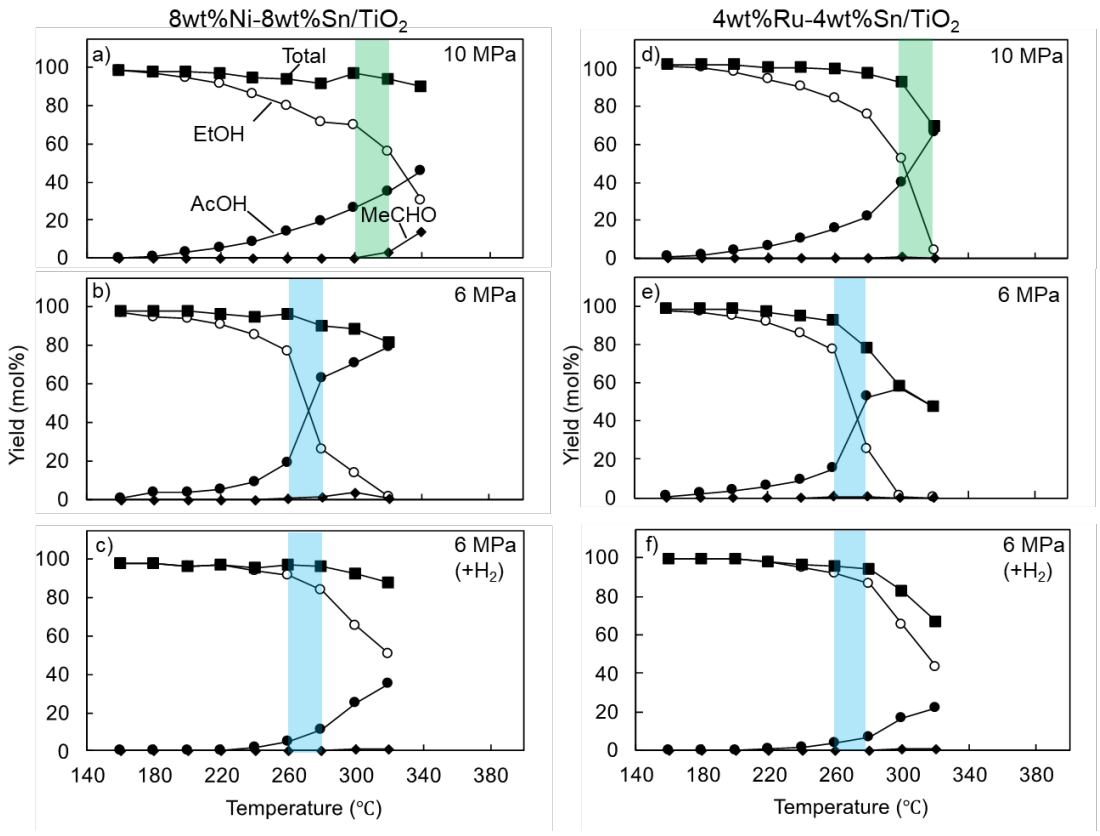

Fig. 4-5 Effect of reaction pressure on the conversion of aqueous ethanol (10 g/L) over 8wt%Ni-8wt%Sn/TiO_2 and 4wt%Ru-4wt%Sn/TiO_2 without hydrogen supply: (a, d) 10MPa (b, e), (c,f) Effect of reaction pressure on the conversion of aqueous ethanol with H_2 (60 mL/min) supply, 6MPa (column size: 3.9-mm inner diameter, 100-mm length; pump flow rate, 0.3 mL/min).

4.3.3.2 Gas formation

Gas formation during the hydrogenation of aqueous acetic acid was not so important for the Ni catalysts but produced CH_4 and CO_2 at the higher reaction temperatures than 340 °C under the 10 MPa trial of Fig. 4-3 (Fig. 4-6), although their yields were quite small even at such high temperatures. As observed with the Ru catalyst (Zhao et al., 2020), CH_4 and CO_2 were produced in similar molar yields,

indicating that the C–C bond in acetic acid is cleaved to produce equimolar amounts of CH_4 and CO_2.

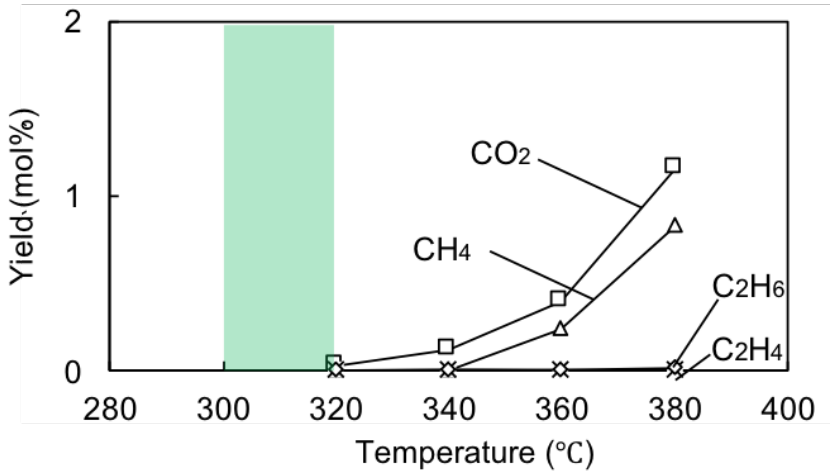

Fig. 4-6 Formation of gaseous products in the hydrogenation of aqueous acetic acid (10 g/L) over 8wt%Ni-8wt%Sn/TiO_2 (column size: 3.9-mm inner diameter, 100-mm length; pump flow rate, 0.3 mL/min; H_2 flow rate, 60 mL/min; pressure, 10 MPa).

The gas formation was more significant for the Ru catalysts. However, the formation mechanisms have not been fully clarified yet. Without the hydrogen supply, both treatment of aqueous acetic acid and aqueous ethanol produced gaseous products at > 300 °C, but the gas yields were greater from ethanol than from acetic acid: gas yield (320 °C, 4wt%Ru-4wt%Sn/TiO_2): CH_4 (13 mol%), CO_2 (21 mol%) from EtOH; CH_4 (5 mol%), CO_2 (3 mol%) from AcOH) (Zhao et al., 2020). Thus, the yields were 2.6-7 times greater from ethanol. In addition, the formation of these gaseous products occurred in the lower temperature range in hydrogenation of aqueous acetic acid. Based on these results, we considered that other gas formation pathways must exist in the hydrogenation using Ru catalysts.

In the present study, we found that, by lowering the reaction pressure from 10 to 6 MPa, the oxidation reaction of ethanol occurred at the lower temperatures and that the decrease in the total recovery (EtOH + AcOH + MeCHO) became greater. This indicates that the gas formation was enhanced by lowering the reaction pressure. Accordingly, the yields of gaseous products during the conversion of aqueous ethanol (no hydrogen supply conditions) are compared at 10 and 6 MPa (Fig. 4-7). The gas formation was significantly improved by lowering the reaction pressure even for the Ni catalyst. Hydrogen may be produced as a by-product in the oxidation of ethanol, in which water (steam) is utilized as an oxidant. In this system, gas formation from acetic acid and acetaldehyde, both of which are the oxidation products of ethanol, must be considered along with ethanol for the discussion of the gas formation pathway.

To understand the role of gasification of acetic acid, recovery data of acetic acid in the conversion of aqueous acetic acid over the Ru and Ni catalysts at 10 and 6 MPa are shown in Fig. 8. In this system, acetaldehyde and ethanol are not produced, and hence, the results indicate the stability of acetic acid against gasification and other reactions. In the previous paper with the Ru catalysts (Zhao et al., 2020), the decrease in the acetic acid recovery at >280 °C (10 MPa) was explained by the formation of CH_4 and CO_2. By lowering the reaction pressure from 10 to 6 MPa, the acetic acid recovery slightly decreased in the case of Ru catalyst, but the degree of decrease was smaller than that observed for the ethanol conversion (Fig. 4-5 and 4-7). No influences were observed in the case of Ni catalyst. Therefore, such large increase in the gas yield by lowering the reaction pressure is not explained by the gasification of acetic acid.

Gas formation pathways can be reasonably drawn in Fig. 4-9 from the viewpoint of synthetic organic chemistry. Because the oxidation states are different, the cleavage of the C–C bonds of acetic acid, acetaldehyde, and ethanol gives CO_2, CO, and formaldehyde, respectively, along with CH_4. The production of CH_4 and CO_2 is

reasonably explained by the acetic acid pathway, and in the acetaldehyde pathway, CO is suggested to be converted to CO_2 and H_2 through water gas shift reaction (equation 4.3) as discussed in our previous study (Zhao et al., 2020) and the literature reporting the catalytic conversion of ethanol in water (Nozawa et al., 2015). However, the selective formation of CO_2 from formaldehyde is difficult to explain. Formaldehyde formed from the ethanol pathway may remain in the reaction mixture or be oxidized to formic acid, instead of the formation of CO_2.

$$CO + H_2O \rightarrow H_2 + CO_2 \quad (4.3)$$

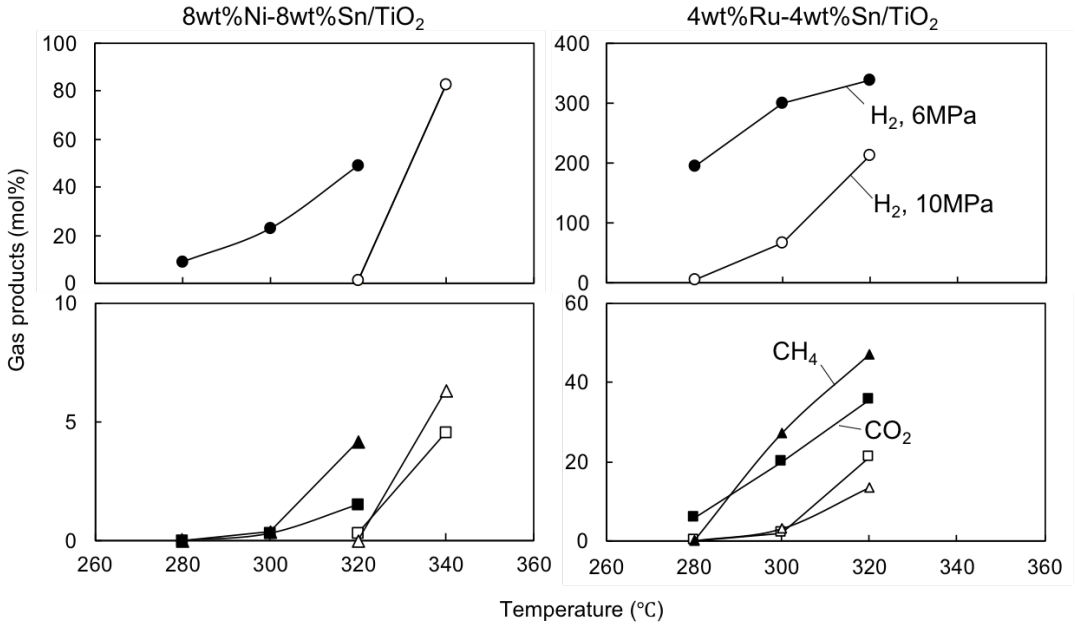

Fig. 4-7 Formation of gaseous products in the conversion of aqueous ethanol (10 g/L) over 8wt%Ni-8wt%Sn/TiO_2 and 4wt%Ru-4wt%Sn/TiO_2 without hydrogen supply at 6 MPa (solid symbols) and 10 MPa (open symbols) (column size: 3.9-mm inner diameter, 100-mm length; pump flow rate, 0.3 mL/min).

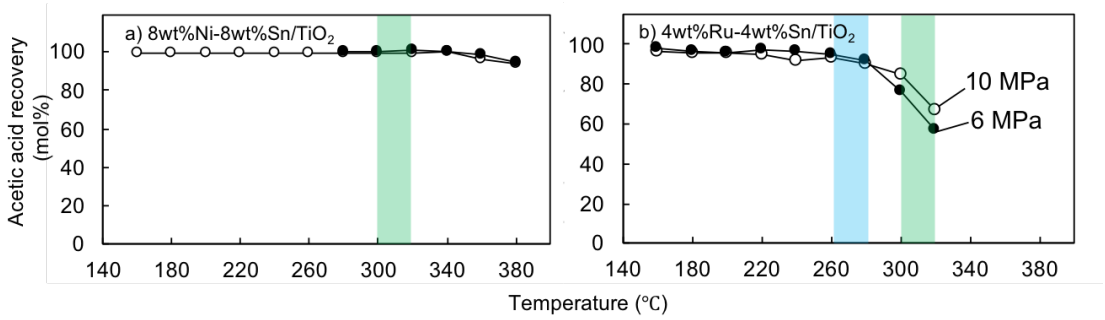

Fig. 4-8 Effect of reaction temperature on the conversion of aqueous acetic acid (10 g/L) over (a) 8wt%Ni-8wt%Sn/TiO_2 and (b) 4wt%Ru-4wt%Sn/TiO_2 without hydrogen supply at 6 MPa (solid symbols) and 10 MPa (open symbols) (column size: 3.9-mm inner diameter, 100-mm length; pump flow rate, 0.3 mL/min).

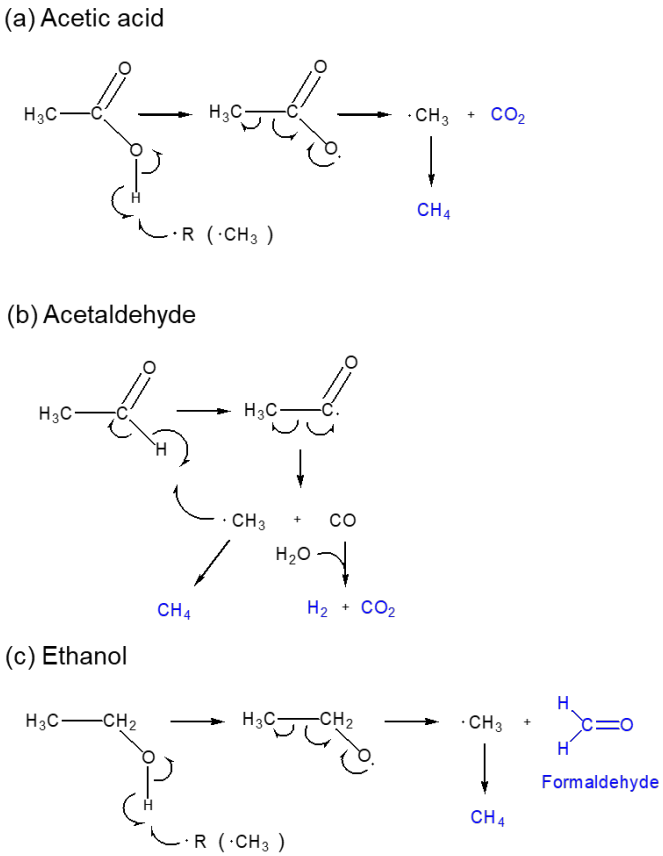

Fig. 4-9 Reasonably drawn fragmentation pathways of acetic acid, acetaldehyde, and ethanol to CH_4, CO_2, and H_2.

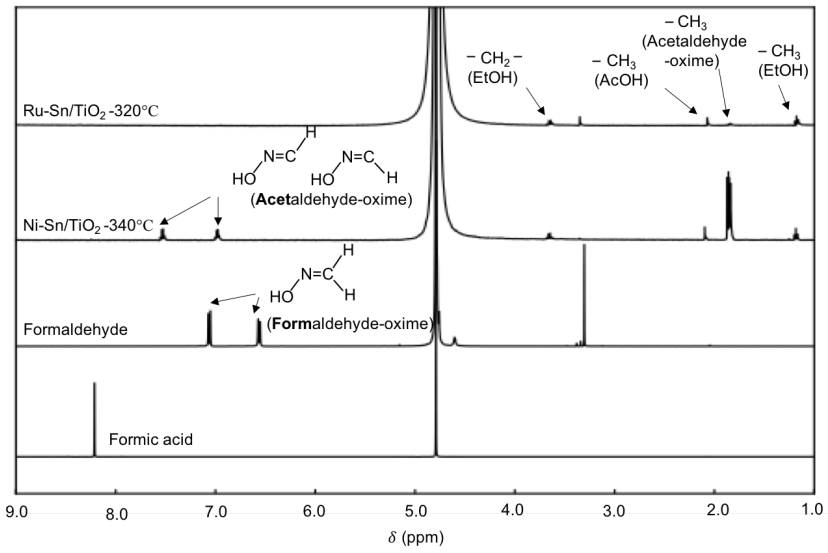

Fig. 4-10 ^{1}H-NMR spectra of the gaseous products from the conversion aqueous ethanol (10 g/L) recovered by bubbling into D_2O containing an oximation reagent (NH_2OH•HCl) for 1 h (8wt%Ni-8wt%Sn/TiO_2 (340 °C) and 4wt%Ru-4wt%Sn/TiO_2 (320 °C); column size, 3.9-mm inner diameter, 100-mm length; pump flow rate, 0.3 mL/min; no H_2 supply; pressure, 6 MPa).

To conclude the above discussion, the gaseous products formed by the conversion of aqueous ethanol using 4wt%Ru-4wt%Sn/TiO_2 at 6 MPa/ 320 °C were collected by bubbling into D_2O that contained an oximation reagent (NH_2OH•HCl) for 1 h. When aldehydes and ketones are included, these are converted to the oxime derivatives during the collection process and can be analyzed by ^{1}H-nuclear magnetic resonance (NMR). Similar experiments were also conducted for the gaseous products by using 8wt%Ni-8wt%Sn/TiO_2 at 6 MPa/ 340 °C. The NMR spectra are shown in Fig. 4-10 along with those of formaldehyde (oxime) and formic acid. Any formaldehyde and formic acid are not detected in these spectra obtained by the conversion of aqueous

ethanol, indicating that the gas formation through the ethanol pathway is not important under the present experimental conditions.

Based on these results, it is suggested that CO_2 and CH_4 were produced from acetic acid and acetaldehyde when the Ru catalyst was used. The greater gas productivity from ethanol than from acetic acid indicates that acetaldehyde is more reactive for the gasification, although the amounts of acetaldehyde detected in the products were only small (Fig. 4-3 and 4-5).

4.3.3.3 Role of acetaldehyde - Cannizzaro reaction

To investigate the role of acetaldehyde detection in acetic acid hydrogenation, 10 g/L aqueous acetaldehyde was subject to hydrogenation reaction under the similar reaction conditions used for acetic acid hydrogenation over 8wt%Ni-8wt%Sn/TiO_2 at 10 MPa, obtained liquid products results shows in Fig. 4-11.

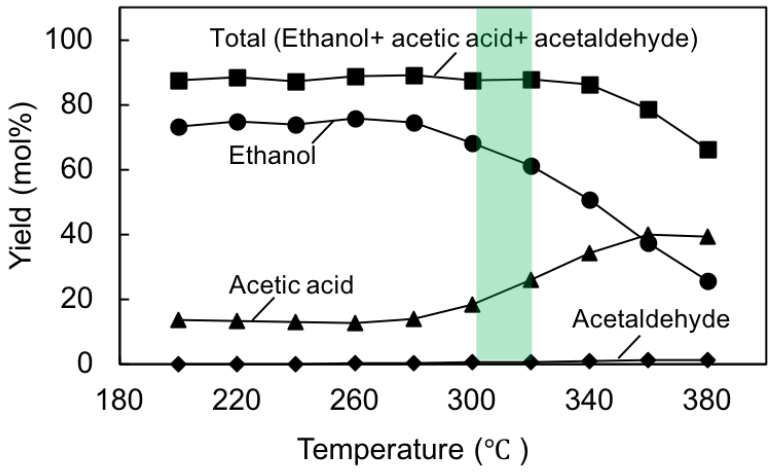

Fig. 4-11 Conversion of aqueous acetaldehyde (10 g/L) under hydrogenation conditions over 8wt%Ni-8wt%Sn/TiO_2 (column size: 3.9-mm inner diameter, 100-mm length; pump flow rate, 0.3 mL/min; H_2 flow rate, 60 mL/min; pressure, 10 MPa).

Acetaldehyde almost completely reacted, and ethanol formed under such conditions. Unexpectedly, acetic acid was found to be produced even under hydrogen conditions, which will be discussed later. When temperature higher than 300 °C ethanol conversion decreased and acetic acid increased, which due to the ethanol oxidation.

It was reported that two molecules of non-enolizable aldehyde give primary alcohol and a carboxylic acid through Cannizzaro-type reaction in either alkaline or hot compress water conditions (Geissman, 2004; Nagai et al., 2003). Since the hydrogenation reaction was conducted with the hot compress water conditions, acetic acid might be produced from Cannizzaro-type reaction. To clarify this hypothesis, the reactivity of 10 g/L aqueous acetaldehyde was investigated under hydrothermal conditions over 8wt%Ni-8wt%Sn/TiO_2 and 4wt%Ru-4wt%Sn/TiO_2 at 10 MPa, and the results show in Fig. 4-12. In the temperature range of 200-260 °C, similar results were obtained using both catalysts, acetaldehyde was completely reacted, and almost equimolar amounts of ethanol and acetic acid were produced, which supports the hypothesis that the acetic acid was produced from Cannizzaro type reaction. When the temperature was higher than 300°C which water started boiling, different performance shows in two catalysts. With the 8wt%Ni-8wt%Sn/TiO_2, acetic acid yield significantly tended to be increased, which indicated the ethanol oxidation promoted, and a light gasification occurred at 380 °C. With the 4wt%Ru-4wt%Sn/TiO_2, and ethanol yield and total yield sharply decreased, which indicated that the gasification and oxidation of acetaldehyde were more selectively under such conditions.

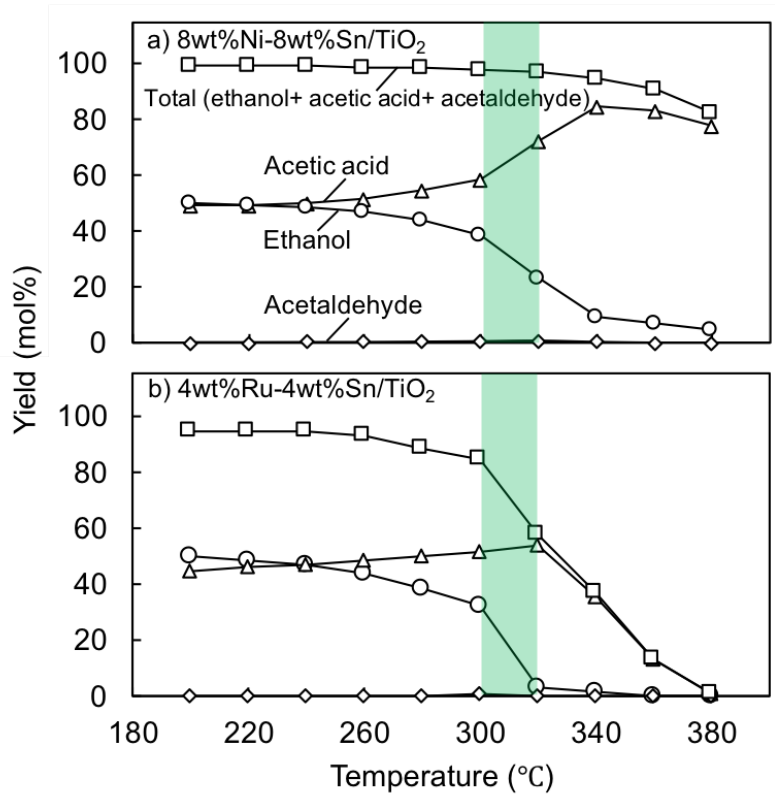

Fig. 4-12 Conversion of 10 g/L aqueous acetaldehyde under hydrothermal conditions over (a) 8wt%Ni-8wt%Sn/TiO_2 and (b) 4wt%Ru-4wt%Sn/TiO_2 (column size: 3.9-mm inner diameter, 100-mm length; pump flow rate, 0.3 mL/min; 10 MPa).

Consequently, based on the present results, the reaction mechanisms during hydrogenation of aqueous acetic acid over Ni-Sn/TiO_2 and Ru-Sn/TiO_2 catalysts in flow reactor are proposed in Fig. 4-13. Oxidation of product ethanol occurs and competes with the hydrogenation of acetic acid to form ethanol. Accordingly, this conversion is characteristic of reversible reaction and the yield of ethanol depends on the equilibrium ethanol/ acetic acid molar ratio (Zhao et al., 2020). The results of current study revealed that the oxidation of ethanol (back reaction) is accelerated when the solvent water is transitioned from liquid to steam (gas), which is governed by the temperature/ pressure conditions. This provide insights into the ethanol production with this method. At a certain temperature, by lowering the reaction pressure enough for solvent water to boil,

the ethanol production (forward reaction) is suppressed by decreasing the reaction time and the partial pressure of hydrogen, whereas the ethanol oxidation (back reaction) becomes very significant. Consequently, the effects of reaction pressure are significant and greater than expected only from the reactivity of the forward reaction (Fig. 4-3).

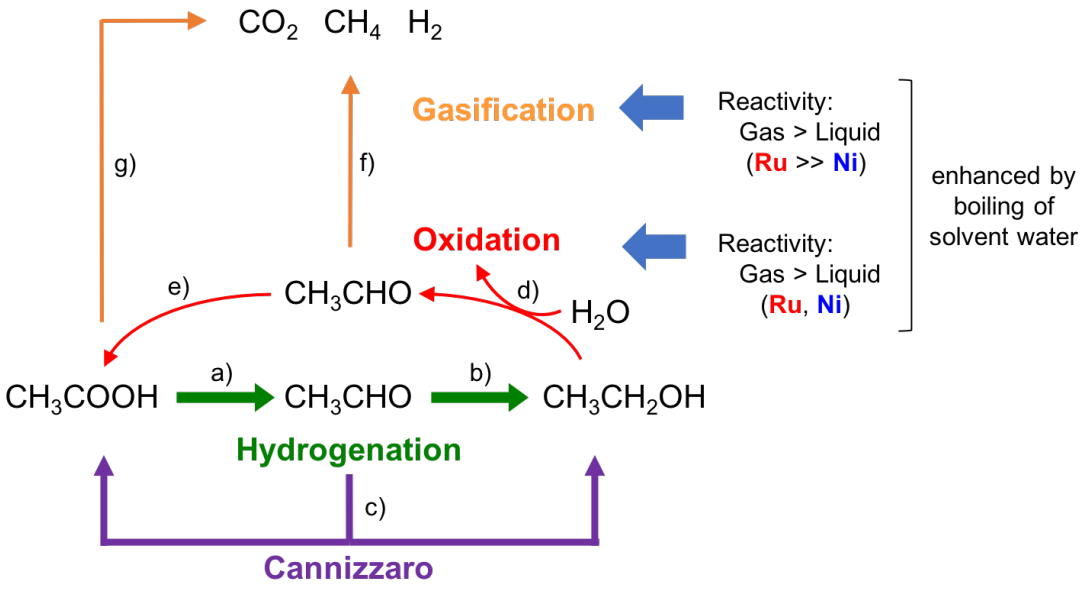

Fig. 4-13 The competitive reaction routes with hydrogenation of aqueous acetic acid.

Another side reaction that reduces the ethanol productivity is gasification to form CO_2, CH_4 and H_2. The catalytic activity for this gasification is much greater for the Ru catalysts than for the Ni catalysts. Gasification would occur via acetic acid and formaldehyde (the hydrogenation/ oxidation intermediate), while the ethanol pathway would not be important. The nature of the reversible reaction (AcOH ⇆ MeCHO ⇆ EtOH) may enhance the gas by-production, since acetaldehyde that is more reactive than acetic acid is continuously regenerated along with acetic acid by the ethanol oxidation. Therefore, in the prolonged reaction, the ethanol yield decreases due to the gasification of acetaldehyde even at relatively low temperatures. Lowering the reaction pressure accelerates the gas production by enhancing the ethanol oxidation.

Moreover, after the ethanol reduce to acetaldehyde, the Cannizzaro type reaction

take place via acetaldehyde in hydrogenation of acetic acid as a side reaction. And the reactivity of Cannizzaro type reaction is extremely high even at the lower temperatures, which actually suppressed the selectivity of gasification which can actually improving the hydrogenation activity.

4.3.4 Catalytic performance at longer residence time

With the fore mentioned hydrogenation conditions using the narrow column, the residence time was too short to convert aqueous acetic acid to ethanol efficiently, particularly for the Ni catalysts. Due to the limitation of the experimental unit (H-Cube Pro^{TM}), we could not change the size of catalyst column freely, but the residence time can be prolonged 12 times by using a wide column, which is 2.4 times wider and 2.1 times longer than the narrow column. Fig. 4-14 shows the results of the trials using this wide column for hydrogenation of 10 g/L aqueous acetic acid over 8wt%Ni-8wt%Sn/TiO_2 and 4wt%Ru-4wt%Sn/TiO_2. Different flow rates of acetic acid solution (0.3, 0.6, 0.9, and 2.4 mL/min) were utilized at a constant rate of hydrogen supply (60 mL/min), because this is the maximum that could be used in this unit. Accordingly, the hydrogen/ acetic acid molar ratio varied depending on the flow rate of acetic acid solution: 54 (0.3), 27 (0.6), 18 (0.9), 6.8 (2.4) (figures in the parentheses: flow rate of acetic acid solution, mL/min). The results using the Ru catalyst at a acetic acid flow rate of 0.3 mL/min are adopted from literature (Zhao et al., 2020). The reaction temperatures used in the experiments are lower than the estimated boiling point of water at 10 MPa (312 °C), and hence undesired gas phase reactions were avoided.

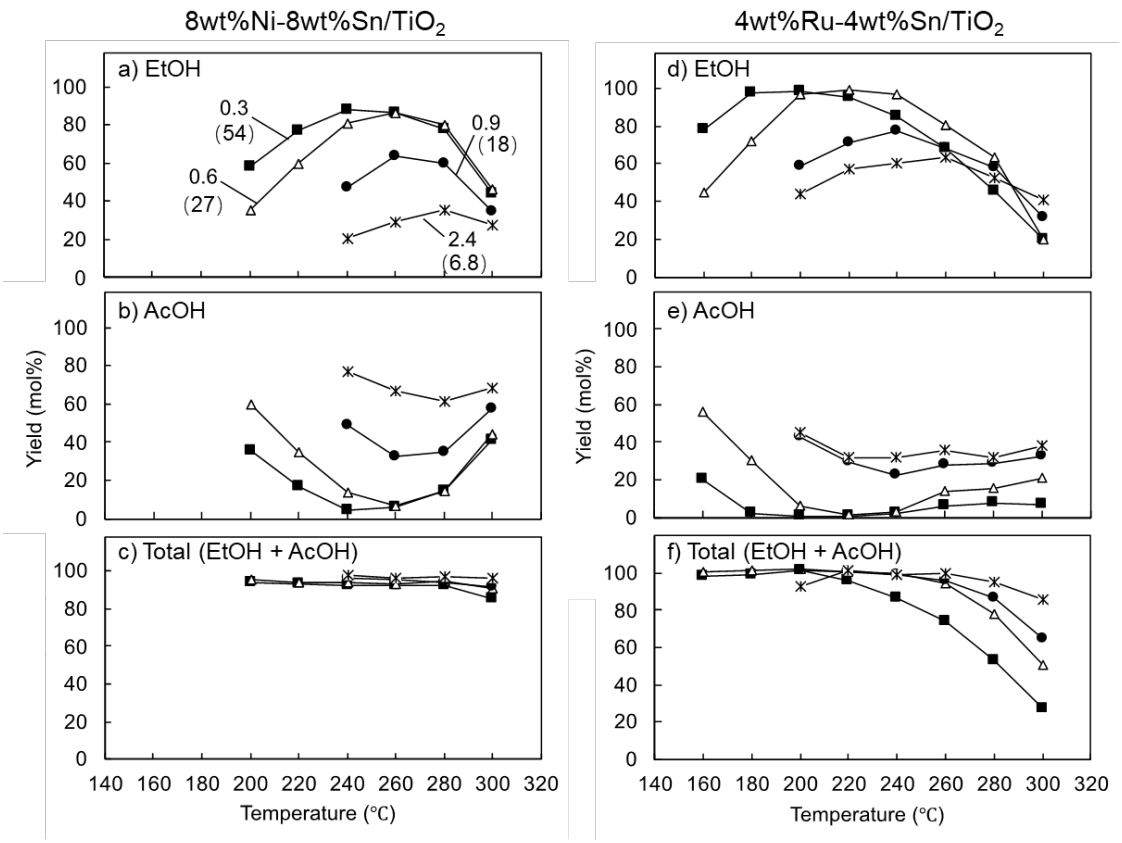

Fig. 4-14 The ethanol productivity of hydrogenation of aqueous acetic acid (10 g/L) over 8wt%Ni-8wt%Sn/TiO_2 and 4wt%Ru-4wt%Sn/TiO_2 with the wide column (a, d) EtOH (b, e) AcOH (c, f) total (EtOH + AcOH + MeCHO) (column size, 9.4-mm inner diameter, 210-mm length; H_2 flow, 60 mL/min; pressure, 10 MPa; flow rate (mL/min) (H_2/ AcOH molar ratio): 0.3 (54), 0.6 (27), 0.9 (18) and 2.4 (6.8)).

For the Ru catalyst, a 98 mol% of ethanol yield was achieved at 200 °C and the residence time of 6.7 min at the acetic acid flow rate of 0.3 mL/min (liquid hourly space velocity (LHSV): 1.23 h^{-1}), although this optimum temperature (200 °C) was lower than that with the narrow column (280 °C) (Zhao et al., 2020). By using the Ni catalyst under the similar flow rate and LHSV conditions, ethanol was obtained in an 88 mol% yield at 240 °C. Accordingly, by prolonging the residence time, the Ni catalyst also effectively produced ethanol from aqueous acetic acid.

For both catalysts, the ethanol yield decreased by raising the reaction temperature further from the optimum due to the increasing efficiency of the ethanol oxidation (back reaction). In the case of Ru, ethanol yields further decreased by the gas production, which can be recognized by the decrease in the total (EtOH + AcOH) recovery. This is an important characteristic of the two catalysts. When the Ru catalyst was used, the gas production occurred at temperatures >220 °C, which is lower than expected from the results with the narrow column (Fig. 4-7 and 4-8). Prolonged residence time enhanced the gas production via the acetaldehyde pathway as discussed earlier. Consequently, the Ni catalyst produced ethanol more efficiently at relatively high temperatures, and it is easier to control the side reactions.

4.4 Conclusions

Hydrogenation of 10 g/L aqueous acetic acid was investigated in a flow reactor and the catalytic activities were compared for 8wt%Ni-8wt%Sn/TiO_2 and 4wt%Ru-4wt%Sn/TiO_2 catalysts, focusing on the effects of reaction pressure and side reactions. The following conclusions were obtained:

1. Catalytic activity for the hydrogenation of aqueous acetic acid was lower for the Ni catalyst than the Ru catalyst, whereas the Ni catalyst was better in terms of the gas by-production.
2. The ethanol productivity showed the maximum at a certain temperature and decreased by increasing the reaction temperature further. This deceleration temperature range decreased by lowering the reaction pressure and well coincided with the boiling point of solvent water at each pressure.
3. The results of model experiments using aqueous ethanol indicated that the oxidation of ethanol (reverse of the hydrogenation of acetic acid) was significantly enhanced by the boiling of solvent water even at the shorter residence time. Therefore, the ethanol oxidation occurred more efficiently under steam than in liquid water, which reasonably explains the deceleration of ethanol production above the boiling point of solvent water.
4. The gasification of aqueous ethanol to CH_4, CO_2 and H_2 was accelerated particularly over the Ru catalyst by the boiling of solvent water. This reduced the ethanol yield further even at relatively low temperature such as 220 °C when the Ru catalyst was used.
5. The gas formation pathways via acetaldehyde and acetic acid were suggested, but the ethanol pathway was not important.
6. The Cannizzaro type reaction take place via acetaldehyde in hydrogenation of acetic acid as a side reaction, which actually suppressed the selectivity of gasification that can actually improving the hydrogenation activity.

7. Reaction mechanisms are proposed to explain the effects of reaction pressure and different performance of the Ni and Ru catalysts.
8. By prolonging the residence time to 6.7 min, the Ni catalyst efficiently produced ethanol from aqueous acetic acid. The Ni catalysts was better than the Ru catalysts in terms of the control of side reactions, particularly gas production.
9. Such information helps to exploit more efficient catalysts and to produce bioethanol from aqueous acetic acid obtained by fermentation.

.

Chapter 5

Stability of Ni-Sn/TiO_2 and Ru-Sn/TiO_2 catalysts in hydrogenation of aqueous acetic acid into ethanol

5.1 Introduction

Declining of the fossil fuel reservoirs and environmental issues drive the development of the utilization of renewable fuels to suppress the reliance on fossil fuel and to minimize the greenhouse gas emissions for the prevention of global warming (Comiso and Hall, 2014; Intergovernmental Panel on Climate Change (IPCC), 2014; "International Energy Agency (IEA): the total primary energy supply (TPES),(2017)," n.d.; International Energy Agency (IEA), 2013). Bioethanol is known as a renewable and environmentally friendly fuel alternative to gasoline (Dodić et al., 2009; Kim and Dale, 2004; Urry, 2014; Yang et al., 2012). Presently, bioethanol is produced by fermenting sugar to alcohol using yeast, which reduces the efficiency of carbon utilization by releasing two carbon atoms in glucose as CO_2 (Schell et al., 1990; Takagi et al., 1977). Hence, a new bioethanol production process using acetic acid fermentation that can theoretically convert all carbon atoms in glucose into acetic acid (Saka et al., 2019).

This new process includes hot-compressed water treatment to hydrolyze lignocellulosics, acetic acid fermentation, and hydrogenation of acetic acid (Saka et al., 2019). This study is focused on the last step, to hydrogenation of aqueous acetic acid numerous metal catalysts supported on metal oxides such as TiO_2 or Al_2O_3 have been studied (Besson et al., 2014; Cheah et al., 1992; Chen et al., 2014; Ito et al., 2016; Kawamoto et al., 2016; Mendes et al., 2001; Tahara et al., 1997; Wan et al., 2013; Zhang et al., 2013; Zhao et al., 2020). Our research group has found that Ru-Sn and Ni-

Sn on titanium oxide (TiO_2) can work as highly efficient catalysts that can convert mire than 90 mol% of ethanol in hydrogenation of aqueous acetic acid with a batch type reactor, but a long reaction time of 12 hours are necessary. (Ito et al., 2016; Zhao et al., 2020).

Furthermore, using a flow reactor has many advantages over batch type for catalytic conversions, such as improve selectivity and reducing reaction time (Durndell et al., 2015; Gómez-Quero et al., 2011; Numwong et al., 2012; Olcay et al., 2014; Osako et al., 2017; Wang et al., 2018; Yu et al., 2020; Zhao et al., 2020). In the previous study, we found that 98 mol% and 88 mol% of ethanol can be obtained over Ru-Sn/TiO_2 and Ni-Sn/TiO_2 with a flow type reactor which shows higher selectivity to ethanol and reduced the reaction time to 6.7 min, which has great advantages for the new bioethanol process (Zhao et al., 2020).

5.2 Experimental

5.2.1 Materials and catalyst preparation

Titanium isopropoxide (>95% purity), ruthenium (III) chloride hexahydrate ($RuCl_3$), nickel (II) chloride hexahydrate ($NiCl_2{\cdot}6H_2O$, >98%), tin (II) chloride dihydrate ($SnCl_2{\cdot}2H_2O$, >97%), sodium hydroxide (NaOH, >97%), 2-propanol (>99%), and aqueous hydrochloric acid (HCl, 6 mol/L) were used for catalyst preparation. Acetic acid (AcOH, >99%), acetaldehyde (AA, >90%), and ethanol (EtOH, >99.5%) were used as aqueous solutions for the hydrogenation reaction. $RuCl_3$ was purchased from Tokyo Chemical Industry Co. Ltd, Tokyo, Japan, and other materials were from

Nacalai Tesque, Inc., Kyoto, Japan. Hydrogen (H_2, > 99.9%) was provided by Imamura Sanso, Co. Ltd., Shiga, Japan.

Catalysts were prepared by the sol-gel sedimentation method (Ito et al., 2016; Zhao et al., 2020). Designated amounts of $NiCl_2 \cdot 6H_2O$ or $RuCl_3$ with $SnCl_2 \cdot 2H_2O$ were added to water (100 mL, 60 °C) as Ni, Ru, and Sn precursors, respectively. A mixture of titanium isopropoxide and 2-propanol was added dropwise to the aqueous solution of $RuCl_3$ + $SnCl_2$ or $NiCl_2$ + $SnCl_2$ with stirring at 60 °C. After stirring for another 30 min, an aqueous NaOH solution (100 mL, sufficient concentration to neutralize the metal chlorides) was added, and the mixture was stirred for 0.5 h. During this period, $RuCl_2$, $NiCl_2$, and $SnCl_2$ were converted to $Ru(OH)_3$, $Ni(OH)_2$, and $Sn(OH)_2$, respectively, and then deposited on the TiO_2 surface. The mixture was allowed to stand for 12 h, and the obtained precipitate was washed five times with water and oven-dried at 105 °C overnight. The precipitate was calcinated at 450 °C under an air flow (100 mL/min) for 1 h and then reduced at 400 °C under a H_2 flow (100 mL/min) for 2 h. The prepared catalysts were sieved to adjust the particle size 50–70 μm and packed into catalyst column.

5.2.2 Catalyst characterization

The fresh and spend catalysts were analyzed by X-ray diffraction (XRD; RINT 2000 V, Rigaku Corp., Tokyo, Japan), and the XRD patterns were identified by comparison to a database (AtomWork, National Institute for Materials Science, Ibaraki, Japan). The catalyst surface, dispersion of metals, and particle size were observed by scanning electron microscope (SEM; SU6600, Hitachi High-Technologies Corp., Tokyo, Japan), and field emission transmission electron microscope (FE-TEM; JEM-2100F, JEOL Ltd., Tokyo, Japan). The states of metals on catalyst surface were

determined by X- ray photoelectron spectroscopy (XPS; JPS-9030, JEOL Ltd., Tokyo, Japan).

5.2.3 Durability study

The flow-type reaction system consists of a flow-type reactor (H-Cube Pro™, ThalesNano Inc., Budapest, Hungary), an electric furnace (Phoenix, ThalesNano Inc.), and a mass flow controller (Gas Module, ThalesNano Inc.) (Jones et al., 2006). The configuration and operation of the flow-type system were introduced in detail in our previous study (Zhao et al., 2020). For durability study, prepared 4wt%Ru-4wt%Sn/TiO_2 and 4wt%Ni-4wt%Sn/TiO_2 catalysts were fixed into the catalyst column (inner diameter, 3.9 mm; catalyst-packed length, 100 mm), the aqueous solution of acetic acid (10 g/L, 0.3 mL/min) and H_2 (60 mL/min) were supplied to the catalyst column by using a pump and the mass flow controller, respectively. The pressure in the reaction system was maintained by a back-pressure regulator, and set at 10 MPa. After being cooled by a heat-exchanger, the resulting liquid was collected and analyzed by HPLC.

5.2.4 Analytical methods

The liquid products were analyzed by high-performance liquid chromatography (HPLC, Prominence, Shimadzu Corp., Kyoto, Japan) under the following conditions: column, Aminex HPX-87H (300×7.8 mm, Bio-Rad Laboratories, Inc., Hercules, CA, USA); eluent, 5 mM sulfuric acid in water; flow-rate, 0.6 mL/min; column temperature, 45 °C; detector, refractive index detector (RID-20A, Shimadzu Corp.).

5.3 Results and discussion

5.3.1 Durability

To investigate the durability of 4wt%Ru-4wt%Sn/TiO_2 and 4wt%Ni-4wt%Sn/TiO_2, changes in the ethanol yield were studied by using the flow-type reactor at 290 °C/10 MPa, results are shown in Fig. 5-1. The 4wt%Ru-4wt%Sn/TiO_2 catalyst performed an excellent activity until 100 hours, and the highest yield was 63 mol%. After 100 hours, the ethanol yield decreased slightly as the reaction time was extended. The 4wt%Ni-4wt%Sn/TiO_2 catalyst performed well until 50 hours with the highest yield at 23 mol%, but the yield showed a declining trend and reached 14 mol% at 192 hours. These results pointed out that Ru-Sn/TiO_2 is more stable than Ni-Sn/TiO_2.

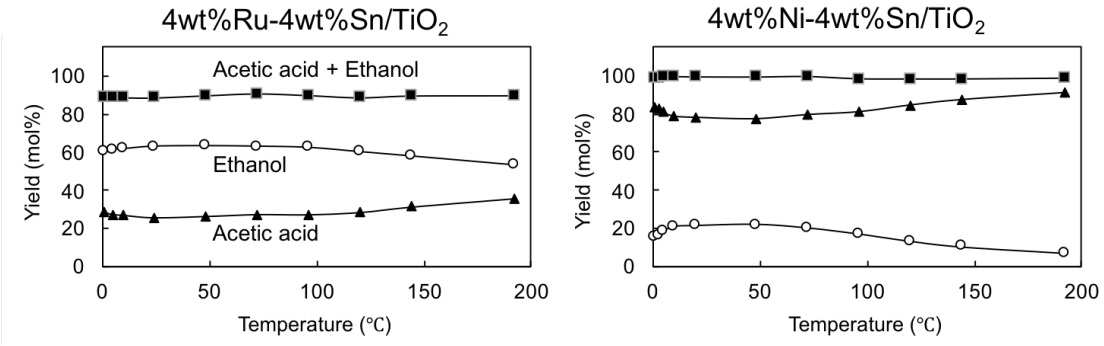

Fig. 5-1 Durability study of 4wt%Ru-4wt%Sn/TiO_2 and 4wt%Ni-4wt%Sn/TiO_2 for hydrogenation of aqueous acetic acid (10g/L, flow rate 0.3 mL/min, 10MPa, 192 h, H_2 60 mL/min).

5.3.2 Characterization of spent catalyst

5.3.2.1 4wt%Ru-4wt%Sn/TiO_2

The influence of 192 hours of reaction on TiO_2 supports of 4wt%Ru-4wt%Sn/TiO_2 catalysts were investigated by comparing with fresh catalyst using XRD, and the results are shown in Fig. 5-2. For the fresh catalyst the typical peaks of anatase and rutile structure of TiO_2 are both observed at 25° and 27°, 50°, and 52° respectively. Ru and SnO_2 were detected at 41° and 36.5° respectively. After 192 hours reaction, the peaks of each particle become sharper, the peak intensity of rutile of TiO_2 become stronger than anatase, and a new peak of rutile detected at 45°. These results indicated that the Ru and SnO_2 particle size become larger and more rutile structures were formed than anatase. We reported that the TiO_2 works as the Lewis acid point for activating the carbonyl carbon in acetic acid which could promote the hydrogenation activity of acetic acid (Ito et al., 2016; Kawamoto et al., 2016; Zhao et al., 2020). The better acceptation of acetic acid with TiO_2 could lead to higher hydrogenation activity. The oxygen interatomic the distance in acetic acid was 0.211 nm, and distance of Ti-Ti in anatase is 0.304 nm and rutile is 0.296 nm, considering that carbonyl oxygen takes an sp^2 hybrid orbital and hydroxyl oxygen takes an sp^3 hybrid orbital, anatase is more advantages than rutile (Kim et al., 1996; Nakabayashi et al., 1999) for hydrogenation of aqueous acetic acid hydrogenation. Hence, the formation of rutile in the spent catalyst is one of the causes of the slight decrease in Ru-Sn/TiO_2 catalytic activity.

SEM images of a fresh and 4wt%Ru-4wt%Sn/TiO_2 catalyst recovered from 192 h reaction are shown in Fig. 5-3. In the SEM images, there were no many differences between the fresh and used catalyst.

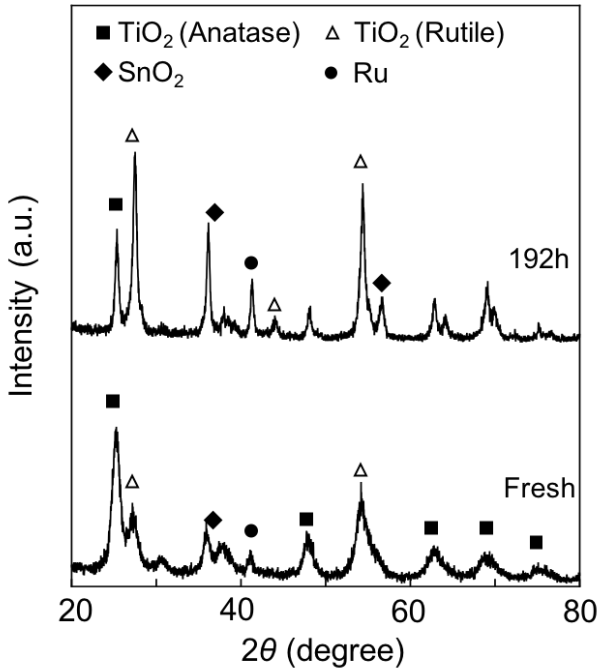

Fig. 5-2 XRD results of fresh and recovered 4wt%Ru- 4wt%Sn/TiO_2 from 192 hours of hydrogenation of aqueous acetic acid (10g/L, flow rate 0.3mL/min, 10MPa, H_2 60 mL/min).

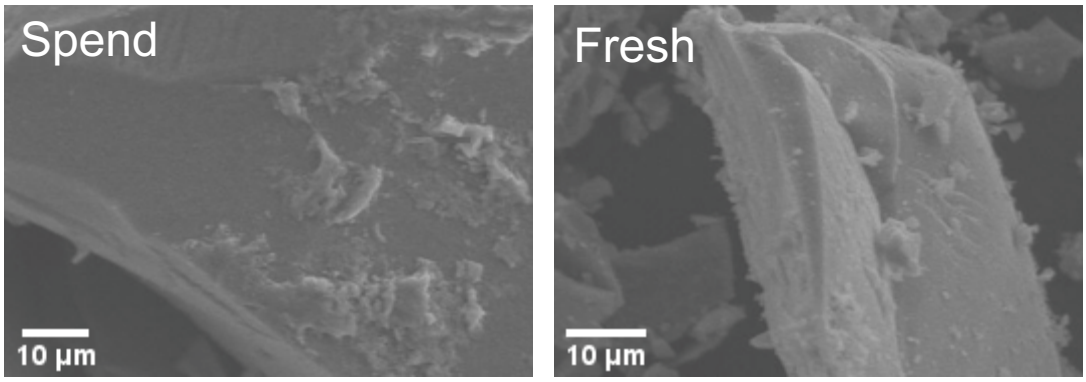

Fig. 5-3 SEM results of recovered 4wt%Ru-4wt%Sn/TiO_2 from 192 hours of hydrogenation of aqueous acetic acid (10g/L, flow rate 0.3mL/min, 10MPa, H_2 60 mL/min).

5.3.2.2 4wt%Ni-4wt%Sn/TiO_2

It is known that the NiSn alloy plays an important role in the hydrogenation of aqueous acetic acid in 4wt%Ni-4wt%Sn/TiO_2 (Zhao et al., 2020). The fresh and recovered 4wt%Ni-4wt%Sn/TiO_2 catalyst from 192 h durability study was observed by FE-TEM, and the results are shown in Fig. 5-4. After 192 hours reaction, the average particle size of Ni_4Sn_3 alloy increased from 13nm to 40 nm, while that of TiO_2 increased from 9 nm to 44 nm (Zhao et al., 2020). In addition, some rutile-like crystal shape of TiO_2 was found in the spent catalyst even though the peaks of rutile crystal were not observed in the XRD chart which will discuss later. As a hypothesis, the crystal moving would help the growth of TiO_2 particles, which also causes the growth of NiSn alloy or metal leaching. The hydrogenation of aqueous acetic acid would take place at the interface between NiSn alloy with TiO_2 supports (Zhao et al., 2020), the growth of NiSn alloy and TiO_2 particles will decrease the interaction area between them and it can decrease the catalyst activity. However, these growth may stop after a certain treatment time and the catalyst will turn stable, but further investigations are necessary.

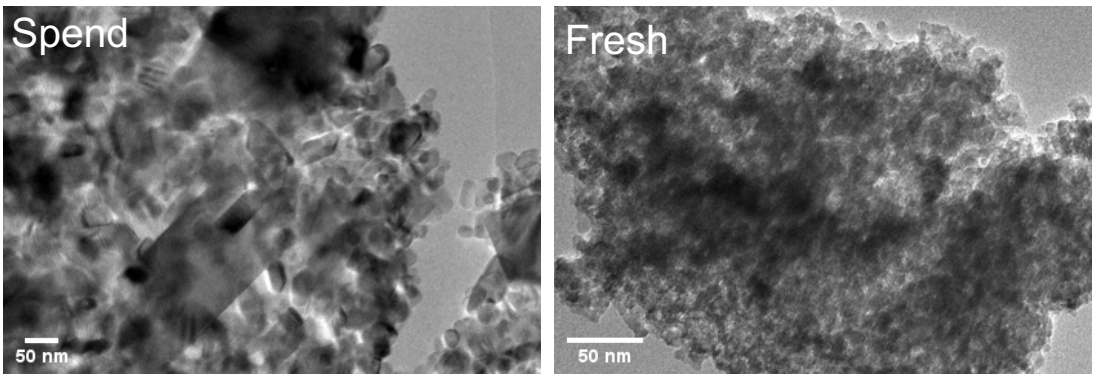

Fig. 5-4 Results of TEM of fresh and recovered 4wt%Ni-4wt%Sn/TiO_2 from 192 hours of hydrogenation of aqueous acetic acid (10g/L, flow rate 0.3mL/min, 10MPa, H_2 60 mL/min).

The composition of each element and the electronic states of Ni and Sn of fresh and recovered 4wt%Ni-4wt%Sn/TiO_2 catalyst from 192 h durability study were evaluated by XPS, and the results are shown in table 5-1 and Fig. 5-5 respectively. In table 5-1, both Ni and Sn ratio were decreased after used for 192 hours, which indicated there were metal leaching taking place while the long-time hydrogenation reaction. The ratio of Ni to Sn also changed which leads an alloy changing which will explain later.

In the spent catalyst, the ratio of Ni^0 to Ni^{2+} with the peak at 852.1 eV (Hengne et al., 2018) and 854.7 eV (Li et al., 2017) decreased from 1:4 to 1:16, and the ratio of Sn^0, Sn^{2+} and Sn^{4+} with the peaks at 485, 486.2, and 487.1 eV were decreased from 1: 3: 1 to 1: 6: 6 (Hanyš et al., 2006; Li et al., 2011; Quackenbush et al., 2013). These results indicated the catalyst have been oxidized, however, it is difficult to conclude this oxidation occurred during the hydrogenation of aqueous acetic acid since the spent catalyst was contacted the air before it was analyzed by XPS. Further discussion about the oxidation of catalysts will be reported later.

Table 5-1 XPS results of the composition change of recovered 4wt%Ni-4wt%Sn/TiO_2 catalyst.

	Ni 2p3/2	Sn 3d5/2	Ti 2p3/2	O 1s
Fresh	17	12	6	64
192 hours	8	10	19	63

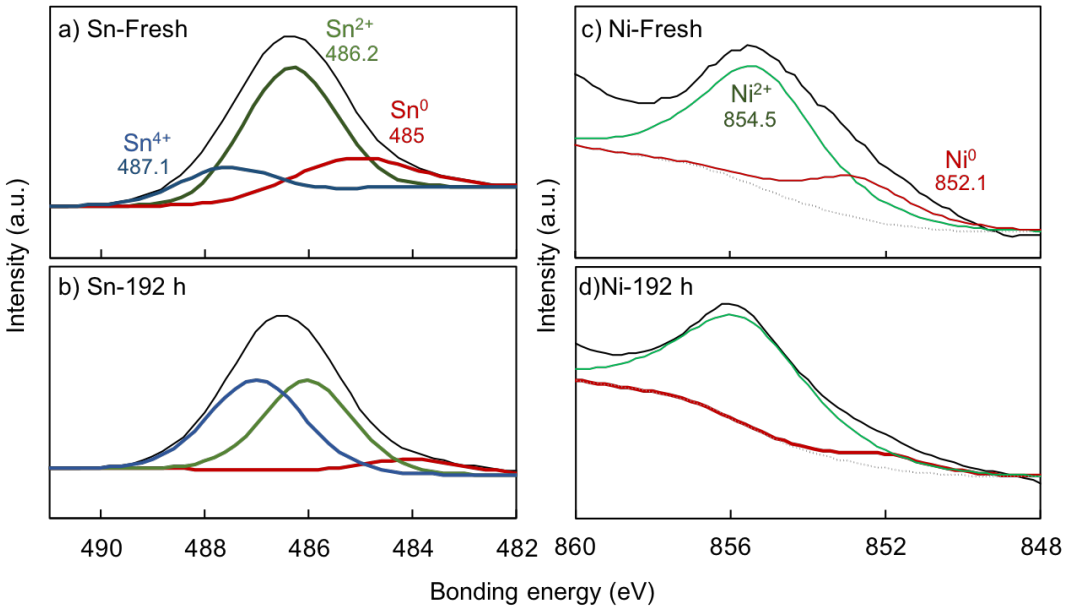

Fig. 5-5 XPS results of recovered 4wt%Ru-4wt%Sn/TiO_2 from 192 hours of hydrogenation of aqueous acetic acid (10g/L, flow rate 0.3mL/min, 10MPa, H_2 60 mL/min).

The changing of alloy can be considered as one of the reasons for catalytic activity decreasing. Therefore, the effects of NiSn alloy changing in spend catalyst were investigated with hot-compressed water treatment was conducted in a batch reactor for 1, 3, 5, and 10 hours at 200 °C/10 MPa and the XRD results are shown in Fig. 5-6. The Ni_3Sn_2 alloy at 41°were getting smaller, and Ni_4Sn_3 alloy peaks around 30° and 42°were getting sharper when the treatment time was prolonged. The metal leaching may cause this alloy changing since in the recovered catalyst Sn content was 55.6 atomic%. And according to the Ni-Sn phase diagram, when there was 56-57 atomic% Sn, rather than Ni_3Sn_2 the Ni_4Sn_3 alloy was easier to form. This alloy changing may result indicates that long-time heating could lead to alloy changing and increasing the alloy size. The peaks of TiO_2 became sharper than fresh, which indicated the size grow to larger, which supported the FE-TEM discussed before.

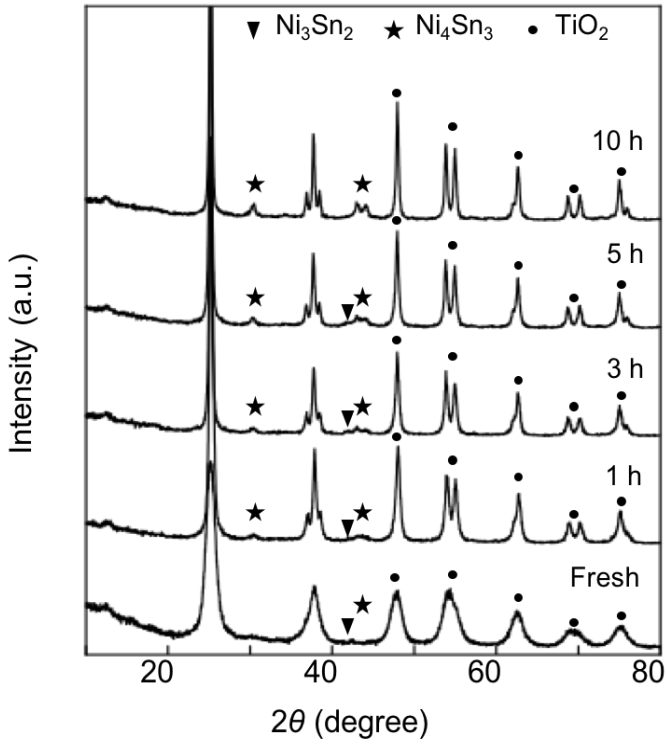

Fig. 5-6 XRD results of fresh and recovered 4wt%Ni-4wt%Sn/TiO_2 from after hot-compressed water treatment in batch reactor for 1, 3, 5, and 10 hours at 200 °C/10 MPa.

Table 5-2. Investigation on oxidation of 4wt%Ni-4wt%Sn/TiO_2 catalyst.

Treatment			Ethanol yield (mol%)
(1)	(2)	(3)	
HCW 10h	-	-	90
HCW 10h	3days in air	-	37
HCW 10h	3days in air	H_2 reduction 1h	71

HCW: hot compress water treatment (200 ℃/ 10MPa/ 10h)

The BET results of treated catalysts were investigated and the surface area of spent Ni-Sn/TiO_2 catalysts after hot-compressed water treatment is decreased from 130 m^2/g along with longer reaction time 1, 3, 5, and 10 hours to 51, 46, 43, and 30 m^2/g, and the NiSn alloy and TiO_2 growing could be the reason for decreasing the BET surface area.

Unexpectedly, the Ni-Sn/TiO_2 catalyst recovered after 10 hours HCW treatment showed no reactivity for hydrogenolysis even under the same conditions as durability study with the flow-type reactor. The only difference of Ni-Sn/TiO_2 catalysts between HCW experiments and durability studies is that the former one was exposed to air for XRD analysis. Therefore, the hot-compressed water (HCW) -treated catalyst may be oxidized in the air. To investigate the effect of oxidation, a series of hydrogenolysis experiments were carried out with 4wt%Ni-4wt%Sn/TiO_2 in the batch-type reactor, as shown in Table 5-1. The amount of 2.4 gram of fresh 4wt%Ni-4wt%Sn/TiO_2 catalyst was under HCW treatment for 10 h at 200 °C/ 10MPa. Then half of the spent catalysts were taken out and rest of them remained inside the reactor. An amount of acetic acid was added to a spent catalyst which remained inside the reactor to make the 10 g/L aqueous acetic acid then followed by the hydrogenation reaction treatment under the same conditions as HCW treatment. It results in a high ethanol yield of 90 mol%. Meanwhile, the spent catalyst which took out from the reactor was exposed to air for 3 days and hydrogenation was conducted. It turns out that the catalyst activity significantly decreased to 37 mol%. It indicates that oxidation occurred during exposure to air. Furthermore, the recovered catalyst was reduced under H_2 gas at 436 °C for 1 h to regenerate its activity and resulted almost as effective as before exposure to air. It is suggested that the oxidized Ni-Sn/TiO_2 catalyst could be removed by reduction to regain its activity. Accordingly, it was found that the Ni-Sn/TiO_2 catalyst after HCW treatment was easy to be oxidized in air, but after hydrogen reduction, the catalyst

activity was recovered appreciably. Therefore, avoiding the exposure of the used Ni-Sn/TiO_2 catalyst to air is more beneficial for the ethanol production process. In other words, the flow-type reactor, which is a closed system, is more appropriate than the batch-type reactor, which always needs to open the system to obtain the products.

5.4 Conclusions

In this study, the durability of 4wt%Ru-4wt%Sn/TiO_2 and 4wt%Ni-4wt%Sn/TiO_2 catalysts were investigated at 290 ℃/10 MPa for 192 hours by flow type reactor.

1. The activity of 4wt%Ru-4wt%Sn/TiO_2 catalyst slightly decreased to 85% (63 mol% to 54 mol%) which was much more stable than 4wt%Ni-4wt%Sn/TiO_2 to 32% (22 mol% to 7 mol%)).
2. The ratio of rutile/anatase (TiO_2) in Ru-Sn/$TiO_2$was increased, which could the main reason for reducing the catalytic activity.
3. The alloy changing from Ni_3Sn_2 to Ni_4Sn_3 in Ni-Sn/TiO_2 occurred, and NiSn alloy and TiO_2 particle size were increased from 13nm to 40 nm and 9 nm to 44 nm respectively by prolonging the reaction time (heating treatment).
4. The Ni_4Sn_3 alloy also had the ability for hydrogenolysis of acetic acid.
5. The XPS results indicated the catalyst oxidation can be considered as one of the main reasons for Ni-Sn/TiO_2 catalyst deactivation. To avoid the catalyst-air contact by using a flow-type reactor will keep the Ni-Sn/TiO_2 catalyst more stable.

Chapter 6

Concluding remarks

6.1 Conclusions

Biomass is known as a renewable and environmentally friendly resource for energy supply which can use as a substitute for fossil energy. To use biomass as an energy resource, bioethanol is attracted attention for its possibility of being an alternative fuel, and it refers to ethanol which is a very important raw material for the modern chemical industry.

The conversional bioethanol production process used alcohol fermentation which will waste carbon by releasing carbon dioxide. Hence, an advanced bioethanol product process by using acetic acid fermentation was investigated in our laboratory. This new process includes three consecutive steps, that is, hot-compressed water treatment to hydrolyze lignocellulosics, acetic acid fermentation, and hydrogenation of acetic acid. This paper focuses on the last hydrogenation step.

Consider the efficient energy-saving, hydrogenation of acetic acid has been investigated under the aqueous phase. Direct hydrogenation of aqueous acetic acid to ethanol reactivity dramatically increased by using Lewis acid support, which coordinates to carbonyl oxygen, resulting in the activation of acetic acid for hydrogenation through increasing δ+ character of the carbonyl carbon. 98 mol% of ethanol from the hydrogenation of 10 g/L aqueous acetic acid over 4wt%Ru-4wt%Sn/TiO_2 catalyst in batch type reactor. Ru is a precious metal, inexpensive catalysts are always more preferable for hydrogenation of aqueous acetic acid and the advanced bioethanol production process. And flow reactor for solid-catalyzed reactions has many advantages over batch reactors. Therefore, in this paper highly efficient catalysts for hydrogenation of aqueous acetic acid were investigated. Moreover, the

catalyst performance in a different types of reactor, and the side reactions in the hydrogenation of acetic acid were reported.

Ni as a cheaper metal than Ru and relatively shows activity on hydrogenation of aqueous acetic acid were used to investigate the new catalyst. In chapter 2, Various Ni and Ni-Sn catalysts supported on TiO_2 were prepared and the catalytic activities were evaluated for ethanol formation from aqueous acetic acid. Although catalytic activities of the Ni/TiO_2 catalysts were limited, the addition of Sn improved the activity dramatically, and the optimum Ni/Sn ratio was approximately 1:1 (w/w). SnO_2, the precursor of Sn, could not be reduced into metal Sn in pure form but did reduce into Ni-Sn alloys in the presence of NiO, the precursor of Ni. Analyses with XRD and SEM-EDS revealed that the Ni-Sn alloys were homogeneously dispersed on the TiO_2 surface. Furthermore, IR analysis indicated that the Ti atoms in the catalyst act as a Lewis acid, which coordinates to the oxygen atoms of acetic acid, enhancing the attack of hydrogens activated on neighboring Ni-Sn alloys. Based on these results, Ni-Sn/TiO_2 is proposed as an effective hydrogenation catalyst for converting aqueous acetic acid into ethanol.

According to our previous study, Ru-Sn/TiO_2 is evaluated as a highly efficient catalyst for the hydrogenation of aqueous acetic acid to ethanol. Hence a similar hydrogenation process was investigated in a flow-type reactor. The optimum temperature was 170 °C for the batch-type reactor because of gas production at higher temperatures; however, for the flow-type reactor, the ethanol yield increased with reaction temperature up to 280 °C and then decreased sharply above 300 °C, owing to an increase in the acetic acid recovery rate. The selectivity for ethanol formation was improved over the batch process, and an ethanol yield of 98 mol% was achieved for a 6.7 min reaction (cf. 12 h for a batch) (liquid hourly space velocity: 1.23 h^{-1}). Oxidation of ethanol to acetic acid (i.e., the reverse reaction) adversely affected the hydrogenation. On the basis of these results, hydrogenation mechanisms that include competing for

side reactions are discussed in relation to the reactor type. These results will help the development of more efficient catalytic procedures. This method was also effectively applied to the hydrogenation of lactic acid to propane-1,2-diol.

Ni-Sn/TiO_2 was found as an efficient catalyst for hydrogenation of aqueous acetic acid to ethanol for bioethanol production. In chapter 4, Ni-Sn/TiO_2 was evaluated and compared with Ru-Sn/TiO_2 in a flow-type reactor under similar conditions as chapter 3. Ni-Sn/TiO_2 catalyst shows lower ethanol conversion, and the ethanol yield was influenced by the amount of H_2 supply. However, at higher temperatures, Ni-Sn/TiO_2 shows a lower selectivity of gasification at higher temperatures. With both Ni and Ru -Sn/TiO_2 catalysts, by increasing the reaction temperature, the catalytic activity became less effective at some temperature, where the recovery of unreacted acetic acid rather increased. This temperature changed depending on the reaction pressure and was close to the boiling point of the solvent water at each pressure. Considering the results of model experiments using ethanol and acetaldehyde, around the water boiling point the oxidation of ethanol becomes significant, especially the gasification was promoted over Ru-SnTiO_2 catalysts. Indicated that the boiling of water interrupted the hydrogenation of acetic acid via acetaldehyde to ethanol, which promotes the ethanol oxidation and slows down the ethanol formation, and increasing the hydrogen amount can suppress these side reactions. Besides, the Cannizzaro reaction was found to occur via acetaldehyde under catalytic conditions. Based on the present results, the competitive reaction routes with hydrogenation of aqueous acetic acid are proposed.

In chapter 5, the durability of 4wt%Ru-4wt%Sn/TiO_2 and 4wt%Ni-4wt%Sn/TiO_2 catalysts were investigated at 290 ℃/10 MPa for 192 hours by flow type reactor. It was found that the activity of 4wt%Ru-4wt%Sn/TiO_2 catalyst slightly decreased to 85% which was much more stable than 4wt%Ni-4wt%Sn/TiO_2 to 32%. The ratio of rutile/anatase (TiO_2) in Ru-Sn/$TiO_2$was increased, which reason for reducing the catalytic activity. The alloy changing from Ni_3Sn_2 to Ni_4Sn_3 in Ni-Sn/TiO_2

occurred, and NiSn alloy and TiO_2 particle size were increased by prolonging the reaction time (heating treatment), and it may decrease the catalyst activity but turns the catalyst more stable. Besides, according to the XPS results and investigation on Ni-Sn/TiO_2 catalyst oxidation indicated the oxidation can be considered as one of the main reasons for Ni-Sn/TiO_2 catalyst deactivation. To avoid the catalyst-air contact by using a flow-type reactor will keep the Ni-Sn/TiO_2 catalyst more stable.

In summary, in this study a new Ni-Sn/TiO_2 catalyst for hydrogenation of aqueous acetic acid has been investigated and compared with Ru-Sn/TiO_2 in a flow type reactor. Both catalysts shown highly efficient, around 90 mol% of ethanol obtain with flow type reactor in 7 min, which has great advantages for the advance bioethanol production process. The side reactions in the hydrogenation of aqueous acetic acid was discussed over both catalysts, and the reaction mechanism of hydrogenation of acetic acid were proposed. Accordingly, it was found that the Ru catalyst shows higher catalytic activity than Ni, but for the selectivity of side reaction of gasification, the Ru also much higher than Ni in flow type reactor, which makes Ni have more advantageous for controlling side reactions. These results provide the possibility for further improving the efficiency of ethanol conversion.

6.2 Prospects for future research

Bioethanol is a potential renewable fuel and energy that can replace part of fossil energy, which can actually reduce the impact of emission from fossil energy to the environment. an advanced bioethanol production has been proposed, this paper focused on the last step of this process, which is catalytically hydrogenated acetic acid to ethanol. New Ni-Sn/TiO_2 catalysts were investigated and compared with Ru-Sn/TiO_2 in a flow type reactor. In the future, the durability of both Ni-Sn/TiO_2 and Ru-Sn/TiO_2 are plan to be discussed. Besides, the role of catalyst for occurring side reactions is still unclear. The effects from TiO_2 support may become one of the reasons, which gives a new

direction for catalyst investigation by exchange different supports work as Lewis acid sites in the future. In addition, in chapter 3 it was found this system shows a good efficiency for aqueous lactic acid. Therefore, the hydrogenation of other organic acids over investigated catalysts will be discussed.

After the research of hydrogenation of aqueous acetic acid (solution from commercial acetic acid), the invented catalyst will be investigated by hydronation of the aqueous acetic acid that recovered from real acetic acid fermentation. Since fermenting acetic acid used nutrient solution that makes the recovered acetic acid may contain some inorganic salt ion may affect the activity of the catalysts. Therefore, the performance of developed catalysts will be further studied in recovered from real acetic acid fermentation in future work.

References

Adkins, H., Folkers, K., 1931. The catalytic hydrogenation of esters to alcohols. J. Am. Chem. Soc. 53, 1095-1097.

Adkins, H., Wojcik, B., 1933. The catalytic hydrogenation of esters to alcohols. III. J. Am. Chem. Soc. 55, 1669-1676.

Ajanovic, A., 2011. Biofuels versus food production: Does biofuels production increase food prices? Energy 36, 2070-2076.

Al-Hasan, M., 2003. Effect of ethanol-unleaded gasoline blends on engine performance and exhaust emission. Energy Convers. Manag. 44, 1547-1561.

Balat, M., Balat, H., Öz, C., 2008. Progress in bioethanol processing. Prog. Energy Combust. Sci. 34, 551-573.

Besson, M., Gallezot, P., Pinel, C., 2014. Conversion of biomass into chemicals over metal catalysts. Chem. Rev. 114, 1827-1870.

Biello, D., 2011. The false promise of biofuels., Scientific American, 59-65.

Bing Li, a Chao Li, b J.C. and J.Z., 2016. Erratum: In situ nano-coating on $Li_{1.2}Mn_{0.52}Ni_{0.13}Co_{0.13}O_2$ with a layered@spinel@coating layer heterostructure for lithium-ion batteries , 2015, J. Mater. Chem. A. 3, 21290-21297.

Bon, E.P.S., Ferrara, M.A., 2010. Bioethanol production via enzymatic hydrolysis of cellulosic biomass. Biotechnology 1-11.

British Petroleum, 2020. Statistical review of world energy, 69th Edition. Bp 69, 66.

Broadbent, H.S., Campbell, G.C., Bartley, W.J., Johnson, J.H., 1959. Rhenium and its compounds as hydrogenation catalysts. Iii. Rhenium Ileptoxide. J. Org. Chem. 24, 1847-1854.

Brown, L.R., 1980. Food or fuel: new competition for the world's cropland. Worldwatch Pap.,1-44.

Cheah, K.Y., Tang, T.S., Mizukami, F., Niwa, S. ichi, Toba, M., Choo, Y.M., 1992. Selective hydrogenation of oleic acid to 9-octadecen-1-ol: Catalyst preparation and optimum reaction conditions. J. Am. Oil Chem. Soc. 69, 410-416.

Chen, H., Chemical composition and structure of natural lignocellulose, in: Biotechnology of lignocellulose: theory and Practice 2014, Beijing and Springer science+business media Dordrecht, 25-71.

Chen, L., Li, Y., Zhang, X., Zhang, Q., Wang, T., Ma, L., 2014. Mechanistic insights into the effects of support on the reaction pathway for aqueous-phase hydrogenation of carboxylic acid over the supported Ru catalysts. Appl. Catal. A Gen. 478, 117-128.

Chen, L., Zhu, Y., Zheng, H., Zhang, C., Zhang, B., Li, Y., 2011. Aqueous-phase hydrodeoxygenation of carboxylic acids to alcohols or alkanes over supported Ru catalysts. J. Mol. Catal. A Chem. 351, 217-227.

Chien, I.L., Zeng, K.L., Chao, H.Y., Liu, J.H., 2004. Design and control of acetic acid dehydration system via heterogeneous azeotropic distillation. Chem. Eng. Sci. 59, 4547-4567.

Church, J.A., White, N.J., 2011. Sea-level rise from the late 19th to the early 21st century. Surv. Geophys. 32, 585-602.

Clarke, C.J., Tu, W.C., Levers, O., Bröhl, A., Hallett, J.P., 2018. Green and sustainable solvents in chemical processes. Chem. Rev. 118, 747-800.

Cleveland, C.J., Costanza, R., Hall, C.A.S., Kaufmann, R., 1984. Energy and the U.S. economy: a biophysical perspective. Science 225, 890-897.

Comiso, J.C., Hall, D.K., 2014. Climate trends in the arctic as observed from space. Wiley Interdiscip. Rev. Clim. Chang., 5, 389-409.

Diagne, C., Idriss, H., Kiennemann, A., 2002. Hydrogen production by ethanol reforming over Rh/CeO_2-ZrO_2 catalysts. Catal. Commun., 3, 565-571.

Dimian, A.C., Kiss, A.A., 2020. Novel energy efficient process for acetic acid production by methanol carbonylation. Chem. Eng. Res. Des. 159, 1-12.

Dodić, S.N., Popov, S.D., Dodić, J.M., Ranković, J.A., Zavargo, Z.Z., 2009. Potential contribution of bioethanol fuel to the transport sector of Vojvodina. Renew. Sustain. Energy Rev. 13, 2197-2200.

Durndell, L.J., Wilson, K., Lee, A.F., 2015. Platinum-catalysed cinnamaldehyde hydrogenation in continuous flow. RSC Adv. 5, 80022-80026.

Eggeman, T., Verser, D., 2006. The importance of utility systems in today's biorefineries and a vision for tomorrow, in: applied biochemistry and biotechnology., 130, 361-381.

Eiichi Kikuchi, 2013. Catalyst characterization, in: new catalytic chemistry. Sankyo Shuppan., Japan, Tokyo, 200-259.

Elliott, D.C., Hart, T.R., 2009. Catalytic hydroprocessing of chemical models for bio-oil. Energy and Fuels 23, 631-637.

Fiume, M.M., Bergfeld, W.F., Belsito, D. V., Hill, R.A., Klaassen, C.D., Liebler, D., Marks, J.G., Shank, R.C., Slaga, T.J., Snyder, P.W., Andersen, F.A., 2012. Safety assessment of propylene glycol, tipropylene glycol, and PPGs as used in cosmetics. Int. J. Toxicol. 31, 245S-260S.

Folkers, K., Adkins, H., 1932. The catalytic hydrogenation of esters to alcohols. II. J. Am. Chem. Soc. 54, 1145-1154.

Geissman, T.A.,2011. The cannizzaro reaction, Organic reactions, Inc. Wiley., 93-114.

Gómez-Quero, S., Cárdenas-Lizana, F., Keane, M.A., 2011. Liquid phase catalytic hydrodechlorination of 2,4-dichlorophenol over Pd/Al_2O_3: batch vs. continuous operation. Chem. Eng. J. 166, 1044-1051.

Hanyš, P., Janeček, P., Matolín, V., Korotcenkov, G., Nehasil, V., 2006. XPS and TPD study of Rh/SnO_2 system - reversible process of substrate oxidation and reduction. Surf. Sci. 600, 4233-4238.

Hartman, R.L., McMullen, J.P., Jensen, K.F., 2011. Deciding whether to go with the flow: evaluating the merits of flow reactors for synthesis. Angew. Chemie - Int. Ed.,50, 7502-7519.

Hasan, R., Mekhilef, S., Seyedmahmoudian, M., Horan, B., 2017. Grid-connected isolated PV microinverters: a review, renewable and sustainable energy reviews., 67, 1065-1080.

Hengne, A.M., Samal, A.K., Enakonda, L.R., Harb, M., Gevers, L.E., Anjum, D.H., Hedhili, M.N., Saih, Y., Huang, K.W., Basset, J.M., 2018. Ni-Sn-supported ZrO_2 catalysts modified by indium for selective CO_2 hydrogenation to methanol. ACS Omega 3, 3688-3701.

Hessel, V., 2009. Novel process windows - gates to maximizing process intensification via flow chemistry. Chem. Eng. Technol. 32, 1641.

Hessel, V., Löb, P., Krtschil, U., Löwe, H., 2007. Microstructured reactors for development and production in pharmaceutical and fine chemistry, in: synthesis new avenues to efficient chemical synthesis; Seeberger, P.H.,Blume, T., Eds.; Springer: Berlin/Heidelberg, Germany, 2007, 205-240.

Intergovernmental Panel on Climate Change (IPCC), 2014. Climate change 2014 synthesis report summary chapter for policymakers. IPCC 31.

International Energy Agency: the total primary energy supply, 2017.

International Energy Agenc: world energy outlook 2019 -analysis - IEA. World energy outlook 2019.

International Energy Agency, 2013. Redrawing the energy-climate map: world energy outlook special report. Int. Energy Agency 134.

InvestmentMine: http://www.infomine.com/investment/metal-prices/, Dec./ 8/ 2020.

Ito, Y., Kawamoto, H., Saka, S., 2016. Efficient and selective hydrogenation of aqueous acetic acid on Ru-Sn/TiO_2 for bioethanol production from lignocellulosics. Fuel 178, 118-123.

Johansson, D.J.A., Azar, C., 2007. A scenario based analysis of land competition between food and bioenergy production in the US. Clim. Change., 82, 267-291.

Jones, R. V., Godorhazy, L., Varga, N., Szalay, D., Urge, L., Darvas, F., 2006. Continuous-flow high pressure hydrogenation reactor for optimization and high-throughput synthesis. J. Comb. Chem. 8, 110-116.

Kampf, G., 2020. Potential role of inanimate surfaces for the spread of coronaviruses and their inactivation with disinfectant agents. Infect. Prev. Pract. 2, 100044.

Kang, Q., Appels, L., Tan, T., Dewil, R., 2014. Bioethanol from lignocellulosic biomass: current findings determine research priorities. Sci. World J., 2014, 1-13.

Kawamoto, H., Fuji, T., Ito, Y., Saka, S., 2016. Effects of different solvents on hydrogenation of acetic acid over Pt/TiO_2 for bioethanol production. J. Japan Inst. Energy 95, 162-166.

Khder, A.E.R.S., 2008. Preparation, characterization and catalytic activity of tin oxide-supported 12-tungstophosphoric acid as a solid catalyst. Appl. Catal. A Gen. 343, 109-116.

Khder, A.S., Ahmed, A.I., 2009. Selective nitration of phenol over nanosized tungsten oxide supported on sulfated SnO_2 as a solid acid catalyst. Appl. Catal. A Gen. 354, 153-160.

Khder, A.S., El-Sharkawy, E.A., El-Hakam, S.A., Ahmed, A.I., 2008. Surface characterization and catalytic activity of sulfated tin oxide catalyst. Catal. Commun. 9, 769-777.

Kim, D.W., Enomoto, N., Nakagawa, Z.E., Kawamura, K., 1996. Molecular dynamic simulation in titanium dioxide polymorphs: Rutile, brookite, and anatase. J. Am. Ceram. Soc. 79, 1095-1099.

Kim, S., Dale, B.E., 2004. Global potential bioethanol production from wasted crops and crop residues. Biomass and Bioenergy 26, 361-375.

Kövér, L., Moretti, G., Kovács, Z., Sanjinés, R., Cserny, I., Margaritondo, G., Pálinkás, J., Adachi, H., 1995. High resolution photoemission and auger parameter studies of electronic structure of tin oxides. J. Vac. Sci. Technol. A Vacuum, Surfaces, Film. 13, 1382-1388.

Lashof, D.A.; Tirpak, D.A. (eds. ., 1990. Policy options for stabilizing global climate. office of policy, planning and evaluation, US Environmental Protection Agency, 401 M Street, S.W., Washington, DC 20460, USA.

Lawal, A.M., Hart, A., Daly, H., Hardacre, C., Wood, J., 2019. Kinetics of hydrogenation of acetic acid over supported platinum catalyst. Energy and Fuels 33, 5551-5560.

Le Berre, C., 2001. Acetic acid. Eur. Chem. News 74, 20.

Lei, Z., Li, C., Li, Y., Chen, B., 2004. Separation of acetic acid and water by complex extractive distillation. Sep. Purif. Technol. 36, 131-138.

Li, J.T., Świątowska, J., Maurice, V., Seyeux, A., Huang, L., Sun, S.G., Marcus, P., 2011. XPS and ToF-SIMS study of electrode processes on Sn-Ni alloy anodes for Li-ion batteries. J. Phys. Chem. C., 115, 7012-7018

Li, X., Xin, M., Guo, S., Cai, T., Du, D., Xing, W., Zhao, L., Guo, W., Xue, Q., Yan, Z., 2017. Insight of synergistic effect of different active metal ions in layered double hydroxides on their electrochemical behaviors. Electrochim. Acta 253, 302-310.

Liu, Q. yan, Yang, F., Liu, Z. hua, Li, G., 2015. Preparation of SnO_2-Co_3O_4/C biochar catalyst as a Lewis acid for corncob hydrolysis into furfural in water medium. J. Ind. Eng. Chem., 26, 45-54.

Luo, G., Yan, S., Qiao, M., Fan, K., 2005. Effect of promoters on the structures and properties of the RuB/γ-Al_2O_3 catalyst. J. Mol. Catal. A Chem. 230, 69-77.

Ma, F., Hanna, M.A., 1999. Biodiesel production: a review. Bioresour. Technol. 70, 1-15.

Mao, B.W., Cai, Z.Z., Huang, M.Y., Jiang, Y.Y., 2003. Hydrogenation of carboxylic acids catalyzed by magnesia-supported poly-γ-aminopropylsiloxane-Ru complex. Polym. Adv. Technol. 14, 278-281.

Matsumura, Y., Sasaki, M., Okuda, K., Takami, S., Ohara, S., Umetsu, M., Adschiri, T., 2006. Supercritical water treatment of biomass for energy and material recovery. Combust. Sci. Technol.

Mendes, M.J., Santos, O.A.A., Jordão, E., Silva, A.M., 2001. Hydrogenation of oleic acid over ruthenium catalysts. Appl. Catal. A Gen. 217, 253-262.

Nagai, Y., Wakai, C., Matubayasi, N., Nakahara, M., 2003. Noncatalytic cannizzaro-type reaction of acetaldehyde in supercritical water. Chem. Lett. 32, 310-311.

Nakabayashi, T., Kosugi, K., Nishi, N., 1999. Liquid structure of acetic acid studied by raman spectroscopy and ab initio molecular orbital calculations. J. Phys. Chem. A 103, 8595-8603.

Nakamura, Y., Miyafuji, H., Kawamoto, H., Saka, S., 2011. Acetic acid fermentability with clostridium thermoaceticum and clostridium thermocellum of standard compounds found in beech wood as produced in hot-compressed water. J. Wood Sci. 57, 331-337.

Nash. A., Nash. P. 1985. The Ni-Sn (nickel-tin) system. Bulletin of alloy phase diagrams. 6, 350-358.

Nozawa, T., Mizukoshi, Y., Yoshida, A., Naito, S., 2014. Aqueous phase reforming of ethanol and acetic acid over TiO_2 supported Ru catalysts. Appl. Catal. B Environ. 146, 221-226.

Nozawa, T., Yoshida, A., Hikichi, S., Naito, S., 2015. Effects of Re addition upon aqueous phase reforming of ethanol over TiO_2 supported Rh and Ir catalysts. Int. J. Hydrogen Energy 40, 4129-4140.

Numwong, N., Luengnaruemitchai, A., Chollacoop, N., Yoshimura, Y., 2012. Partial hydrogenation of polyunsaturated fatty acid methyl esters over Pd/activated carbon: effect of type of reactor. Chem. Eng. J. 210, 173-181.

Olcay, H., Xu, L., Xu, Y., Huber, G.W., 2010. Aqueous-phase hydrogenation of acetic acid over transition metal catalysts. ChemCatChem 2, 1420-1424.

Olcay, H., Xu, Y., Huber, G.W., 2014. Effects of hydrogen and water on the activity and selectivity of acetic acid hydrogenation on ruthenium. Green Chem. 16, 911-924.

Osako, T., Torii, K., Hirata, S., Uozumi, Y., 2017. Chemoselective continuous-flow hydrogenation of aldehydes catalyzed by platinum nanoparticles dispersed in an amphiphilic resin. ACS Catal. 7, 7371-7377.

Osei, G., Arthur, R., Afrane, G., Agyemang, E.O., 2013. Potential feedstocks for bioethanol production as a substitute for gasoline in Ghana. Renew. Energy 55, 12-17.

Owusu, P.A., Asumadu-Sarkodie, S., 2016. A review of renewable energy sources, sustainability issues and climate change mitigation. Cogent Eng., 3, 1167990.

Phaiboonsilpa, N., Kawamoto, H., Minami, E., Masuda, S., Wakagi, R., Sunayama, T., Saka, S., 2020. Two-step conversion of acetic acid to bioethanol by ethyl esterification and catalytic hydrogenolysis. J. Japan Pet. Inst. 63, 196-203.

Pimentel, D., Marklein, A., Toth, M., Karpoff, M., Paul, G., McCormack, R., Kyriazis, J., Krueger, T., 2008. Biofuel impacts on world food supply: use of fossil fuel, land and water resources. Energies. 1, 41-78.

Quackenbush, N.F., Allen, J.P., Scanlon, D.O., Sallis, S., Hewlett, J.A., Nandur, A.S., Chen, B., Smith, K.E., Weiland, C., Fischer, D.A., Woicik, J.C., White, B.E., Watson, G.W., Piper, L.F.J., 2013. Origin of the bipolar doping behavior of SnO from X-ray spectroscopy and density functional theory. Chem. Mater. 25, 3114-3123.

Rabemanolontsoa, H., Kuninori, Y., Saka, S., 2016. High conversion efficiency of Japanese cedar hydrolyzates into acetic acid by co-culture of clostridium thermoaceticum and clostridium thermocellum. J. Chem. Technol. Biotechnol. 91, 1040-1047.

Rabemanolontsoa, H., Saka, S., 2016. Various pretreatments of lignocellulosics. Bioresour. Technol., 199, 83-91.

Rachmady, W., Vannice, M.A., 2000. Acetic acid hydrogenation over supported platinum catalysts. J. Catal. 192, 322-334.

Rathmann, R., Szklo, A., Schaeffer, R., 2010. Land use competition for production of food and liquid biofuels: An analysis of the arguments in the current debate. Renew. Energy., 35, 14-22.

Roberge, D.M., Bieler, N., Mathier, M., Eyholzer, M., Zimmermann, B., Barthe, P., Guermeur, C., Lobet, O., Moreno, M., Woehl, P., 2008a. Development of an industrial multi-injection microreactor for fast and exothermic reactions - Part II. Chem. Eng. Technol. 31, 1155-1161.

Roberge, D.M., Zimmermann, B., Rainone, F., Gottsponer, M., Eyholzer, M., Kockmann, N., 2008b. Microreactor technology and continuous processes in the

fine chemical and pharmaceutical industry: is the revolution underway? Org. Process Res. Dev. 12, 905-910.

Rodiansono, Khairi, S., Hara, T., Ichikuni, N., Shimazu, S., 2012. Highly efficient and selective hydrogenation of unsaturated carbonyl compounds using Ni-Sn alloy catalysts. Catal. Sci. Technol. 2, 2139-2145.

Rodríguez, L.A., Toro, M.E., Vazquez, F., Correa-Daneri, M.L., Gouiric, S.C., Vallejo, M.D., 2010. Bioethanol production from grape and sugar beet pomaces by solid-state fermentation. Int. J. Hydrogen Energy 35, 5914-5917.

S. Saka, 2001. Baioetanoru, in: Baiomasu・Enerugi・Kankyou. Industrial Publishing & Consulting Inc., Tokyo, 380-388.

Saka, S., Ehara, K., Minami, E., 2005. Efficient utilization of woody biomass with supercritical fluid technologies. Mokuzai Gakkaishi/Journal Japan Wood Res. Soc. 51, 207-217.

Saka, S., Rabemanolontsoa, H., Minami, E., Kawamoto, H., 2019. Advanced ethanol production with acetic acid fermentation from lignocellulosics. J. Japan Pet. Inst. 62, 199-204.

Sauer, M., Porro, D., Mattanovich, D., Branduardi, P., 2008. Microbial production of organic acids: expanding the markets. Trends Biotechnol., 26, 100-108.

Schell, D.J., Hinman, N.D., Wyman, C.E., Werdene, P.J., 1990. Whole broth cellulase production for use in simultaneous saccharification and fermentation. Appl. Biochem. Biotechnol. 24-25, 287-297.

Shen, J., Feng, X., Liu, R., Xu, X., Rao, C., Liu, J., Fang, X., Tan, C., Xie, Y., Wang, X., 2019. Tuning SnO_2 surface with CuO for soot particulate combustion: the effect of monolayer dispersion capacity on reaction performance. Chinese J. Catal. 40, 905-916.

Shiro Saka, 2010. Saiseikanou bioenerugi no gijyutsusenryaku, in: Gurin Sangyou Kakumei-Shakai Keizai Shisutemu no Kaihen to Gijyutsu Senryaku. Nikkei Business Publications Inc., Tokyo, 127-144.

Simmons, B.A., Loque, D., Blanch, H.W., 2008. Next-generation biomass feedstocks for biofuel production. Genome Biol. 9, 242.

Tahara, K., Nagahara, E., Itoi, Y., Nishiyama, S., Tsuruya, S., Masai, M., 1997. Liquid-phase hydrogenation of carboxylic acid on supported bimetallic Ru-Sn-alumina catalysts. Appl. Catal. A Gen. 154, 75-86.

Takagi, M., Abe, S., Suzuki, S., Emert, G., Yata, N., 1977. A method for production of alcohol directly from cellulose using cellulase and yeast. Bioconversion Symp. New Dehli. 551-571.

Urry, J., 2014. The Problem of Energy. Theory, Cult. Soc. 31, 3-20.

Voeste, T., Buchold, H., 1984. Production of fatty alcohols from fatty acids. J. Am. Oil Chem. Soc. 61, 350-352.

Voloshin, R.A., Rodionova, M. V., Zharmukhamedov, S.K., Nejat Veziroglu, T., Allakhverdiev, S.I., 2016. Review: Biofuel production from plant and algal biomass. Int. J. Hydrogen Energy., 41, 17257-17273.

Wan, H., Chaudhari, R. V., Subramaniam, B., 2013. Aqueous phase hydrogenation of acetic acid and its promotional effect on p-cresol hydrodeoxygenation. Energy and Fuels 27, 487-493.

Wang, Y., Prinsen, P., Triantafyllidis, K.S., Karakoulia, S.A., Yepez, A., Len, C., Luque, R., 2018. Batch versus continuous flow performance of supported mono- and bimetallic nickel catalysts for catalytic transfer hydrogenation of furfural in isopropanol. ChemCatChem 10, 3459-3468.

Wang, Z., Li, G., Liu, X., Huang, Y., Wang, A., Chu, W., Wang, X., Li, N., 2014. Aqueous phase hydrogenation of acetic acid to ethanol over Ir-MoOx/SiO_2 catalyst. Catal. Commun. 43, 38-41.

Wei, Y.J., Yan, L.Y., Wang, C.Z., Xu, X.G., Wu, F., Chen, G., 2004. Effects of Ni doping on [MnO_6] octahedron in $LiMn_2O_4$. J. Phys. Chem. B 108, 18547-18551.

Wiles, C., Watts, P., 2012. Continuous flow reactors: a perspective. Green Chem., 14, 38-54.

Yang, Y., Bae, J., Kim, J., Suh, S., 2012. Replacing gasoline with corn ethanol results in significant environmental problem-shifting. Environ. Sci. Technol. 46, 3671-3678.

Yu, T., Jiao, J., Song, P., Nie, W., Yi, C., Zhang, Q., Li, P., 2020. Recent progress in continuous-flow hydrogenation. ChemSusChem 13, 2876-2893.

Zhang, S., Duan, X., Ye, L., Lin, H., Xie, Z., Yuan, Y., 2013. Production of ethanol by gas phase hydrogenation of acetic acid over carbon nanotube-supported Pt-Sn nanoparticles, Catalysis Today. 215, 260-266.

Zhang, Z., Jackson, J.E., Miller, D.J., 2001. Aqueous-phase hydrogenation of lactic acid to propylene glycol. Appl. Catal. A Gen. 219, 89-98.

Zhao, Y., Konishi, K., Minami, E., Saka, S., Kawamoto, H., 2020. Hydrogenation of aqueous acetic acid over Ru-Sn/TiO_2 Catalyst in a flow-type reactor, governed by reverse reaction. Catalysts, 10, 1270.

Zhao, Y., Nishida, T., Minami, E., Saka, S., Kawamoto, H., 2020. TiO_2-supported Ni-Sn as an effective hydrogenation catalyst for aqueous acetic acid to ethanol. Energy Reports, 6, 2249-2255.

Acknowledgements

This thesis becomes a reality with the kind support and help of many indiciduals. I would like to extend my sincere thanks to all of them.

Firstly, I would like to express my deep and sincere gratitude to my research supervisor, Professor Haruo Kawamoto, Department of Socio-Environmental Science, Graduate School of Energy Science, Kyoto University, for giving me the opportunity to do research and providing invaluable guidance throughout this research. His dynamism, vision, sincerity and motivation have deeply inspired me. He has taught me the methodology to carry out the research and to present the research works as clearly as possible. It was a great privilege and honor to study under his guidance. I am extremely grateful for what he has offered me. I would also like to thank him for his kindness and patient that his office was always open whenever I had a question about my research or writing.

I would like to express my thanks to Specially-Appointed Professor Shiro saka, Department of Socio-Environmental Science, Graduate School of Energy Science, Kyoto University, for let me take apart in the ALCA project, that gives me a chance to enrich my research experiences.

I would like to express my high appreciations to Prof. Keiichi Ishihara, Department of Socio-Environmental Science, Graduate School of Energy Science, Kyoto University, and Prof. Hiroshi Kamitakahara, Division of Forest and Biomaterials Science, Graduate School of Agriculture, Kyoto University, for their comments, advices and valuable discussions of the manuscript.

I would also like to thank Assistant Professor Eiji Minanami, Department of Socio-Environmental Science, Graduate School of Energy Science, Kyoto University, for his patience and willingness to share his experiences, and giving valuable ideas or advices for my research.

My grateful thanks are also extended to Ms. Rie Nakanishi for her help in arranging experiment materials and communicating necessary documents.

I would like to say thanks to my friends and research colleagues, Dr. Kiky Corneliasari Sembiring, Mr. Jiawei Wang, Mr. Nomura Takashi, Ms. Latifa Seniorita, Mr. Jiaqi Wang, Ms. Yilin Yao, Ms. Rui Fang, Mr. Qiming Jin, Ms. Luthfiana Nurul

Hidayati for their constant encouragement. I express my special thanks to Dr. Wan Zurina Samad, JSPS researcher, Department of Socio-Environmental Science, Graduate School of Energy Science, Kyoto University, for her genuine sharing the experiences which relate to my research work.

I would also like to thanks all my lab mates for the stimulating discussions, for the sleepless nights we were working together before deadlines, and for all the fun we have had in these years.

I must express my very profound gratitude to my parents for providing me with unfailing support and continuous encouragement throughout my years of study and through the process of researching. This accomplishment would not have been possible without them. Thank you.

Finally, my thanks go to all the people who have supported me to complete the research work directly or indirectly.

List of publications

Original Papers

1. Yuanyuan Zhao, Takayuki Nishida, Eiji Minami, Shiro Saka, Haruo Kawamoto (2020) TiO_2-supported Ni-Sn as an effective hydrogenation catalyst for aqueous acetic acid to ethanol, *Energy reports* 6: 2249-2255 (DOI: 10.1016/j.egyr.2020.08.007)

2. Yuanyuan Zhao, Kansei Konishi, Eiji Minami, Shiro Saka and Haruo Kawamoto (2020) Hydrogenation of aqueous acetic acid over Ru-Sn/TiO_2 catalyst in a flow-type reactor, governed by reverse reaction, *Catalysts* 10: 1270 (DOI: 10.3390/catal10111270)

3. Yuanyuan Zhao, Eiji Minami, Shiro Saka, Haruo Kawamoto (2021) Effects of water boiling on hydrogenation of aqueous acetic acid over Ni-Sn/TiO_2 and Ru-Sn/TiO_2 in a flow type reactor. (Submitted to *Chemical engineering journal*)

4. Yuanyuan Zhao, Eiji Minami, Shiro Saka, Haruo Kawamoto (2021) Cannizzaro reaction occurring in hydrogenation of aqueous acetic acid over Ni-Sn/TiO_2 and Ru-Sn/TiO_2. (in preparation)

5. Yuanyuan Zhao, Luthfiana Nurul Hidayati, Eiji Minami, Haruo Kawamoto (2021) Stability of Ni-Sn/TiO_2 and Ru-Sn/TiO_2 catalysts in hydrogenation of aqueous acetic acid into ethanol. (in preparation)

Abstracts and proceedings of international conferences

6. Kansei Konishi, Yuanyuan Zhao, Haruo Kawamoto, Shiro Saka (2017) Hydrogenation of aqueous acetic acid from lignocellulosics for bioethanol production over Ru-Sn/TiO_2 with a flow-type reactor, *The 8th Japan-China*

workshop on environmental catalysis and eco-materials, P 60-61, December 5, 2017, Tsukuba, Japan

7. Yuanyuan Zhao, Haruo Kawamoto (2019) Competitive reactions in hydrogenation of aqueous acetic acid by flow-type reactor with Ni-Sn/TiO_2 catalyst for bioethanol production, *4th edition of international conference on catalysis and green chemistry*, P 71, May 13-14, 2019, Tokyo, Japan

8. Yuanyuan Zhao, Eiji Minami, Shiro Saka, Haruo Kawamoto (2019) Side reactions and their influence in hydrogenation of aqueous acetic acid into bioethanol in flow-type reactor using Ni-Sn/TiO_2 catalyst, *9th East Asia joint symposium on environmental catalysis and eco-materials,* Poster, November 5-8, 2019, Yancheng, China

9. Yuanyuan Zhao, Eiji Minami, Shiro Saka, Haruo Kawamoto (2019) Side reactions and their influence in hydrogenation of aqueous acetic acid into bioethanol in flow-type reactor using Ni-Sn/TiO_2 catalyst, *3rd Kyoto—Zhejiang—Ajou joint symposium on energy*, P 11, December 5-7, 2019, Kyoto, Japan

10. Yuanyuan Zhao, Esmaeil Ahmadi , Seyed Mostafa Mortazavi, Nesreen Hamad, Peng Lin, Zhihao Qin (2019) Characterization of household energy services in China, Egypt and Iran, *3rd Kyoto —Zhejiang —Ajou joint symposium on energy*, P 53 (poster), December 5-7, 2019, Kyoto, Japan

Abstracts and proceedings of domestic conferences

11. Yuanyuan Zhao, Haruo Kawamoto, Shiro Saka (2018) Hydrogenation of aqueous acetic acid by flow-type reactor with Ni-Sn/TiO_2 catalyst for bioethanol production, *68th annual meeting of the Japan wood research society*, P14-08-1330, March 14-16, 2018, Kyoto, Japan

12. Yuanyuan Zhao, Haruo Kawamoto, Shiro Saka (2018) Characterization of aqueous acetic acid hydrogenation over Ni-Sn/TiO_2 catalyst in flow-type reactor for

bioethanol production, *27th annual meeting of the Japan Institute of energy*, P 82-83, August 8-9, 2018, Tokyo, Japan

13. Yuanyuan Zhao, Haruo Kawamoto, Shiro Saka (2019) Role of cannizzaro reaction in hydrogenation of aqueous acetic acid by flow-type reactor with Ni-Sn/TiO_2 catalyst for bioethanol production, *69th annual meeting of the Japan wood research society*, P14-06-1500, March 14-16, 2019, Hakotate, Japan

14. Luthfiana Nurul Hidayati, Yuanyuan Zhao, Haruo Kawamoto, Shiro Saka (2019) Hydrogenation of aqueous acetic acid obtained from Japanese cedar fermentation over TiO_2-supported Ru-Sn and Ni-Sn for bioethanol production, *69th annual meeting of the Japan wood research society*, P14-06-1515, March 14-16, 2019, Hakotate, Japan

15. Yuanyuan Zhao, Eiji Minami, Shiro Saka, Haruo Kawamoto (2019) Side reactions and their roles in hydrogenation of aqueous acetic acid into bioethanol in flow-type reactor using Ni-Sn/TiO_2 catalyst, *28th annual meeting of the Japan Institute of energy,* P 108-109, August 7-8, 2019, Suita, Japan

16. Luthfiana Nurul Hidayati, Yuanyuan Zhao, Eiji Minami, Shiro Saka, Haruo Kawamoto (2019) Catalytic hydrogenation of aqueous acetic acid obtained by fermentation into bioethanol over TiO_2-supported Ru-Sn and Ni-Sn catalysts, *28th annual meeting of the Japan Institute of energy,* P 110-111, August 7-8, 2019, Suita, Japan

17. Luthfiana Nurul Hidayati, Yuanyuan Zhao, Eiji Minami, Haruo Kawamoto (2019) Stability of Ni-Sn/TiO_2 and Ru-Sn/TiO_2 catalysts in hydrogenation of aqueous acetic acid into ethanol, *70th annual meeting of the Japan wood research society*, P16-02-1530, March 16-18, 2020, Totori, Japan

Awards

1. Best student oral presentation award. *69th annual meeting of the Japan wood research society*, March 14-16, 2019, Hakotate, Japan

2. Best presentation award. Master thesis presentation of department of social environmental energy science, March 20-21, 2018, Kyoto, Japan